Spring 2022

Mechanistic Understanding of Catalytic Processes for Sustainable Chemical Transformations

Pooja J. Ayare

Recommended Citation

Ayare, P. J.(2022). *Mechanistic Understanding of Catalytic Processes for Sustainable Chemical Transformations.* (Doctoral dissertation). Retrieved from https://scholarcommons.sc.edu/etd/6618

MECHANISTIC UNDERSTANDING OF CATALYTIC PROCESSES FOR SUSTAINABLE CHEMICAL TRANSFORMATIONS

by

Pooja J. Ayare

Bachelor of Science
Kelkar Education Trust's Vinayak Ganesh Vaze College, 2013

Master of Science
Institute of Chemical Technology, 2015

Submitted in Partial Fulfillment of the Requirements

For the Degree of Doctor of Philosophy in

Chemistry

College of Arts and Sciences

University of South Carolina

2022

Accepted by:

Aaron K. Vannucci, Major Professor

Dmitry Peryshkov, Committee Member

Linda S. Shimizu, Committee Member

John R. Regalbuto, Committee Member

Tracey L. Weldon, Interim Vice Provost and Dean of the Graduate School

DEDICATION

To my grandmothers, who I love and miss every day.

ACKNOWLEDGEMENT

First and foremost, I would like to extend my deepest gratitude to my research advisor, Prof. Aaron Vannucci for his unwavering support and invaluable insights in my graduate research, presented in this dissertation. He is the best mentor I could have ever asked for and his guidance has helped me throughout my graduate career. I also sincerely thank my dissertation research committee: Prof. Dmitry Peryshkov, Prof. Linda Shimizu and Prof. John Regalbuto for their insightful suggestions, which helped advance my perspectives and research in new directions. I am grateful for their invaluable time and assistance they proffered whenever needed.

I am particularly thankful to all the current and former members of Vannucci Research Group; Dr. Mevan Dissanayake, Dr. Nicholas Delucia, Dr. Ryan Key, Dr. Victoria Bobo, James Sitter, Jake Tillou, Joseph Kuchta, Maizie Helton and Mollie Morrow. for their support and motivation. It's been an absolute pleasure to have been a member of Vannucci Research Group alongside these brilliant minds. I am no less grateful to Prof. Mark Losego and Prof. Kenneth Hanson for their contributions to my research work. I would also like to thank members of Linda Shimizu group, Shustova group, Peryshkov group and John Regalbuto group for graciously extending the resources needed for my research.

Finally, I am forever indebted to my parents, who have always been supportive of my career pursuit. I owe it all to them and cannot express how

fortunate I consider myself to be your daughter. Special thanks to my younger brother, Omkar, for all his love and for being my virtual connection to celebrations back home. I would like to thank my incredible fiancé, Sumedh, for patiently supporting me through every up and down of this journey. You mean the world to me. To my Aatya, for her unwavering belief in me and for all that she has done for me. I appreciate all the support and love showered on me by the rest of my family. Lastly but most importantly, I would like to thank all my dear friends here and back home for keeping me sane in this graduate school journey. Grateful to have y’all.

Forever to thee!

ABSTRACT

The current field of catalysis is notably advanced in terms of both conceptual and technical innovation. There is a constant need to design new catalysts and develop catalytic processes to improve the scope, efficiency, and selectivity of various chemical transformations. It is also imperative to design catalytic systems which are effective, truly-recyclable and energy efficient for a sustainable future. This can be done through comprehensive knowledge and understanding of catalyst behavior, reaction kinetics and process designing.

For most industrial processes, the preferred catalysts are heterogeneous because these solid catalysts can be easily separated from the final product. However, they often lack selectivity and produce waste due to unwanted side reactions. Traditional homogeneous molecular catalysts are highly selective but lack practical industrial utility due to challenges in catalyst separation, final product separation and catalyst degradation in aqueous medium and thus face manufacturing scale-up complexities. *To address these challenges and build an active, robust and highly selective catalytic system, designing a hybrid catalyst by immobilizing these molecular catalysts onto a solid support is a viable solution for sustainable catalysis. This could transform the practical utility of molecular catalysts, increase the reaction selectivity with simplified catalyst separation and product recovery,*

and prevent catalyst decomposition by impeding any bimolecular catalyst interactions. Thus, Chapter 2 details this study based on the well-studied Suzuki carbon– carbon cross-coupling reaction, to demonstrate the ability to achieve catalytic performance using a non-noble nickel-based molecular catalyst in high aqueous content solvents. Furthermore, this study demonstrates a new paradigm in the design of hybrid catalysts in which Atomic Layer Deposition (ALD) is used to improve the attachment and stability of molecular catalysts on solid metal oxide supports. This research has helped achieve a combination of ligand first surface attachment with molecular design and ALD application for new approaches in catalyst discovery. Encouraged by the results from this study, further study on synthesizing nickel bipyridine based hybrid catalysts anchored onto the silica oxide support via carboxylic acid and silatrane linking group was undertaken to analyze if covalent binding of the silatrane linker promotes stronger immobilization of the molecular catalyst onto the oxide support. Comparative analysis on synthesis and characterization of molecular and hybrid versions of carboxylic acid and silatrane linker is discussed in Chapter 3.

Another foremost area which has gained increased momentum is developing hydrocarbon-free, green energy technologies and exploring promising solutions for utilizing and producing sustainable energy to meet our current and future energy needs. In this regard, the aims for Chapter 4, are to study energy-efficient photocatalytic hydrogen production and investigate the catalytic pathway as part of the solution to the green energy transition. Natural photosynthesis uses an elaborate array of chemical structures to absorb multiple photons of light and

convert that energy into chemical bonds in a “Z-scheme” process. Extensive research has been performed in the field of artificial photosynthesis to mimic this natural Z-scheme. To date, however, an artificial Z-scheme composed only of molecular components has yet to be realized. *Here, we have developed a novel Z-scheme based molecular photocatalytic system by utilizing the light absorbing properties of aryl-alcohol photocatalysts for hydrogen production at significantly lower reaction overpotentials (≤40meV).* Chemical, electrochemical, and spectroscopic data studies supports a Z-scheme based pathway and provides mechanistic insights into hydrogen production via dual photoexcitation. This research can open new avenues for further study of molecular photocatalytic hydrogen production.

TABLE OF CONTENTS

LIST OF TABLES

LIST OF FIGURES

CHAPTER 1

INTRODUCTION

1.1 Catalysis for sustainable synthesis

Transition metal-based catalysis has become an indispensable tool and is at the core of chemistry in developing viable strategies for an array of chemical transformations in pharmaceutical and fine chemical industry. However, many catalytic processes operate using decades old practices which rely on non-sustainable expensive metals, generate tons of waste, and lead to significant energy wastage. The challenge of moving towards an economical and greener society, inevitably requires developing high performing sustainable alternatives to the pre-existing, environmentally hazardous processes. Driven by both public demand and government regulations, pharmaceutical and fine chemical manufacturers are increasingly seeking to replace stoichiometric reagents used in synthetic transformations with sustainable catalytic routes to develop greener, safer, and more cost-effective chemical processes. Moreover, the ACS Green Chemistry Institute® Pharmaceutical Roundtable (GCIPR) established in 2005 encourages the integration of green chemistry and green engineering into the pharmaceutical industry. While considerable progress has been attained in developing alternative green routes, from an ecological and economic standpoint, there are still opportunities for further enhancements in the design of these chemical transformations. Thus, to engineer a sustainable world through catalysis it is imperative to design alternative catalytic routes with improved reactivity and recovery efficiency, while utilizing cost effective abundant metals, wherever possible.

With the goal of achieving sustainable catalysis, one area of my dissertation research focuses on developing a sustainable, earth abundant metal-based hybrid molecular catalyst for Suzuki cross-coupling in green chemical solvents. In this regard, utilizing nickel catalysts for cross-coupling reactions, not only minimizes the waste footprint of the process but also offers cost-effective synthetic routes. Due to the ever-increasing demand and continuous efforts towards developing sustainable catalysts, significant progress in nickel based cross-coupling catalysis has been achieved. However, performing transition metal catalysis in aqueous media, particularly nickel-based catalysis is often challenging due to the instability and insolubility of nickel complexes in water, therefore, limiting their practical utility. This study, thus, sets an example for extending the current literature on Suzuki cross-coupling reactions by utilizing a ligand-first binding approach to support molecular [(2,2′:6′,2″-terpyridine-4′-benzoic acid)Ni(II)]Cl_2 catalyst onto metal oxide support via atomic layer deposition for organic cross-coupling reactions in green aqueous medium. Encouraged by the successful results and applicability of this report, study on syntheses and analysis of two bidentate nickel complexes with different molecular precursors for surface-anchoring to metal oxide support groups was undertaken. Silatrane anchoring groups form strong covalent siloxane surface bonds to metal oxide supports and are known to be water stable. These properties of silatranes can be utilized for increasing the surface stability of inorganic complexes onto metal oxide support. Thus, synthesis and preliminary characterization data of [(2,2’-bipyridine-4,4’-dicarboxylic acid)Ni(II)]Cl_2 and [(2,2’-bipyridine-4,4’-diamidopropylsilatrane)Ni(II)]Cl_2 molecular hybrid catalyst for comparative analysis of molecular and hybrid versions of carboxylic acid and silatrane anchoring groups have been discussed.

Another area of interest for my dissertation research is designing environmentally benign and sustainable transformations by utilizing renewable energy sources for steering energy efficient solar fuel generation. Thus, with the objective to design and study a solar energy based efficient catalytic pathway, my research focuses on designing a sustainable molecular photocatalytic system for renewable solar fuel generation and interpreting thorough mechanistic understanding for the same. The ever-increasing energy demands as well as rising global warming by CO_2 emissions, and the existing nature of fossil fuels have led us to focus on developing technologies driven by enhanced efficiencies and sustainable resources for secure and clean, carbon-free fuel production. In this regard, 'photocatalysis' can be considered to be the holy grail for driving thermodynamically unfavorable reactions for light-driven hydrogen generation. Despite extensive study on the components and dynamics of these systems, current state-of-the-art photocatalytic systems designed for hydrogen production face challenges. Namely, they still operate at overpotentials, low turnovers and, at times, lack detailed probing of the underlying reaction pathways. Nature is remarkable at efficiently producing hydrogen via photosynthesis catalyzed by hydrogenase enzymes. Thus, inspired by nature, this study presents first successful implementation of a *molecular 'Z-scheme'* or artificial photosynthesis for photocatalytic hydrogen production at negative overpotential, termed as *'Underpotential'*. A detailed report on the fundamentals associated with system design and mechanistic analysis via various spectroscopic techniques corroborate that this approach establishes a promising new direction in the field of molecular photocatalytic hydrogen production.

1.2. Traditional Nickel-based molecular catalysts

The current field of catalysis is notably advanced in terms of both conceptual and technical innovation. Great successes and significance of transition metal-catalyzed coupling reactions were highlighted by the Nobel Prize in chemistry in 2010.[1] Over the last 50 years, transition metal catalyzed cross coupling reactions, have become one of the most efficient and direct strategies for organic transformations. With access to multiple oxidation states, bonding modes, and coordination environments, the novel chemical reactivity afforded to organotransition metal complexes has led to innovative solutions to long-standing synthetic challenges.[2] Furthermore, extensive variations and modifications of transition-metal catalyzed coupling reactions have enabled wide applications in organic and inorganic synthesis and are regarded as one of the most reliable, accurate, and important facets of synthetic chemistry.

Transition metal catalyzed, especially, palladium catalyzed cross-coupling reactions have been extensively studied, with applications ranging from complex natural product synthesis to drug discovery and manufacturing. While palladium catalysts are remarkable, there is a push towards development of cross-coupling catalysts based on first-row, earth abundant transition metals. In this regard, utilizing nickel metal for catalysis can be an advantageous, inexpensive alternative owing to its unique reactivity and chemical properties. Nickel complexes can adopt both high- and low-spin configurations and are stable in a variety of oxidation states ranging from Ni(0) to Ni(IV).[3-4] Additionally, being less electronegative in comparison to palladium, oxidative addition step is very facile during catalysis. An important difference of the nickel species in comparison to palladium is the easy involvement of one electron processes.[4] Thus, advancing nickel based cross-coupling catalysts is of particular interest, due to its diverse reactivity, versatile intrinsic properties, and cost efficiency. Studies have shown nickel to be an effective catalyst for a range of valuable and difficult organic transformations,[4] Kumada-Corriu,[5] Suzuki-Miyaura, Negishi,[6-7] Nickel catalyzed C-X cross-coupling of electrophiles,[8-10] Mizoroki-Heck reaction,[11-12] photoredox catalysis.[13-16] This versatility and ability of nickel in activating less reactive substrates can be attributed to easy accessibility and tunability of its oxidation states. Generally, Ni-catalyzed Suzuki cross-coupling includes three steps: oxidative addition (OA), transmetalation (TM), and reductive elimination (RE). As shown in Figure 1.1, the catalytic cycle can proceed similar to palladium based systems via Ni(0)/Ni(II) cycle, which proceeds by OA, followed by TM and RE.

Alternatively, a Ni(I)/Ni(III) cycle, which proceeds by TM first, followed by OA and RE is also possible. Although, Ni(0)/Ni(II) catalytic cycles are widespread, the easy accessibility of Ni(I) and Ni(III) oxidation states allows different modes of reactivity and thus, several transformations are based on Ni(I)/Ni(III), Ni(0)/Ni(II)/Ni(I), or even cycles in which nickel remains in the Ni(I) state for the entire catalytic cycle.[17-18]

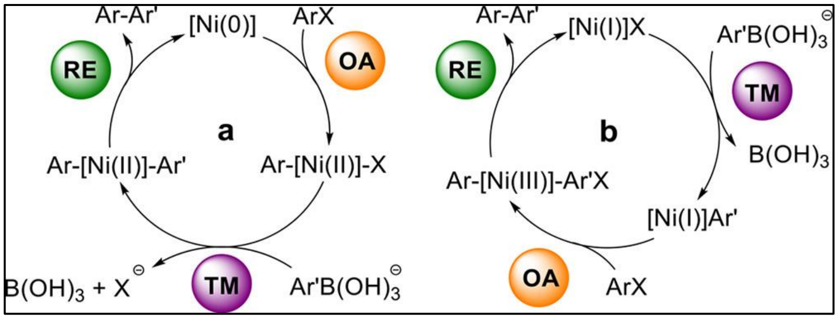

Figure 1.1: Proposed mechanistic pathways for Ni-catalyzed Suzuki Cross-coupling. Adapted with permission from reference[19]

However, an important study based on studying nickel catalysis by Payard and co-workers indicated the formation of inactive nickel dimers as a competing pathway during nickel catalyzed Suzuki cross coupling reaction.[19] Based on this finding, a revised catalytic cycle as shown in Figure 1.2 was proposed. As shown in Figure 1.2, this dimer complex formation prior to transmetalation step deactivates the catalyst, inhibits catalytic activity and is thus a critical shortcoming in traditional molecular nickel catalysts.

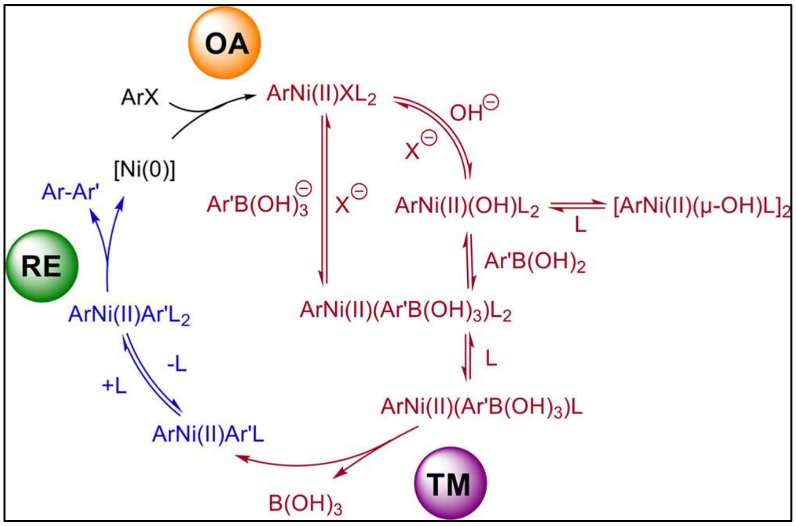

Figure 1.2: Revised catalytic cycle proposed by Payard and co-workers. Reprinted with permission from reference[19]

1.3 Challenges in molecular Nickel-based catalytic systems

Nickel catalysts demonstrate outstanding diversity of reactivity patterns. However, without a suitable ligand many Ni-mediated transformations are likely to fail because of easy catalyst deactivation, poor functional group tolerance or initiation of unwanted side reactions leading to byproducts and thus leading to lower selectivity.[17] Studies have also shown that Ni-mediated catalytic system is difficult to control or predict owing to nickel's high reactivity. Furthermore, compared to palladium catalysts, nickel catalysts exhibit a high degree of sensitivity to the choice of solvent and base during Suzuki cross-coupling.[20] As previously discussed, studies reported by Payard and co-workers, have shown the formation of inactive nickel dimers/multimers and catalyst deactivation during homogenous nickel-based catalysis.[19, 21] In addition to this, higher concentrations of nickel catalysts generally increases the rate of bimolecular decomposition pathways and can also lead to unwanted byproducts or metal poisoning of products.[4, 22] Another limitation of molecular catalysts is the difficulty in separation and post reaction analysis. It has been studied that the limited stability of some organometallic species toward oxygen, water, and temperature is often sustained upon immobilizing onto supports.[23] Immobilizing the molecular catalyst onto a surface stabilizes individual catalyst molecules on solid oxide supports through direct binding of transition metal complexes to the oxide supports. This prevents the immobilized molecular catalyst from undergoing bi- or multimolecular degradation and thus, results in more persistent reactive catalytic species. Thus, based on the discussion above, immobilizing a molecular nickel catalyst onto support is a viable approach to address these primary challenges.

1.4 Molecular/hybrid surface supported catalysts

Similar to the limitations of molecular catalysts, heterogeneous catalysts, preferred by industry, also are far from perfect, since, high temperatures lead to energetic over-consumption, low selectivity raises environmental concerns, and deactivation can render processes complex, unecological, and uneconomical.[24] Therefore, utilizing a molecular/hybrid catalytic system can facilitate ease of synthetic modification for heterogeneous applications and further help gain mechanistic insights into molecular catalytic pathways with a promise of higher reactivity under milder conditions. This also permits well-defined surface species to be prepared and fully characterized with techniques complementary to those of molecular homogeneous catalysts. In an attempt to utilize the positive aspects from both fields for developing active and recoverable catalysts, numerous catalytic transformations have been achieved via utilization of these hybrid surface organometallic chemistry (SOMC) catalysts on metal oxide supports.[23, 25-27] Figure 1.3 represents an example of a hybrid surface supported organometallic catalyst.

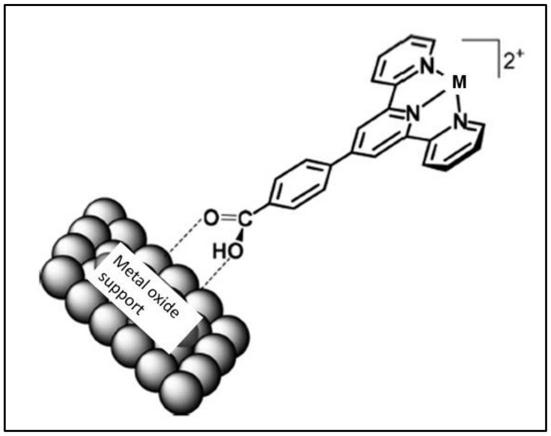

Figure 1.3: General representation of a molecular catalyst immobilized on metal oxide support.

Several articles on design and stability of molecular/hybrid catalysts have been reported.[26] DeLucia and co-workers reported a Palladium-terpyridine based molecular catalyst supported on silica surface for selective hydrodeoxygenation of biomass. The hybrid catalyst was found to be more active and recyclable than its analogous homogenous catalysts.[28] This molecular/heterogeneous hybrid catalyst presented the combined advantages of each system and helped access desired reactivity in solvents that were not suitable for a molecular homogeneous catalyst to work.[28] Kuehnel and co-workers reported a hybrid photocatalytic system of water tolerant Nickelbis(terpyridine) complexes anchored onto CdS to achieve visible-light driven reduction of aqueous CO_2.[29] The performance of this hybrid system was found to be crucially dependent on the interface between the nanoparticulate photosensitizer and the molecular catalyst, thus, demonstrating that catalyst immobilization is key to achieve selective CO_2 reduction in water. Another study reported a polymer-cross-linking ligand design for immobilizing bisphosphine ligands-based nickel catalyst. The catalyst exhibited remarkable reactivity towards C-N coupling with high selectivity and thermal stability. This study revealed that immobilization on polymer support, enabled challenging molecular transformations that were not possible through unsupported homogeneous ligands.[30] Key and co-workers also have shown that immobilization of a molecular nickel catalyst on solid support isolates individual nickel catalyst molecules and helps prevent bimolecular decomposition of the catalyst, which can occur in homogeneous solution.[20] Thus, developing a molecular/heterogeneous hybrid catalyst can fully exploit the strengths of traditional molecular and heterogeneous catalysis in order to yield suitable alternatives and help access previously unattainable reactivities and catalytic transformations.

1.5 Atomic Layer Deposition

The most important factor to consider when designing these hybrid catalysts is the stability of the ligand anchoring groups in aqueous solvents. It is well-known that a significant barrier to utilizing this ligand-first hybrid catalyst design approach arises from the limited stability of surface binding ligands. For example, studies have shown the surface-bound carboxylates to undergo hydrolysis in water.[26, 31-32] Another key stability issue for molecular catalysts heterogenized onto oxide supports is their gradual desorption from the surface during catalysis, thus, inhibiting catalytic activity and recyclability. Therefore, to address the abovementioned limitations in molecular nickel catalyzed cross-coupling, in Chapter 2 we have discussed a sustainable approach based on ligand-first binding to an oxide support for studying nickel catalyzed cross-coupling in aqueous solvents. We have developed a green catalytic system wherein a molecular nickel catalyst was immobilized onto a solid support via atomic layer deposition (ALD) to help increase catalyst stability and selectivity.

Atomic layer deposition (ALD) is a technique capable of systematic stabilizing of molecular catalysts on variety of surfaces. It is a self-limiting thin-film deposition technique in which reactive vapor phase precursors are sequentially exposed to a substrate surface.[33] Through controlled surface reactions and sequential precursor delivery, ALD permits exquisite control over layer thickness and conformality. Figure 1.4 shows the sequential deposition process in a typical ALD cycle. $Al(Me)_3$ is introduced in gas phase which reacts exclusively with oxygen atoms. Once oxygen atoms are all reacted, the $Al(Me)_3$ is purged and an oxidant such as water vapor is introduced. This reacts with the remaining Al-Me bonds to form a new oxide layer. The water is then purged, and the cycle can be repeated as many times as necessary to yield uniformly coated ALD surface.

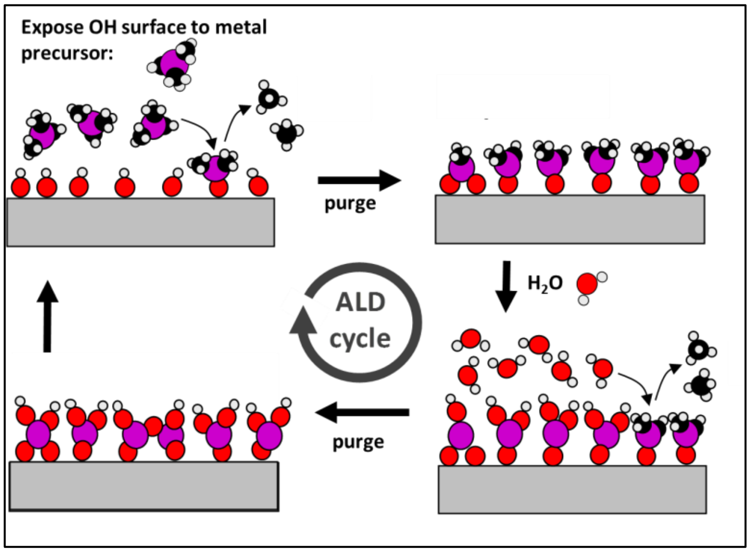

Figure 1.4: A typical representation of ALD cycle.

In recent years, ALD has proven effective for supported catalyst synthesis since it offers molecular-level control and relies on surface chemical bonds rather than electrostatic interactions. It is a highly effective method for suppressing nanoparticle agglomeration and can conceivably be used to stabilize single atoms. Also, it has demonstrated excellent ability to maximize the benefits of high surface area supports.[33] Furthermore, ALD has shown to address the typical inhomogeneity of heterogeneous catalysts and helped enhance the understanding of catalyst composition/ structure/function relationships.[34] It has been demonstrated to be an exceptionally powerful tool for catalysis research in the field of nanoparticle chemistry, metal organic frameworks, zeolites, photoelectrolysis and carbon nanotubes.[35-36] Reports based on new ALD catalysts show improved selectivity for specific catalytic reactions and to be more stable, even in the high temperature ranges. ALD primarily prevents any ligand or complex leaching from the surface, thus leading to longer catalytic activity. Additionally, ALD coating improved selectivity in reactions where undercoordinated active sites catalyzed unfavorable side reactions, as was shown for Pd and Ni catalysts on which side reactions were reduced after the introduction of ALD coating.[33, 37]

Metal oxides are common catalysts in photoelectrolysis and photocatalytic water splitting because they can reduce or eliminate the required bias, and ALD catalysts have made important contributions in the improvement of these catalysts.[33] For example, Vannucci and co-workers earlier reported on the utilization of TiO_2 ALD layers to stabilize surface binding of the chromophore $[Ru(bpy)_2(4,4'\text{-}(PO_3H_2)bpy)]^{2+}$ on TiO_2 surfaces and demonstrated enhanced performance toward water oxidation catalysis.[26] Figure 1.5 shows how ALD layers protect molecular catalyst stabilized on a metal oxide support, without altering the functionality of the molecular catalyst.

ALD techniques have shown remarkable promise; however, its application in cross-coupling reactions and advantages over traditional molecular catalysts still needs to be investigated. Based on abovementioned advantages of ALD coating, it can be considered to be a sustainable solution for increasing catalyst activity and

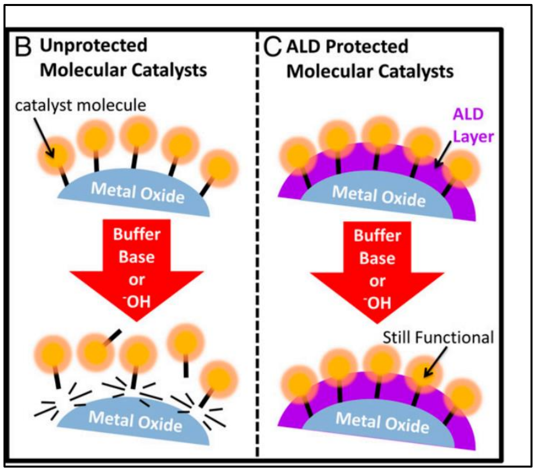

Figure 1.5: General representation of ALD coated catalyst. Reprinted from reference[26]

molecular/heterogeneous catalysis. *Thus, a proof-of-concept study on designing and immobilizing a molecular nickel catalyst onto oxide support via ALD and its application in Suzuki cross-coupling reaction will be discussed in Chapter 2, with consideration that this highly selective sustainable Suzuki transformation was achieved in green aqueous solvent with minimal nickel loading.*

1.6 Anchoring groups for immobilizing inorganic complexes onto oxide support

As previously discussed, modification of metal oxide surfaces by anchoring transition metal complexes onto the surface both helps understand interesting fundamental questions in interfacial science and leads to a variety of potential practical applications.[38-41] Homogeneous catalysis is very selective and generally operates at lower energy reaction conditions, however, time-consuming expensive separation process and catalyst loss during extraction is not always economically tolerable.[42] Immobilization onto a solid support not only offers the benefits of easier separation, but further increases the applicability and effectiveness of molecular catalysts irrespective of the catalyst concentration and solubility. Thus, designing molecular/hybrid catalysts by immobilizing them onto a surface is imperative for producing catalysts that are both selective and robust. This strategy promotes a commercially applicable catalytic system. This merger can further both the catalysis fields as new synthetic routes and novel applications can be established to meet the expected requirements for sustainable applications.

Recent developments to increase the stability of covalently bound dyes and catalysts onto metal oxide surfaces involve using atomic layer deposition (ALD) of metal oxides as a protecting layer.[43-44] Another approach to increase surface stability of molecular complexes is to utilize water-stable surface anchoring groups linked to the molecules for strong surface attachment. An important parameter to consider when designing these molecular/hybrid catalysts is the nature of the binding between the metal complex and the oxide support since it directly corelates to the long-term stability and activity of the catalytic system. Surface attachment of the anchoring groups on the metal complex to the oxide support commonly involves electrostatic interactions, hydrophobic effects, or covalent bonding, the latter tending to have the advantage of greater stability.[39] The judicious choice of an anchoring group can provide custom-tailored performance parameters for catalyst stability and overall conversion efficiency.

Carboxylic acids have been the most widely utilized functional groups for anchoring complexes to metal oxide supports in dye sensitized solar cells.[45-46] However, the bonds formed during the adsorption process are not stable in all solvents. Also, carboxylic acids are prone to dissociate from the metal oxide surface under conditions such as including exposure to aqueous and alkaline solutions.[26, 38, 47] Furthermore, some studies have shown carboxylate linkages can leach from the metal oxide surfaces in certain mixtures of organic solvents.[48] Such instability decreases the range of compatible solvents that can be used.

Alternatively, the enhanced surface functionalization properties of silatranes, coupled with the great stability of the silyl ether covalent bonding to the oxide support, suggests that silatranes could be superior to other surface attachment methods for functional linkages in variety of applications. Preparation of the silatrane precursor requires additional synthetic steps compared to the often-used carboxylate derivative. Since linkage to the metal oxide by the silatrane involves much stronger covalent attachment via silyl ether bonds, it allows for a wider range of solvent and pH conditions than carboxylate and phosphonate linkages. Moreover, as surface-anchoring functional groups consist of metal chelating ligands, ligand stability during formation of an inorganic complex is crucial. In this regard, silatrane can be considered to be stable and protected from side-reactions due to its caged structure and thus should stay intact during the chemical reaction.[43]

Different types of linkages will tend to exhibit different reactivity based on their stability and binding strength to the oxide support. *Thus, to study the interfacial chemistry of different anchoring groups, Chapter 3, will be discussing synthesis, immobilization and characterization of two nickel bipyridine complexes* [(2,2’-bipyridine-4,4’-dicarboxylic acid)Ni(II)]Cl_2 and [(2,2’-bipyridine-4,4’-diamidopropylsilatrane)Ni(II)]Cl_2 *onto metal oxide support via carboxylic acids and* *silatrane surface binding groups*. Direct comparison of these anchoring groups in nickel catalyzed cross-coupling reaction will help understand if catalytic activity and robustness can be fostered by the additional strength of covalent linkages in silatrane anchoring group.

1.7 Hydrogen: Applications and Limitations

A great technological challenge facing our global future is the development of a secure, clean, and renewable energy source.[49] Hydrogen is a clean, limitless energy source with potential applications in sustainable energy storage and ammonia production. Despite the illusion of simplicity in the nature of hydrogen bonds, the kinetic barrier for making hydrogen without a catalyst is very high, and therefore many creative approaches to lower the energy barrier for hydrogen evolution have been explored.[50] Currently, about 96% of the worldwide industrial production of hydrogen is achieved by steam reforming of natural gas, oil, or coal. These current industrial hydrogen production technologies consume fossil resource, require high temperature and high pressure and generate a greenhouse gas (i.e. CO_2), making them unsustainable and incompatible for a large scale production.[51-52] Thus, alternative solutions need to be developed. Although the catalytic performances of platinum group metals for hydrogen production are unrivaled, the limited supply of noble-metal would not sustain a low-cost and wide-scale production of technological devices.[53]

1.8 Electrocatalytic systems for production hydrogen production

Nature has shown us that hydrogenase enzymes are remarkably efficient catalysts for molecular hydrogen production.[54-55] In this regard, remarkable progress has been made by developing hydrogenase enzymes based on inexpensive, earth abundant metals such as nickel,[56-58] iron,[55, 59-61] cobalt[62-63] or molybdenum[64] as electrocatalysts for the production of molecular hydrogen.[55] Particularly, the Fe-only hydrogenase containing an Fe_2S_2 core as their active sites, shown in Figure 1.6[50, 54, 60] are well-suited for reductive hydrogen generation.

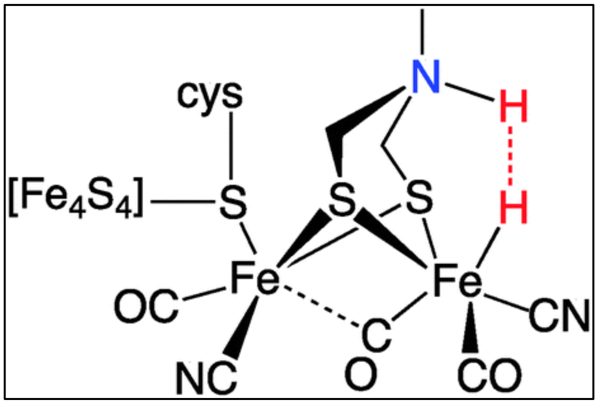

Figure 1.6: Fe_2S_2 hydrogenase showing formation of H-H bond. Reprinted from reference[50]

To realize non-platinum based effective electrocatalysts, understanding the fundamental trends in catalytic activity during electrocatalytic hydrogen production is essential for designing sustainable catalytic routes. The “best” electrocatalysts are the ones that produce a large increase in the catalytic current and work at potentials closer to thermodynamic potentials for acid reduction, i.e. they work at lower overpotentials.[65] A variety of complexes based on Fe_2S_2 core have been well studied.[54-55, 59] Felton and coworkers reported a diiron cyclopentadienyl carbonyl complex Fp_2 as a procatalyst for the reduction of weak acids in acetonitrile.[66] The understanding of reactivity provided from these studies led to new insights into designing catalysis for hydrogen generation, however, the fundamental challenge of energy efficient catalysis at minimum overpotential for acid reduction still needs to be surmounted.

1.9 Molecular photocatalytic systems for hydrogen production

Advancing molecular systems that based on renewable solar energy can be an alternative route to combat the energy wastage from catalytic overpotential. A molecular catalytic system that efficiently exploits excited-state electron transfers for the proton reduction step could help minimize reaction overpotentials and would represent a breakthrough in hydrogen production.[67] Noteworthy advances in the design, synthesis and study of molecular catalytic systems for photocatalytic or photo-electrocatalytic hydrogen production have been reported.[51, 68-71] Figure 1.7 represents a typical multi-component molecular photocatalytic system for hydrogen production consisting of a photocatalyst/photosensitizer (PS), an acid reducing catalyst and a sacrificial electron donor (SED). The general mechanism for the photocatalytic cycle is initiated by the absorption of a photon by the photosensitizer/photocatalyst, yielding PS* excited state. From here, an electron transfer may take place by either an oxidative or reductive quenching process between the sacrificial electron donor and excited PS*. This results in formation of either an oxidized PS^+ or reduced PS^-, which subsequently then reduces the acid reducing catalyst to its active state for molecular hydrogen formation. The light-driven electron transfer process in such multi-component systems is generally governed by the photophysical and redox properties of PS (e.g., large absorption bands in the visible, long lifetimes of the excited state, etc.) and by the redox properties of the catalyst and the sacrificial electron donor.

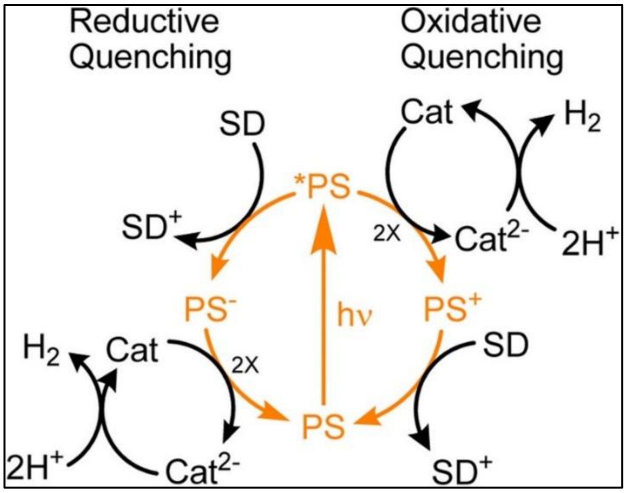

Figure 1.7: A general representation of photocatalytic pathway in a multi-component system. Reprinted from reference[51]

Encouraging results have been obtained by employing a combination of photocatalysts with transition metal based[72-74] acid reducing catalysts. Figure 1.8 shows a photocatalytic system consisting of Fluorescein as the photocatalyst, nickel-pyridinethiolate complex as the acid reducing catalyst for hydrogen production in presence of triethylamine as the sacrificial electron donor, reported by Eisenberg and group.

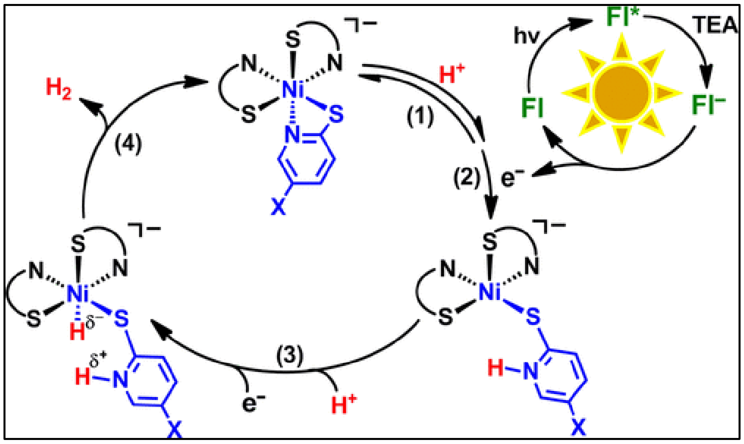

Figure 1.8: Multicomponent photocatalytic system for molecular hydrogen production. Reprinted from reference[75]

The initial photochemical step is reductive quenching in which the Fl* excited state is reduced to Fl^- by reaction with TEA. This generates a very high energy reductant which can cause unwanted side reactions. Furthermore, it is important to note that the pyridinethiolate ligand used for catalysis plays a dual role in stabilizing the reduced Ni center and providing a means for transferring protons from solution to the suggested hydride intermediate, which adds further strain on the catalyst itself. Besides, the acid reducing nickel thiolate catalyst still works at an overpotential (~0.5V) to reduce acetic acid.[75]

The photocatalytic studies described above imply that optimization of the experimental conditions and the catalytic system for developing an energy efficient pathway is not a trivial process. Indeed, its efficiency strongly relies on a broad range of parameters that cannot be independently optimized. Despite extensive experimental investigations and mechanistic studies of these systems, several systems suffer from low activity, catalyst degradation or overpotential. Some photocatalytic systems suffer from an important limitation wherein hydrogen generation is driven by a sacrificial donor.[49, 76] This can lead to incorrect claims and undermines advances in the field. Thus, in order to make significant progress in the solar production of H_2 on a globally significant scale, new systems and design strategies must be pursued that allow H_2 to be photogenerated at low electrochemical overpotential.[49]

1.10 Z-scheme based systems for hydrogen production

Along with the advancements in molecular photocatalytic systems for hydrogen production, significant efforts have been devoted towards the development of Z-scheme based efficient artificial photosynthetic systems, which utilize solar energy for solar fuel production.[77-78] In this context, natural photosynthesis is a great source of inspiration for developing energy efficient hydrogen producing systems. Incited by natural photosynthesis, an artificial Z-scheme as shown in Figure 1.9 was proposed by Sayama and co-workers.[77] In such a system, artificial photosynthesis is achieved by coupling two narrow band gap semiconductors/photocatalysts, namely, an oxygen evolution photocatalyst (OEP) and hydrogen evolution photocatalyst (HEP).

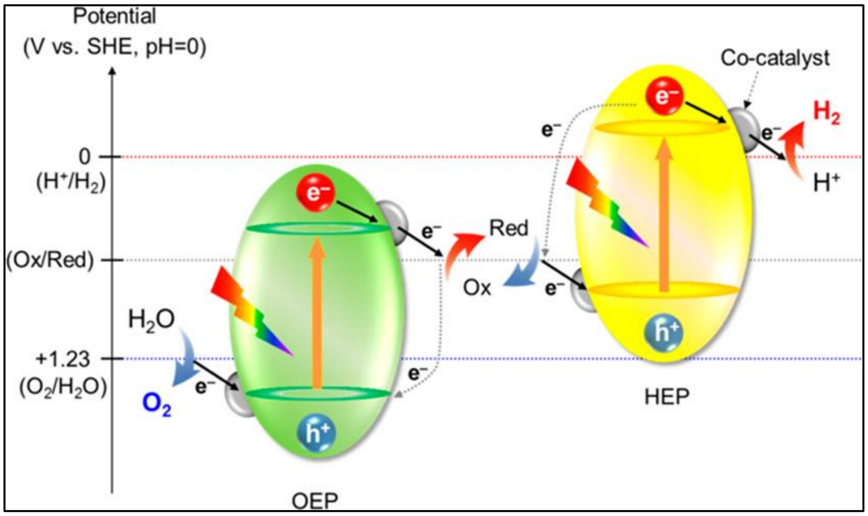

Figure 1.9: Artificial Z-scheme based hydrogen production. Reprinted from reference[77]

The reaction is initiated by absorption of photons by OEP, resulting in excitation of electrons to conduction band with formation of holes in valence band of OEP. This results in oxidation of water. Conversely, the excited electrons in conduction band of HEP reduce protons to hydrogen. The electrons are then transferred between two photocatalysts by the appropriate shuttle redox couple in solution continuously.[77] The last decade has seen tremendous achievements and sustained efforts in the development of photoelectrocatalytic Z-schemes, however, there are issues which should be carefully considered for the future optimizations in these heterogeneous Z-scheme systems. More importantly, the photocatalytic efficiency of previously reported Z-scheme hydrogen evolving systems is still low.[79] Also, the charge transfer mechanisms in these Z-scheme based systems have been less investigated, thus, limiting the progress of developing these systems for solar fuel synthesis.[77] Moreover, different electronic configurations, defects, and lattice mismatches at the interface lower the charge carrier transport.[80] Thus, although promising approaches have been reported, efforts towards developing systems that exhibit high light utilization efficiency, low resistance to charge carrier transfer and high chemical and physical stability with minimal photodegradation over time need to be undertaken. Even in the most efficient photocatalytic system, overpotentials > 0.1V are still observed.

In particular, to date, no molecular or artificial photosynthetic system has been reported that is capable of H_2 evolution at an electrochemical underpotential.[67] In order to address this limitation of overpotential, gain maximum catalytic activity and reduce energy wastage in hydrogen production, it is necessary to understand and consider the inherent thermodynamic aspects involved in proton reduction.

1.11 Thermodynamic parameters involved in reduction of weak acids

Various reports have studied catalytic hydrogen production via reduction of organic acids which act as proton sources for hydrogen formation. In order to construct energy efficient routes with maximum catalytic activity it is important to study the relation between pK_a of these acids and their reduction potentials. Evans and co-workers[81] reported a method to calculate the thermodynamic standard reduction potential for reduction of acid and its correlation with pK_a of the acid in a non-aqueous solvent as shown in equation 1.1:

$$E_{HA}^{o} = E_{H+}^{o} - \frac{2.303RT}{F}\mathrm{p}K_{a,HA} \quad (1.1)$$

where $E°_{HA}$ is the reduction potential of the weak acid in its ground-state, $E°_{H^+}$ is the thermodynamic potential required to reduce a proton in a given solvent, R and F are the gas and Faraday's constants respectively, and T is the temperature. It is thermodynamically impossible for reduction of acid to occur at a potential of lower magnitude than the standard potential, and the most effective catalysts will operate at potentials as close as possible to the standard potential. The thermodynamic minimum for the reduction of weak acids in acetonitrile solution is between -0.3 to -1.5 eV versus the saturated calomel electrode (SCE). However, as aforementioned, most of the catalytic systems designed to reduce these weak acids operate at more negative potentials beyond this thermodynamic reduction potential, termed as overpotential. Furthermore, experimental results consistently show that an additional overpotential energy between 0.1 and 1.0 eV is necessary even for platinum catalysts. [59, 81-82]

1.12 Introduction to Photoacids.

The catalytic systems based on reduction of weak organic acids, in general, operate at high energy, and in turn are less catalytically active. An attractive alternative to employing traditionally weak organic acids for hydrogen production, can be utilizing excited state proton transfer properties of light absorbing acids, termed photoacids. A photoacid is a molecule whose pK_a in an electronically excited state is much lower than in the ground state. Following electronic excitation, the charge distribution of the photoacid is dramatically altered, which, in turn, reduces the pK_a of the molecule.[83] Thus, in its excited state it is a much better acid and can be easily reduced at more positive potentials compared to its ground state. For example, pK_a of 7-bromo-2-naphthol in the ground state in acetonitrile solution is 26.1, while the singlet and triplet excited states have pK_a values of approximately 13.7 and 14.6 (estimated from a Forster cycle), respectively, suggesting that the photoacid, 7-bromo-2-naphthol is a better acid in its excited state compared to its ground state.[63, 84] Although these pK_a jumps often are constricted to the nanosecond lifetimes of singlet excited states, substitution with bromine facilitates intersystem crossing to generate high yields of long-lived triplet excited states, enabling bimolecular proton transfer reactions.[63] These light absorbing acids have been well studied in the literature,[83, 85] however, hydrogen production by utilizing the excited state electron transfers of these photoacids has not been yet studied.

1.13 Molecular Z-scheme for hydrogen production

As stated previously, although significant advances in the field of Z-scheme based artificial photosynthesis and multi-component molecular photocatalytic systems for hydrogen production have been achieved, a molecular Z-scheme based system that works at '*Underpotential'* by exploiting the photophysical properties of both the photocatalyst and photoacid has not been yet accomplished. Furthermore, utilizing the dual photon absorption-based pathway eliminates the need of a secondary acid-reducing catalyst and therefore promotes energy efficiency and limits additional energy wastage. *Thus, in Chapter 4 we have shown for the first time a novel molecular Z-scheme based photocatalytic route for hydrogen production by using light absorbing aryl alcohols at remarkably low reaction overpotentials.* We believe that the in-depth mechanistic understanding of this molecular photocatalysis via dual photon absorption Z-scheme based pathway will greatly stimulate the applications of photocatalysis in solar fuel production.

1.14 References

1. Sun, C.-L.; Shi, Z.-J., Transition-Metal-Free Coupling Reactions. *Chem Rev* **2014**, *114* (18), 9219-9280.

2. Trowbridge, A.; Walton, S. M.; Gaunt, M. J., New Strategies for the Transition-Metal Catalyzed Synthesis of Aliphatic Amines. *Chem Rev* **2020**, *120* (5), 2613-2692.

3. Diccianni, J.; Lin, Q.; Diao, T., Mechanisms of Nickel-Catalyzed Coupling Reactions and Applications in Alkene Functionalization. *Accounts of Chemical Research* **2020**, *53* (4), 906-919.

4. Ananikov, V. P., Nickel: The “Spirited Horse” of Transition Metal Catalysis. *ACS Catalysis* **2015**, *5* (3), 1964-1971.

5. Tamao, K.; Kodama, S.; Nakajima, I.; Kumada, M.; Minato, A.; Suzuki, K., Nickel-phosphine complex-catalyzed Grignard coupling—II: Grignard coupling of heterocyclic compounds. *Tetrahedron* **1982**, *38* (22), 3347-3354.

6. Smith, S. W.; Fu, G. C., Nickel-catalyzed Negishi cross-couplings of secondary nucleophiles with secondary propargylic electrophiles at room temperature. *Angew Chem Int Ed Engl* **2008**, *47* (48), 9334-9336.

7. Zhou, J.; Fu, G. C., Cross-Couplings of Unactivated Secondary Alkyl Halides: Room-Temperature Nickel-Catalyzed Negishi Reactions of Alkyl Bromides and Iodides. *J Am Chem Soc* **2003**, *125* (48), 14726-14727.

8. Beletskaya, I. P.; Ananikov, V. P., Transition-Metal-Catalyzed C−S, C−Se, and C−Te Bond Formation via Cross-Coupling and Atom-Economic Addition Reactions. *Chem Rev* **2011**, *111* (3), 1596-1636.

9. Phan, N. T. S.; Van Der Sluys, M.; Jones, C. W., On the Nature of the Active Species in Palladium Catalyzed Mizoroki–Heck and Suzuki–Miyaura Couplings – Homogeneous or Heterogeneous Catalysis, A Critical Review. *Advanced Synthesis & Catalysis* **2006**, *348* (6), 609-679.

10. Frisch, A. C.; Beller, M., Catalysts for Cross-Coupling Reactions with Non-activated Alkyl Halides. *Angewandte Chemie International Edition* **2005**, *44* (5), 674-688.

11. Kwiatkowski, M. R.; Alexanian, E. J., Nickel-Catalyzed Mizoroki–Heck-Type Reactions of Unactivated Alkyl Bromides. *Angewandte Chemie International Edition* **2018**, *57* (51), 16857-16860.

12. Gøgsig, T. M.; Kleimark, J.; Nilsson Lill, S. O.; Korsager, S.; Lindhardt, A. T.; Norrby, P.-O.; Skrydstrup, T., Mild and Efficient Nickel-Catalyzed Heck Reactions with Electron-Rich Olefins. *J Am Chem Soc* **2012**, *134* (1), 443-452.

13. Twilton, J.; Le, C.; Zhang, P.; Shaw, M. H.; Evans, R. W.; MacMillan, D. W. C., The merger of transition metal and photocatalysis. *Nature Reviews Chemistry* **2017**, *1* (7), 0052.

14. Tellis John, C.; Primer David, N.; Molander Gary, A., Single-electron transmetalation in organoboron cross-coupling by photoredox/nickel dual catalysis. *Science* **2014**, *345* (6195), 433-436.

15. Zhu, C.; Yue, H.; Chu, L.; Rueping, M., Recent advances in photoredox and nickel dual-catalyzed cascade reactions: pushing the boundaries of complexity. *Chemical Science* **2020**, *11* (16), 4051-4064.

16. Thoi, V. S.; Kornienko, N.; Margarit, C. G.; Yang, P.; Chang, C. J., Visible-Light Photoredox Catalysis: Selective Reduction of Carbon Dioxide to Carbon Monoxide by a Nickel N-Heterocyclic Carbene–Isoquinoline Complex. *J Am Chem Soc* **2013**, *135* (38), 14413-14424.

17. Tasker, S. Z.; Standley, E. A.; Jamison, T. F., Recent advances in homogeneous nickel catalysis. *Nature* **2014**, *509* (7500), 299-309.

18. Cornella, J.; Gómez-Bengoa, E.; Martin, R., Combined Experimental and Theoretical Study on the Reductive Cleavage of Inert C–O Bonds with Silanes: Ruling out a Classical Ni(0)/Ni(II) Catalytic Couple and Evidence for Ni(I) Intermediates. *J Am Chem Soc* **2013**, *135* (5), 1997-2009.

19. Payard, P.-A.; Perego, L. A.; Ciofini, I.; Grimaud, L., Taming Nickel-Catalyzed Suzuki-Miyaura Coupling: A Mechanistic Focus on Boron-to-Nickel Transmetalation. *ACS Catalysis* **2018**, *8*, 4812-4823.

20. Key, R. J.; Tengco, J. M. M.; Smith, M. D.; Vannucci, A. K., A Molecular/Heterogeneous Nickel Catalyst for Suzuki–Miyaura Coupling. *Organometallics* **2019**, *38* (9), 2007-2014.

21. Rull, S. G.; Funes-Ardoiz, I.; Maya, C.; Maseras, F.; Fructos, M. R.; Belderrain, T. R.; Nicasio, M. C., Elucidating the Mechanism of Aryl Aminations Mediated by NHC-Supported Nickel Complexes: Evidence for a Nonradical Ni(0)/Ni(II) Pathway. *ACS Catalysis* **2018**, *8* (5), 3733-3742.

22. Jo, J.; Tu, Q.; Xiang, R.; Li, G.; Zou, L.; Maloney, K. M.; Ren, H.; Newman, J. A.; Gong, X.; Bu, X., Metal Speciation in Pharmaceutical Process Development:

Case Studies and Process/Analytical Challenges for a Palladium-Catalyzed Cross-Coupling Reaction. *Organometallics* **2019**, *38* (1), 185-193.

23. Witzke, R. J.; Chapovetsky, A.; Conley, M. P.; Kaphan, D. M.; Delferro, M., Nontraditional Catalyst Supports in Surface Organometallic Chemistry. *ACS Catalysis* **2020**, *10* (20), 11822-11840.

24. Samantaray, M. K.; Pump, E.; Bendjeriou-Sedjerari, A.; D'Elia, V.; Pelletier, J. D. A.; Guidotti, M.; Psaro, R.; Basset, J.-M., Surface organometallic chemistry in heterogeneous catalysis. *Chemical Society Reviews* **2018**, *47* (22), 8403-8437.

25. Pelletier, J. D. A.; Basset, J.-M., Catalysis by Design: Well-Defined Single-Site Heterogeneous Catalysts. *Acc. Chem. Res.* **2016**, *49* (4), 664-677.

26. Vannucci, A. K.; Alibabaei, L.; Losego, M. D.; Concepcion, J. J.; Kalanyan, B.; Parsons, G. N.; Meyer, T. J., Crossing the divide between homogeneous and heterogeneous catalysis in water oxidation. *Proceedings of the National Academy of Sciences* **2013**, *110* (52), 20918-20922.

27. Materna, K. L.; Crabtree, R. H.; Brudvig, G. W., Anchoring groups for photocatalytic water oxidation on metal oxide surfaces. *Chemical Society Reviews* **2017**, *46* (20), 6099-6110.

28. DeLucia, N. A.; Jystad, A.; Laan, K. V.; Tengco, J. M. M.; Caricato, M.; Vannucci, A. K., Silica Supported Molecular Palladium Catalyst for Selective Hydrodeoxygenation of Aromatic Compounds under Mild Conditions. *ACS Catalysis* **2019**, *9* (10), 9060-9071.

29. Kuehnel, M. F.; Orchard, K. L.; Dalle, K. E.; Reisner, E., Selective Photocatalytic CO2 Reduction in Water through Anchoring of a Molecular Ni Catalyst on CdS Nanocrystals. *J Am Chem Soc* **2017**, *139* (21), 7217-7223.

30. Iwai, T.; Harada, T.; Shimada, H.; Asano, K.; Sawamura, M., A Polystyrene-Cross-Linking Bisphosphine: Controlled Metal Monochelation and Ligand-Enabled First-Row Transition Metal Catalysis. *ACS Catalysis* **2017**, *7* (3), 1681-1692.

31. Brown, D. G.; Schauer, P. A.; Borau-Garcia, J.; Fancy, B. R.; Berlinguette, C. P., Stabilization of Ruthenium Sensitizers to TiO2 Surfaces through Cooperative Anchoring Groups. *Journal of the American Chemical Society* **2013**, *135* (5), 1692-1695.

32. Martini, L. A.; Moore, G. F.; Milot, R. L.; Cai, L. Z.; Sheehan, S. W.; Schmuttenmaer, C. A.; Brudvig, G. W.; Crabtree, R. H., Modular Assembly of High-Potential Zinc Porphyrin Photosensitizers Attached to TiO2 with a Series of Anchoring Groups. *The Journal of Physical Chemistry C* **2013**, *117* (28), 14526-14533.

33. O’Neill, B. J.; Jackson, D. H. K.; Lee, J.; Canlas, C.; Stair, P. C.; Marshall, C. L.; Elam, J. W.; Kuech, T. F.; Dumesic, J. A.; Huber, G. W., Catalyst Design with Atomic Layer Deposition. *ACS Catalysis* **2015**, *5* (3), 1804-1825.

34. Wegener, S. L.; Marks, T. J.; Stair, P. C., Design Strategies for the Molecular Level Synthesis of Supported Catalysts. *Accounts of Chemical Research* **2012**, *45* (2), 206-214.

35. Lauinger, S. M.; Piercy, B. D.; Li, W.; Yin, Q.; Collins-Wildman, D. L.; Glass, E. N.; Losego, M. D.; Wang, D.; Geletii, Y. V.; Hill, C. L., Stabilization of

Polyoxometalate Water Oxidation Catalysts on Hematite by Atomic Layer Deposition. *ACS Applied Materials & Interfaces* **2017**, *9* (40), 35048-35056.

36. Zhao, J.; Nunn, W. T.; Lemaire, P. C.; Lin, Y.; Dickey, M. D.; Oldham, C. J.; Walls, H. J.; Peterson, G. W.; Losego, M. D.; Parsons, G. N., Facile Conversion of Hydroxy Double Salts to Metal–Organic Frameworks Using Metal Oxide Particles and Atomic Layer Deposition Thin-Film Templates. *J Am Chem Soc* **2015**, *137* (43), 13756-13759.

37. Gould, T. D.; Izar, A.; Weimer, A. W.; Falconer, J. L.; Medlin, J. W., Stabilizing Ni Catalysts by Molecular Layer Deposition for Harsh, Dry Reforming Conditions. *ACS Catalysis* **2014**, *4* (8), 2714-2717.

38. Brennan, B. J.; Llansola Portolés, M. J.; Liddell, P. A.; Moore, T. A.; Moore, A. L.; Gust, D., Comparison of silatrane, phosphonic acid, and carboxylic acid functional groups for attachment of porphyrin sensitizers to TiO2 in photoelectrochemical cells. *Physical Chemistry Chemical Physics* **2013**, *15* (39), 16605-16614.

39. Troiano, J. L.; Crabtree, R. H.; Brudvig, G. W., Optimization of Surface Loading of the Silatrane Anchoring Group on TiO2. *ACS Applied Materials & Interfaces* **2022**.

40. Hagfeldt, A.; Boschloo, G.; Sun, L.; Kloo, L.; Pettersson, H., Dye-Sensitized Solar Cells. *Chemical Reviews* **2010**, *110* (11), 6595-6663.

41. Chen, Z.; Concepcion, J. J.; Hull, J. F.; Hoertz, P. G.; Meyer, T. J., Catalytic water oxidation on derivatized nanoITO. *Dalton Transactions* **2010**, *39* (30), 6950-6952.

42. Robinson, A. L., Homogeneous Catalysis (II): Anchored Metal Complexes. *Science* **1976**, *194* (4271), 1261-1263.

43. Materna, K. L.; Brennan, B. J.; Brudvig, G. W., Silatranes for binding inorganic complexes to metal oxide surfaces. *Dalton Transactions* **2015**, *44* (47), 20312-20315.

44. Hanson, K.; Losego, M. D.; Kalanyan, B.; Parsons, G. N.; Meyer, T. J., Stabilizing Small Molecules on Metal Oxide Surfaces Using Atomic Layer Deposition. *Nano Letters* **2013**, *13* (10), 4802-4809.

45. Polo, A. S.; Itokazu, M. K.; Murakami Iha, N. Y., Metal complex sensitizers in dye-sensitized solar cells. *Coordination Chemistry Reviews* **2004**, *248* (13), 1343-1361.

46. Zhang, L.; Cole, J. M., Anchoring Groups for Dye-Sensitized Solar Cells. *ACS Applied Materials & Interfaces* **2015**, *7* (6), 3427-3455.

47. Brewster, T. P.; Konezny, S. J.; Sheehan, S. W.; Martini, L. A.; Schmuttenmaer, C. A.; Batista, V. S.; Crabtree, R. H., Hydroxamate Anchors for Improved Photoconversion in Dye-Sensitized Solar Cells. *Inorganic Chemistry* **2013**, *52* (11), 6752-6764.

48. Brennan, B. J.; Keirstead, A. E.; Liddell, P. A.; Vail, S. A.; Moore, T. A.; Moore, A. L.; Gust, D., 1-(3′-amino)propylsilatrane derivatives as covalent surface linkers to nanoparticulate metal oxide films for use in photoelectrochemical cells. *Nanotechnology* **2009**, *20* (50), 505203.

49. Esswein, A. J.; Nocera, D. G., Hydrogen Production by Molecular Photocatalysis. *Chemical Reviews* **2007**, *107* (10), 4022-4047.

50. Bullock, R. M.; Appel, A. M.; Helm, M. L., Production of hydrogen by electrocatalysis: making the H-H bond by combining protons and hydrides. *Chem Commun (Camb)* **2014**, *50* (24), 3125-43.

51. Stoll, T.; Castillo, C. E.; Kayanuma, M.; Sandroni, M.; Daniel, C.; Odobel, F.; Fortage, J.; Collomb, M.-N., Photo-induced redox catalysis for proton reduction to hydrogen with homogeneous molecular systems using rhodium-based catalysts. *Coordination Chemistry Reviews* **2015**, *304-305*, 20-37.

52. Seo, B.; Joo, S. H., Recent advances in unveiling active sites in molybdenum sulfide-based electrocatalysts for the hydrogen evolution reaction. *Nano Converg* **2017**, *4* (1), 19.

53. Andreiadis, E. S.; Chavarot-Kerlidou, M.; Fontecave, M.; Artero, V., Artificial photosynthesis: from molecular catalysts for light-driven water splitting to photoelectrochemical cells. *Photochem Photobiol* **2011**, *87* (5), 946-64.

54. Tye, J. W.; Hall, M. B.; Darensbourg, M. Y., Better than platinum? Fuel cells energized by enzymes. *Proceedings of the National Academy of Sciences of the United States of America* **2005**, *102* (47), 16911.

55. Gloaguen, F.; Rauchfuss, T. B., Small molecule mimics of hydrogenases: hydrides and redox. *Chemical Society Reviews* **2009**, *38* (1), 100-108.

56. Tsay, C.; Yang, J. Y., Electrocatalytic Hydrogen Evolution under Acidic Aqueous Conditions and Mechanistic Studies of a Highly Stable Molecular Catalyst. *J Am Chem Soc* **2016**, *138* (43), 14174-14177.

57. Wiese, S.; Kilgore, U. J.; Ho, M.-H.; Raugei, S.; DuBois, D. L.; Bullock, R. M.; Helm, M. L., Hydrogen Production Using Nickel Electrocatalysts with Pendant

Amines: Ligand Effects on Rates and Overpotentials. *ACS Catalysis* **2013**, *3* (11), 2527-2535.

58. Vij, V.; Sultan, S.; Harzandi, A. M.; Meena, A.; Tiwari, J. N.; Lee, W.-G.; Yoon, T.; Kim, K. S., Nickel-Based Electrocatalysts for Energy-Related Applications: Oxygen Reduction, Oxygen Evolution, and Hydrogen Evolution Reactions. *ACS Catalysis* **2017**, *7* (10), 7196-7225.

59. Felton, G. A. N.; Mebi, C. A.; Petro, B. J.; Vannucci, A. K.; Evans, D. H.; Glass, R. S.; Lichtenberger, D. L., Review of electrochemical studies of complexes containing the Fe2S2 core characteristic of [FeFe]-hydrogenases including catalysis by these complexes of the reduction of acids to form dihydrogen. *Journal of Organometallic Chemistry* **2009**, *694* (17), 2681-2699.

60. Felton, G. A. N.; Vannucci, A. K.; Chen, J.; Lockett, L. T.; Okumura, N.; Petro, B. J.; Zakai, U. I.; Evans, D. H.; Glass, R. S.; Lichtenberger, D. L., Hydrogen Generation from Weak Acids: Electrochemical and Computational Studies of a Diiron Hydrogenase Mimic. *Journal of the American Chemical Society* **2007**, *129* (41), 12521-12530.

61. Liu, T.; DuBois, D. L.; Bullock, R. M., An iron complex with pendent amines as a molecular electrocatalyst for oxidation of hydrogen. *Nature Chemistry* **2013**, *5* (3), 228-233.

62. Baffert, C.; Artero, V.; Fontecave, M., Cobaloximes as Functional Models for Hydrogenases. 2. Proton Electroreduction Catalyzed by Difluoroborylbis(dimethylglyoximato)cobalt(II) Complexes in Organic Media. *Inorganic Chemistry* **2007**, *46* (5), 1817-1824.

63. Dempsey, J. L.; Winkler, J. R.; Gray, H. B., Mechanism of H2 Evolution from a Photogenerated Hydridocobaloxime. *Journal of the American Chemical Society* **2010**, *132* (47), 16774-16776.

64. Stewart, M. P.; Ho, M. H.; Wiese, S.; Lindstrom, M. L.; Thogerson, C. E.; Raugei, S.; Bullock, R. M.; Helm, M. L., High catalytic rates for hydrogen production using nickel electrocatalysts with seven-membered cyclic diphosphine ligands containing one pendant amine. *J Am Chem Soc* **2013**, *135* (16), 6033-46.

65. Felton, G. A. N.; Glass, R. S.; Lichtenberger, D. L.; Evans, D. H., Iron-Only Hydrogenase Mimics. Thermodynamic Aspects of the Use of Electrochemistry to Evaluate Catalytic Efficiency for Hydrogen Generation. *Inorganic Chemistry* **2007**, *46* (19), 8098-8098.

66. Felton, G. A. N.; Vannucci, A. K.; Okumura, N.; Lockett, L. T.; Evans, D. H.; Glass, R. S.; Lichtenberger, D. L., Hydrogen Generation from Weak Acids: Electrochemical and Computational Studies in the [(η5-C5H5)Fe(CO)2]2 System. *Organometallics* **2008**, *27* (18), 4671-4679.

67. Stratakes, B. M.; Miller, A. J. M., H2 Evolution at an Electrochemical “Underpotential” with an Iridium-Based Molecular Photoelectrocatalyst. *ACS Catal.* **2020**, *10* (16), 9006-9018.

68. Han, Z.; Eisenberg, R., Fuel from water: the photochemical generation of hydrogen from water. *Acc Chem Res* **2014**, *47* (8), 2537-44.

69. Lv, H.; Ruberu, T. P.; Fleischauer, V. E.; Brennessel, W. W.; Neidig, M. L.; Eisenberg, R., Catalytic Light-Driven Generation of Hydrogen from Water by Iron Dithiolene Complexes. *J Am Chem Soc* **2016**, *138* (36), 11654-63.

70. Ashford, D. L.; Gish, M. K.; Vannucci, A. K.; Brennaman, M. K.; Templeton, J. L.; Papanikolas, J. M.; Meyer, T. J., Molecular Chromophore–Catalyst Assemblies for Solar Fuel Applications. *Chemical Reviews* **2015**, *115* (23), 13006-13049.

71. Duan, L.; Bozoglian F Fau - Mandal, S.; Mandal S Fau - Stewart, B.; Stewart B Fau - Privalov, T.; Privalov T Fau - Llobet, A.; Llobet A Fau - Sun, L.; Sun, L., A molecular ruthenium catalyst with water-oxidation activity comparable to that of photosystem II. (1755-4349 (Electronic)).

72. Eckenhoff, W. T.; Brennessel, W. W.; Eisenberg, R., Light-driven hydrogen production from aqueous protons using molybdenum catalysts. *Inorg Chem* **2014**, *53* (18), 9860-9.

73. McNamara, W. R.; Han, Z.; Alperin, P. J.; Brennessel, W. W.; Holland, P. L.; Eisenberg, R., A cobalt-dithiolene complex for the photocatalytic and electrocatalytic reduction of protons. *J Am Chem Soc* **2011**, *133* (39), 15368-71.

74. Xue, L. X.; Meng, T. T.; Yang, W.; Wang, K. Z., Recent advances in ruthenium complex-based light-driven water oxidation catalysts. *J Photochem Photobiol B* **2015**, *152* (Pt A), 95-105.

75. Han, Z.; Shen, L.; Brennessel, W. W.; Holland, P. L.; Eisenberg, R., Nickel pyridinethiolate complexes as catalysts for the light-driven production of hydrogen from aqueous solutions in noble-metal-free systems. *J Am Chem Soc* **2013**, *135* (39), 14659-69.

76. Costantino, F.; Kamat, P. V., Do Sacrificial Donors Donate H2 in Photocatalysis? *ACS Energy Letters* **2022**, *7* (1), 242-246.

77. Wang, Y.; Suzuki, H.; Xie, J.; Tomita, O.; Martin, D. J.; Higashi, M.; Kong, D.; Abe, R.; Tang, J., Mimicking Natural Photosynthesis: Solar to Renewable H2 Fuel Synthesis by Z-Scheme Water Splitting Systems. *Chemical Reviews* **2018**, *118* (10), 5201-5241.

78. Yu, Z.; Li, F.; Sun, L., Recent advances in dye-sensitized photoelectrochemical cells for solar hydrogen production based on molecular components. *Energy & Environmental Science* **2015**, *8* (3), 760-775.

79. Guo, H.-L.; Du, H.; Jiang, Y.-F.; Jiang, N.; Shen, C.-C.; Zhou, X.; Liu, Y.-N.; Xu, A.-W., Artificial Photosynthetic Z-scheme Photocatalyst for Hydrogen Evolution with High Quantum Efficiency. *The Journal of Physical Chemistry C* **2017**, *121* (1), 107-114.

80. Li, X.; Garlisi, C.; Guan, Q.; Anwer, S.; Al-Ali, K.; Palmisano, G.; Zheng, L., A review of material aspects in developing direct Z-scheme photocatalysts. *Materials Today* **2021**, *47*, 75-107.

81. Zuo, Z.; Ahneman Derek, T.; Chu, L.; Terrett Jack, A.; Doyle Abigail, G.; MacMillan David, W. C., Merging photoredox with nickel catalysis: Coupling of α-carboxyl sp3-carbons with aryl halides. *Science* **2014**, *345* (6195), 437-440.

82. Appel, A.; Helm, M., Determining the Overpotential for a Molecular Electrocatalyst. *ACS Catalysis* **2014**, *4*, 630–633.

83. Spry, D. B.; Fayer, M. D., Observation of slow charge redistribution preceding excited-state proton transfer. *J Chem Phys* **2007**, *127* (20), 204501.

84. Grabowski, Z. R.; Rubaszewska, W., Generalised Förster cycle. Thermodynamic and extrathermodynamic relationships between proton transfer,

electron transfer and electronic excitation. *Journal of the Chemical Society, Faraday Transactions 1: Physical Chemistry in Condensed Phases* **1977**, *73* (0), 11-28.

85. Strada, A.; Fredditori, M.; Zanoni, G.; Protti, S., Acid Catalyzed Formation of C–C and C–S Bonds via Excited State Proton Transfer. *Molecules* **2019**, *24* (7).

CHAPTER 2

IMMOBILIZATION OF MOLECULAR CATALYSTS ON SOLID SUPPORTS VIA ATOMIC LAYER DEPOSITION FOR CHEMICAL SYNTHESIS IN SUSTAINABLE SOLVENTS.[1]

---

[1] Ayare, P. J.; Gregory, S. A.; Key, R. J.; Short, A. E.; Tillou, J. G.; Sitter, J. D.; Yom, T.; Goodlett, D. W.; Lee, D.-C.; Alamgir, F. M.; Losego, M. D.; Vannucci, A. K., Green Chemistry, 2021. Reprinted with permission from Royal Society of Chemistry.

2.1 Abstract

Homogeneous molecular catalysts are valued for their reaction specificity but face challenges in manufacturing scale-up due to complexities in final product separation, catalyst recovery, and instability in the presence of water. Immobilizing these molecular catalysts, by attachment to a solid support, could transform the practical utility of molecular catalysts, simplify catalyst separation and recovery, and prevent catalyst decomposition by impeding bimolecular catalyst interactions. Previous strategies to heterogenize molecular catalysts via ligand-first binding to supports have suffered from reduced catalytic activity and leaching (loss) of catalyst, especially in environmentally friendly solvents like water. Herein, we describe an approach in which molecular catalysts are first attached to a metal oxide support through acidic ligands and then “encapsulated” with a metal oxide layer via atomic layer deposition (ALD) to prevent molecular detachment from the surface. For this initial report, which is based upon the well-studied Suzuki carbon-carbon cross-coupling reaction, we demonstrate the ability to achieve catalytic performance using a non-noble metal molecular catalyst in high aqueous content solvents. The catalyst chosen exhibits limited catalytic reactivity under homogeneous conditions due to extremely short catalyst lifetimes, but when heterogenized and immobilized with an optimal ALD layer thickness product yield > 90% can be obtained in primarily aqueous solutions. Catalyst characterization before and after ALD application and catalytic reaction is achieved with infrared, electron paramagnetic resonance, and X-ray spectroscopies.

2.2 Introduction

Molecular transition metal catalysts in homogeneous solutions tend to exhibit high catalytic activity and reaction selectivity, but also exhibit poor stability and short lifetimes.[1] One major pathway to molecular catalyst deactivation is the formation of off-cycle intermediates via intermolecular catalyst interactions. While catalyst dimers or trimers are sometimes necessary for catalytic activity,[2] most catalyst “multi”-mers result in catalytic dead ends.[3-5] Multimer formation is often promoted by water in the reaction solution, as shown in Figure 2.1A,[3, 6-7] thus limiting the ability to utilize highly environmentally safe solvents. One common approach to minimizing intermolecular catalyst interactions is to perform catalytic reactions under very low catalyst loadings.[7-10] This approach has led to impressively high initial turnover frequencies (TOFs) but often times does not appreciably increase catalyst lifetimes.[7]

The immobilization of molecular catalysts onto solid supports is an approach designed towards preventing intermolecular catalyst interactions and extending molecular catalysts lifetimes.[11] The isolation of molecular catalysts on solid supports inhibits bimolecular catalyst interactions and thus takes advantage of the inherent catalyst activity. This approach of creating a molecular/heterogeneous catalyst has the added benefits of increased solvent compatibility, increased ease of catalyst separation from reaction mixtures, possible incorporation into flow reactors, and potential for catalyst recycling.[6, 12] This approach, however, can have its own set of drawbacks including increased cost of catalyst synthesis, possible decreases in catalyst selectivity, and difficulty in preventing catalyst leaching from the solid support.[13] The increased cost of both the materials and catalyst preparation can be overcome by achieving previously unattainable reactivity through extending catalyst lifetimes and recyclability.

Extensive research has been reported on immobilized catalysts in the field of surface organometallic chemistry (SOMC). This approach generates individual catalyst molecules on solid oxide supports through direct binding of transition metals to the oxide supports. This binding occurs after a thorough preparation of the oxide surface to create sites capable of strong binding to individual metal atoms.[14] The metal atoms that bind the oxide support can be introduced to the support through solution phase chemistry[15] or directly via ALD methods.[16] Many of these SOMC catalysts are composed of early transition metals due to their oxophilicity,[17] but recent reports have extended SOMC to the late transition metals.[18-21] An impressive array of catalytic transformations has been achieved with this class of SOMC catalyst.[22-23] Similar to polymer-supported[24-26] and MOF-supported[27-28] catalysts, SOMC catalysts utilize the support as a ligand for the catalysts, therefore, there is no direct analogous homogeneous catalysts for comparison. Iterative design of SOMC catalysts, hence, cannot directly benefit from homogeneous catalyst studies.

Ligand-first binding of molecular catalysts to a support is an alternative approach to catalyst immobilization on solid metal oxides that could benefit from previous understandings of homogeneous catalysis. The ligand-first class of molecular/heterogeneous catalysts on oxide supports is inspired by the design of dye sensitized solar cells,[29-32] and electrocatalysis.[33-35] In this approach catalytic activity and selectivity of homogeneous catalyst can often be translated to the molecular/heterogeneous system.[36-37] Furthermore, the lifetimes of homogeneous catalysts that rapidly deactivate in solution through bimolecular routes such as dimerization, may have their lifetimes greatly enhanced by isolation on a solid support as illustrated in Figure 2.1B. However, detachment of ligand-first molecules from metal oxide supports remains a problem.[13, 36-38] Detachment, or leaching, of the molecular catalysts into solution is typically promoted by water or highly polar organic solvents disrupting the ligand binding to the support. Metal oxide supports can even accelerate decomposition and nanoparticle formation of leached molecular catalysts.[13] Many strategies for increasing the binding strength between molecular catalysts and metal oxide surfaces have been explored.[35, 39] While these binding motifs have been successful to varying degrees, most still have limited stability under reaction conditions, especially in the presence of water.[40-41]

Herein, we describe a potentially universal method for reliably attaching and isolating molecular catalysts ligand-first to solid metal oxide supports for solution-based chemical catalysis. This paradigm uses atomic layer deposition (ALD) to physically encapsulate pre-bound molecular catalysts to solid metal oxides. ALD allows for precise control of oxide layer growth and has been used to isolate single-site heterogeneous catalysts.[42-43]

As shown in Figure 2.1C, this precise control allows for encasing the hybrid catalyst binding sites while leaving the catalyst active site exposed to solvent and

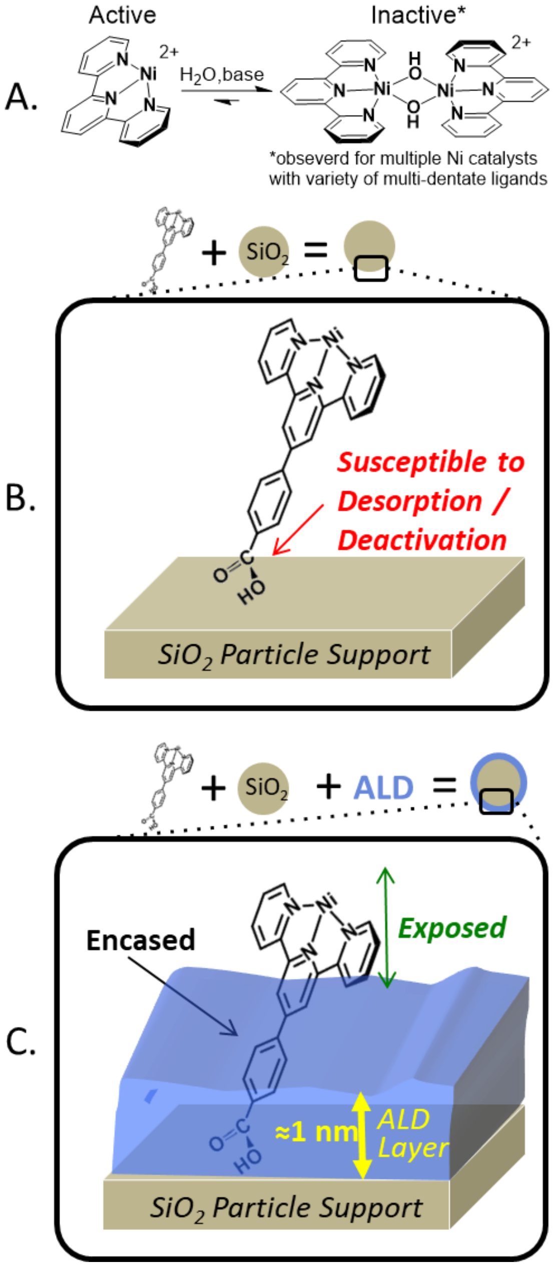

Figure 2.1: Comparison of previous work to current study. A. Example of molecular nickel catalyst deactivation in homogeneous solution. B. Depiction of molecular catalyst (**1**) loaded onto an SiO_2 support susceptible to desorption and subsequent deactivation. C. This work, stabilization of molecular catalyst **1** with an ALD encapsulation layer.

substrate. The ALD layer thus immobilizes and strongly adheres the molecular catalyst onto the solid oxide support. This immobilization generates a hybrid single molecule catalyst and allows for the use of green, polar solvents, such as water. It is worth noting, that cross-coupling reactivity with nickel catalysts in water has been achieved with the addition of micelles in the reaction solution.[44-45] In addition, this approach allows for the use of nickel-based catalysts for reactions that are typically performed by palladium.[46-47] Both the ACS Pharmaceutical Round Table and the Green Chemistry Institute have called for increased use of nickel catalysts in cross-coupling reactions,[48] however, nickel catalysts are not being widely employed in the fine chemical industry.[49] Controlled reactivity, catalyst stability, and batch-to-batch consistency of nickel catalysts is still lacking. Often nickel catalysts exhibit a high degree of sensitivity to the choice of solvent, base, moisture levels, and substrates employed during coupling reactions. The ALD immobilization of molecular nickel catalysts onto solid supports has been designed to overcome these shortcomings and create a general catalyst motif for use in fine chemical synthesis.

This approach builds upon prior work that used ALD to attach active molecular photosensitizers to nanostructured electrodes for photoelectrochemical devices.[12, 50-52] However, in those systems, device performance required careful design of ALD encapsulation layers that permitted proper electron transfer between molecule and oxide support. For chemical catalysis, this requirement is no longer necessary, simplifying the design. Moreover, as shown here, attachment of molecular catalysts to solid supports can lead to new reactivity not seen under homogeneous conditions. Most approaches to molecular catalyst immobilization involve developing, or taking from literature, successful homogeneous catalysts and attempting to adapt them for use as immobilized catalysts on heterogeneous supports. Poor homogeneous catalysts, however, are rarely considered for immobilization. Many poor homogeneous catalysts only suffer from very short catalyst lifetimes due to being susceptible to the catalyst deactivation pathways discussed above (e.g., dimerization). Deactivation through routes such as dimerization should be less likely, or even completely prevented when catalysts are immobilized. Herein, we show that immobilization via ALD of a poor homogeneous molecular catalyst significantly extends its lifetime as a hybrid heterogeneous catalyst for chemical synthesis. Thus, using ALD to create hybrid catalysts via immobilization of molecular catalysts without concern for their homogeneous reactivity opens a new approach and chemical space for catalyst discovery. As a demonstration, we report the design and synthesis of a hybrid nickel catalyst using ALD, characterize the synthesis steps with spectroscopic techniques, and show proof-of-concept Suzuki cross-coupling reactions to illustrate consistent catalytic activity in green solvents with high aqueous content.

2.3 Results and Discussion

We recently reported on the design and catalytic testing of a molecular/heterogeneous nickel catalyst.[6] The catalyst in Figure 2.1B was composed of a molecular terpyridine nickel catalyst bound to a solid SiO_2 support through a carboxylic acid linker. This molecular/heterogeneous catalyst exhibited prolonged catalyst lifetimes for Suzuki cross-coupling using dioxane as the solvent for the coupling partners, in addition the benefits of utilizing terpyridine ligands for nickel catalysts have also been explored.[53] The analogous homogeneous molecular catalyst quickly dimerized and became catalytically inactive. A series of control reactions and characterization of the molecular/heterogeneous catalyst pre- and post-reaction strongly supported the surface-bound catalyst being the active catalyst for cross-coupling reactivity. This molecular/heterogeneous catalyst, however, still required the toxic organic solvent dioxane to operate. Attempts to achieve cross-coupling reactivity in green solvents such as ethanol and water were unsuccessful. These failures were attributed to the protic, polar solvents disrupting catalyst binding to the SiO_2 support, resulting in desorption of the catalyst from the surface. Upon catalyst desorption, the molecular catalyst in solution quickly dimerized and deactivated. In this report, ALD is utilized (Figure 2.1C) to overcome the previously observed catalyst deactivation and perform catalytic chemical synthesis in solvents containing a high-volume ratio of water.

*Synthesis of **1|SiO_2|TiO_2***

The molecular catalyst [(2,2':6',2''-terpyridine-4'-benzoic acid)Ni(II)]Cl_2 (**1**) was synthesized following a previously reported procedure.[6] Loading of **1** onto Aerosil A300 SiO_2 support to form **1|SiO_2** (Figure 2.1B) followed a one-step method also previously reported.[6] Catalyst **1|SiO_2** was characterized before atomic layer deposition to examine how ALD may affect the structure or binding of **1** to the SiO_2 support. ICP-MS analysis indicates that **1|SiO_2** contains 0.4 weight% nickel pre-ALD treatment, which equates to roughly 2x10^{-7} mols of catalyst per m^2 of support surface area. In addition, elemental analysis from scanning transmission electron microscopy - energy dispersive spectroscopy (STEM-EDS) confirmed nickel was present on the SiO_2 particles. X-ray diffraction (XRD) analysis of **1|SiO_2** does not show any evidence for crystalline nickel particles, suggesting that the molecular nickel catalyst, not metallic nickel or nickel oxide particles, are present on the SiO_2 support pre-ALD treatment. Infrared attenuated total reflection (FTIR-ATR) spectroscopy was used to characterize the ligand binding to the support. Figure 2.2 shows the comparison of the FTIR of the molecular catalyst **1** to the FTIR-ATR of **1|SiO_2**

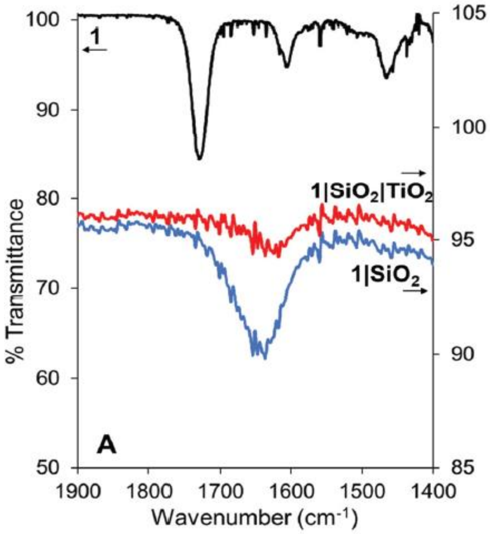

Figure 2.2: Overlay of FT-IR spectra of 1 and 1ISiO_2

The molecular catalyst **1** has a prominent C-O stretching frequency at 1729 cm^{-1}. Upon attachment of **1** to the SiO_2 support to form **1|SiO_2**, this prominent C-O stretching frequency remains present but shifts to 1636 cm^{-1}. This shift is consistent with carboxylate binding to metal oxide supports as has been previously observed.[54-55]

Catalyst **1|SiO_2** was then immobilized using TiO_2 ALD (10 cycles of $TiCl_4$ + H_2O as described in section 2.5). The ALD procedure was designed to coat **1|SiO_2** with a ~1.0 nm thick layer of TiO_2 to create the hybrid catalyst **1|SiO_2|TiO_2** as depicted in Figure 2.1C. ICP-MS analysis reveals that **1|SiO_2|TiO_2** catalyst contains 0.35 weight% nickel, indicating minimal, if any, loss of nickel catalyst during ALD. We mainly attribute the lower weight% nickel to the increased weight of the solid catalyst with the addition of the TiO_2 layer. STEM-EDS analysis on **1|SiO_2|TiO_2** also detected the presence of Ni and Ti as expected. As shown in Figure 2.3 XRD analysis of **1|SiO_2|TiO_2** again shows no evidence for nickel nanoparticles nor were any nanoparticles ever observed with STEM imagining.

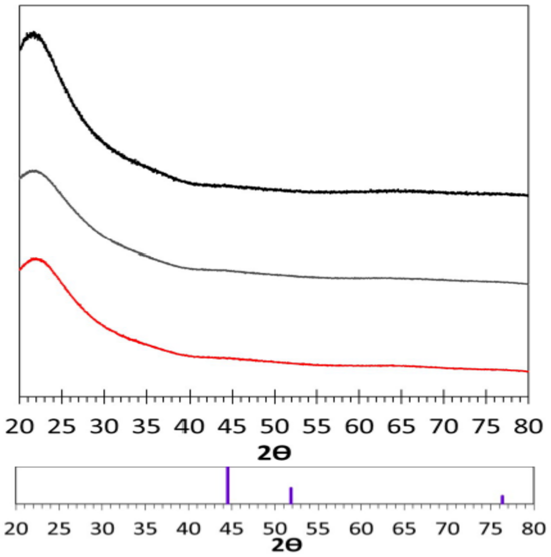

Figure 2.3: XRD overlay of **1|SiO_2** (black),**1|SiO_2|TiO_2**,(grey) post reaction **1|SiO_2|TiO_2** (red)

The FTIR-ATR spectrum of **1|SiO_2|TiO_2**, plotted in Figure 2.2, continues to show the existence of the C-O stretching frequencies that are indicative of carboxylate binding to metal oxides. No measurable shift in the C-O stretching frequencies between **1|SiO_2** and **1|SiO_2|TiO_2** suggests that the ALD treatment did not significantly alter the binding of the ligand to the SiO_2 support.

To investigate the stability of the nickel center of the catalyst, electron paramagnetic resonance (EPR) spectroscopy was utilized as shown in Figure 2.4. The EPR spectrum of a solid sample of the molecular catalyst **1** obtained at room temperature is shown in the center of Figure 2.4. The spectrum of catalyst **1|SiO_2|TiO_2** catalyst after ALD coatings is shown at the top of 2.4. The similar spectral splitting and shifts indicates the nickel centers between the two samples

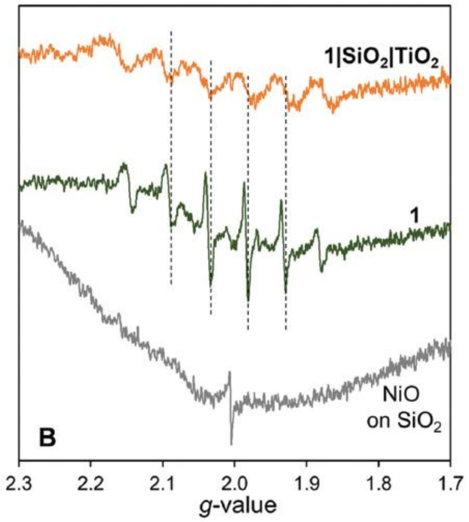

Figure 2.4: EPR overlay of molecular catalyst **1** and catalyst **1|SiO_2|TiO_2** post ALD. Reference EPR of NiO on SiO_2

(**1** and **1|SiO_2|TiO_2**) have the same oxidation-states and chemical binding environment. For comparison, the EPR spectrum of nickel oxide on SiO_2 support is shown in the bottom of Figure 2.4. Nickel oxide particles exhibit a clearly distinct EPR spectrum. Thus, the combined data analysis indicates that the molecular nickel catalyst is stable and maintains molecular integrity throughout the ALD coating process. Differences in reactivity between **1|SiO_2** and **1|SiO_2|TiO_2** as discussed in the next section lend further support for the structure of **1|SiO_2|TiO_2** proposed here (*vide infra*).

Catalytic Performance

To illustrate the advantage of this hybrid ALD catalyst approach, and to determine the optimized ALD layer thickness, a series of catalytic Suzuki cross-coupling reactions were performed. Table 1 presents the results of these test reactions along with illustrations of the proposed ligand-first bound catalyst compositions. The reaction shown in Table 2.1 was chosen as a simple test reaction to determine the optimal conditions and catalyst composition. The reaction conditions were chosen to highlight the green chemistry possibilities of this catalytic system. For solid support hybrid catalysts, 0.9 mol% nickel catalyst was used per reaction with respect to the limiting reagent iodotoluene. The solvent system chosen was a 1:1 ratio of ethanol and water, with the ethanol serving to help increase the solubility of the organic substrates. The only reaction additive was K_3PO_4 base, where base is a mechanistic requirement for boronic acid activation.[56] Lower reaction temperatures (80 °C) and shorter reaction times (12 hrs.) resulted in lower yields than compared to the optimal reaction temperature and time (105 °C and 24 hrs). The results in Table 2.1 indicate that the optimal catalyst design consists of **1** attached to a SiO_2 support with approximately 1.0 nm thickness of TiO_2 applied via 10 ALD cycles (**1|SiO_2|TiO_2**).

Table 2.1. Determining optimal ALD layer thickness for cross-coupling reactions in ethanol:water solvent.

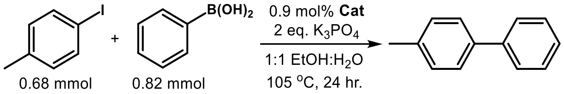

Cat	Yield
1	0%
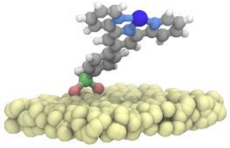 **1|SiO_2**	5%
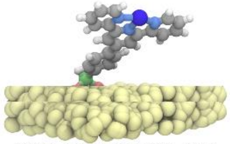 **1|SiO_2** with 0.5 nm TiO_2 ALD	32%
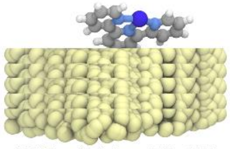 **1|SiO_2** with 1.0 nm TiO_2 ALD (**1|SiO_2|TiO_2**)	90%
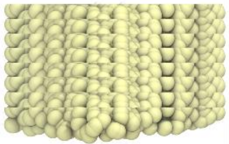 **1|SiO_2** with 1.5 nm TiO_2 ALD	2%

For molecular catalyst **1** in homogeneous solution, no product formation was detected. This result is due to rapid catalyst dimerization and deactivation promoted by water (Table 2.1A). The dimer, $[(\mu\text{-X})Ni(tpy)]_2$ where X = Cl^- or OH^-, has been shown to be inactive for this catalytic transformation.[6] The molecular catalyst **1** attached to an SiO_2 support without applied ALD layers (**1|SiO_2**), is able to generate product at a 5% yield, and post reaction analysis of **1|SiO_2** with ICP-MS revealed that the solid support no longer contained any detectable nickel. Thus, without an ALD layer, the polar ethanol water solvent mixture promotes the detachment of the molecular nickel catalyst from the surface of the SiO_2 support and the catalyst then deactivates in solution. A thin layer (less than 1 nm, see experimental section) of TiO_2 was then applied to the **1|SiO_2** structure via 5 ALD cycles and this catalyst produced the cross-coupled product with 32% yield. This non-optimal yield suggests that "thin" ALD layers are insufficient to fully protect the catalyst binding sites from solvent attack and subsequent desorption. The reason for incomplete protection is not entirely clear, but it is likely due to either poor coating uniformity at these thicknesses (i.e., nucleation delay) or simply insufficient thickness to block attack of the binding groups by the polar solvent.

Next, a roughly 1 nm layer of TiO_2 was applied to the **1|SiO_2** structure via 10 ALD cycles to yield catalyst **1|SiO_2|TiO_2**. As can be seen in Table 2.1, the 10 ALD cycle layer results in a catalyst capable of achieving optimal yields of the desired product. Computations on the Pd analogue of **1**, calculated a distance between the C atom of the COOH group and the metal center was nearly 1.2 nm,[57] indicating that an average 1 nm thick ALD layer would still expose the Ni center to the reaction solution. Post reaction ICP-MS indicates that 0.31 wt% nickel remained on the **1|SiO_2|TiO_2** catalyst, indicating that minimal nickel loss during the 24-hour reaction. ICP-MS analysis of the reaction solution post reaction did detect 1.77 µg of nickel per gram of solution. This minimal nickel in solution could occur due to nickel loss from the terpyridine ligand and not from complete molecular catalyst desorption from the surface of the oxide support. EDS analysis of the post-reaction catalyst also detected the continued presence of Ni and Ti on the SiO_2 surface, and an elemental map showed highly dispersed Ni on the surface with no evidence of nanoparticle formation, which was also supported by XRD patterns as shown in Figure 2.3. In addition to the detected Ni and Ti, the STEM-EDS analysis shows potassium and phosphorous content on the surface, likely arising from the K_3PO_4 base used during the reaction. FTIR-ATR analysis of the solid molecular/heterogeneous catalyst post reaction also showed C-O stretching frequencies assigned to the ligand binding to the oxide support.

These results suggest that the 10 ALD cycle TiO_2 layer now sufficiently coats the SiO_2 surface, fully immobilizing the molecular catalyst by stabilizing the ligand COOH binding to the oxide surface. This stabilized ligand binding prevents catalyst desorption and protects the catalyst from bimolecular degradations. Furthermore, BET analysis of **1|SiO_2** and **1|SiO_2|TiO_2** indicated that the ALD layer does not lead to an appreciable difference in surface area of the solid support (216 ± 0.8 m^2/g and 223 ± 0.8 m^2/g). The surface area analysis implies the ALD uniformly coats the SiO_2 support without clogging the micropores. It is also worth noting that molecular catalyst **1** attached to a TiO_2 support without ALD applied

(**1|TiO_2**) did achieve a 38% yield of the cross-coupled product. This indicates the ligand binding to TiO_2 is stronger than to SiO_2, likely due to the higher isoelectric point of TiO_2 compared to SiO_2. The 38% yield from this reaction is considerably lower than optimized yields obtained through ALD coating, indicating that the catalyst does not just migrate to the TiO_2 layers, and the binding sites are “buried” by the TiO_2 ALD as depicted in Table 2.1. Furthermore, post-reaction ICP-MS analysis of the **1|TiO_2** catalyst revealed that the molecular catalyst **1** detaches from the surface of this support after a single reaction cycle, which is not consistent with catalysts coated with ALD layers (*vide infra*).

Lastly, a 2.0 nm layer of TiO_2 was applied to the catalyst via 20 ALD cycles. This “thick” coating results in almost no yield of the desired product, as shown in Table 2.1. ICP-MS analysis of the 2.0 nm thick TiO_2 catalyst revealed that the nickel is still present at levels nearly identical to the pre-reaction levels. Therefore, this result supports that ALD layers can be applied that are too thick and thus fully encase the molecular catalyst. This full enclosure of the catalyst strongly binds the catalyst to the surface but also prevents catalyst activity due to preventing the active nickel center from accessing the reaction substrates.

With the optimized ALD layer thickness determined, control reactions were performed to help further identify the active catalyst species. Results from these control reactions are summarized in Table 2.2. Reaction 1 in Table 2.2 shows the designed hybrid catalyst **1|SiO_2|TiO_2** leads to an efficient product yield of 90%. For reaction. 3 in Table 2.2, the solid **1|SiO_2|TiO_2** catalyst was filtered from reaction mixture and additional substrate was added to the filtrate solution and a second reaction was performed. No new product formation or substrate consumption was observed after the second reaction showing that the active catalyst is not present in the reaction filtrate post reaction.

Table 2.2. Control Reactions Performed to Identify the Catalytically Active Species.

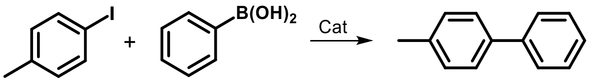

Rxn.	Catalyst	Yield[a]
1	**1|SiO_2|TiO_2**	90%
2	**1|TiO_2**	32%
3	Reaction Filtrate	0%
4	Only SiO_2	0%
5	Only TiO_2	0%
6	1 nm TiO_2 on SiO_2	0%
7	1 mol% **1** + SiO_2 *in situ*	0%
8	1 mol% **1** + TiO_2 *in situ*	4%
9	1 mol% $NiCl_2$ in solution	0%
10	1 mol% Rainey Ni in solution	1%
11	1 mol% $NiCl_2$ + SiO_2 *in situ*	0%
12	1 mol% Raney Ni + SiO_2 *in situ*	0%
13	Ni nanoparticles|SiO_2 (CEDI)	1%
14	**1|SiO_2|TiO_2** + Hg drop	82%

Conditions: 0.82 mmol phenylboronic acid, 0.68 mmol iodotoluene, 1.7 mmol K_3PO_4 in 20 ml 1:1 ethanol/water. 105 ^oC 24 hr. 0.9 mol% **1|SiO_2|TiO_2**, 1.1 mol% CEDI. [a]Determined by GC-MS analysis.

To confirm the necessity of the **1|SiO_2|TiO_2** structure, numerous other active catalysts were also considered. As indicated by reactions 4 and 5, the untreated metal oxides powders are not catalytically active for this cross-coupling transformation. SiO_2 ALD coated with TiO_2 without molecular nickel catalyst present was also not active (reaction 6). A mixture of homogenous molecular catalyst and fresh oxide particles, reactions 7 and 8, did not result in appreciable product formation, indicating that the ligand-first surface-attachment of the molecular catalyst is necessary in the hybrid design. Decomposition of the molecular nickel catalyst to nickel salts ($NiCl_2$) or metallic nickel during the reaction could have also been possible. Testing of $NiCl_2$ or metallic Rainey Ni both in solution and in the presence of oxide support (reactions 9 - 12) resulted in poor product yields (< 5%), indicating that these possible decomposition products are not responsible for the observed catalytic activity of **1|SiO_2|TiO_2**. We further examined the possibility that reduced nickel nanoparticles act as the catalytically active species. We synthesized 0.5 weight% nickel nanoparticle catalyst on the SiO_2 support using charge enhanced dry impregnation (CEDI).[58] The nickel nanoparticles did not exhibit catalytic activity in the water : ethanol mixture (reaction. 13), further illustrating an advantage of the designed hybrid ALD catalyst. To test for possible advantageous metallic species being catalytically active, the hybrid ALD catalyst was exposed to the mercury drop test. Mercury is known to poison heterogeneous metal nanoparticle catalysts.[59] In the presence of Hg, the hybrid catalyst maintained catalytic activity (reaction. 13), which strongly indicates that the active catalytic species is molecular in nature. Furthermore, nickel first binding to the oxide surface to generate a SOMC moiety is highly unlikely, as SOMCs require extensive oxide surface preparation under air-free conditions,[14] while **1|SiO_2|TiO_2** was prepared in air without prior conditioning of the oxide surface.

A further summary of the reactivity and stability of **1|SiO$_2$|TiO$_2$** in comparison to **1** and **1|SiO$_2$** can be found in Table 2.3. The data in Table 2.3 supports the conclusion that the hybrid catalyst containing an ALD overcoating (**1|SiO$_2$|TiO$_2$**) exhibits increased Suzuki cross-coupling reactivity due to the construction of the catalyst leading to extended lifetimes for the molecular component of the catalyst.

Table 2.3: Summary of the Characterization Data Comparing Homogeneous Catalyst (**1**), Hybrid Catalyst without ALD (**1|SiO$_2$**), and Hybrid Catalyst with ALD Overcoating (**1|SiO$_2$|TiO$_2$**).

		IR (COOH cm^{-1})		ICPMS (Ni wt%) catalyst		ICPMS (Ni) solution	EDS elements detected*		XRD (Ni particles?)	
Catalyst	%Yield	Pre	Post	Pre	Post	Post	Pre	Post	Pre	Post
1	0	1729	N/A	N/A	N/A	N/A	N/A	N/A	N/A	N/A
1|SiO$_2$	5	1639	*N.S.*	0.35	0.06	170 µg	Ni	*N.S.*	No	No
1|SiO$_2$|TiO$_2$	90	1640	1640	0.35	0.31	35 µg	Ni, Ti	Ni, Ti, K, P	No	No

N/A: data not collected/not applicable. *N.S.*: no signal. Pre and Post refer to pre-reaction and post-reaction, reaction details in Table 1. *EDS detected Si and O in every measurement.

IR spectroscopy focusing on the carboxylic frequencies indicates prolonged binding of the ligand to the oxide surface only when the ALD overcoat is applied. In addition, ICPMS analysis of the catalyst and the reaction solution shows retention of the majority of the nickel on the solid catalyst with **1|SiO$_2$|TiO$_2$.** STEM-EDS analysis supports the ICPMS data, and elemental mapping of **1|SiO$_2$|TiO$_2$** post-reaction shows a uniform coating of the TiO$_2$ layer and well-dispersed nickel on the surface of the SiO$_2$ support. The characterization data in Table 2.3

combined with the reactivity data in Tables 2.1 and 2.2 provide compelling evidence that the designed hybrid catalyst **1|SiO₂|TiO₂** is the catalytically active species for the test Suzuki cross-coupling reaction under the chosen conditions.

To further evaluate the chemical stability of this catalysts design, **1|SiO₂|TiO₂** was examined with X-ray emission spectroscopy (XES) before and after use in a Suzuki cross-coupling reaction. Figure 2.5 overlays the XES spectra at the Ni K$\beta_{1,3}$ and Kβ' emission for five different nickel samples. Here, the emission energy is indicative of the nickel chemical binding state.

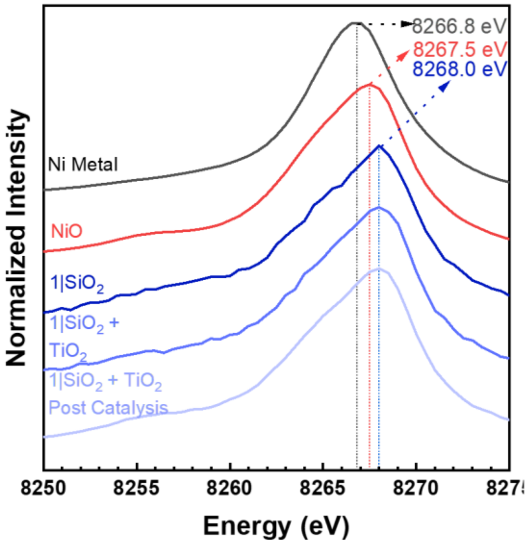

Figure 2.5: Overlay of XES spectra to compare emission of five different nickel samples

The top two spectra are reference scans made on nickel metal and nickel oxide (NiO) powders. Here, we observe a clear shift in peak emission intensity from 8266.8 eV to 8267.5 eV, as would be expected for these reference materials differences in chemical states. Next are scans for **1** in various states. First is the XES spectrum of **1|SiO₂**, the catalyst before ALD coating. This catalyst exhibits a peak intensity at 8268.0 eV. This peak intensity is 0.5 eV shifted from the oxide state, indicating that XES is capable of detecting the difference in chemical states between NiO and the molecular catalyst **1**. Shown next is the XES spectrum for **1|SiO$_2$|TiO$_2$**, which exhibits an identical peak emission energy to **1|SiO$_2$** (8268.0 eV). This result again indicates that the catalyst maintains its molecular nature after ALD coating. Lastly is the spectrum for the **1|SiO$_2$|TiO$_2$** catalyst after a 24 hour reaction in 1:1 ethanol:water solvent. This “used” catalyst once again shows its maximum peak intensity at 8268.0 eV, further confirming the molecular stability of the hybrid catalyst. In fact, direct overlays of these three spectra, showed that all three samples have nearly identical XES spectra, which demonstrates the increased hybrid catalyst stability afforded by ALD overlayers.

This hybrid catalyst exhibits desirable green chemistry principles[48, 60] such as the use of earth abundant nickel, low metal loadings which help prevent product contamination,[61] ease of catalyst separation from reaction mixtures without the need for column chromatography, and a green solvent mixture of H_2O and ethanol. To test the longer-term stability of **1|SiO$_2$|TiO$_2$**, consecutive reactions were performed, and product yield was monitored. After each reaction the used catalyst was filtered, rinsed, dried, and added to a fresh reaction solution. This procedure was repeated for multiple reactions and roughly 500 catalytic turnovers were achieved with **1|SiO$_2$|TiO$_2$** for the reaction shown in Table 2.1. Conversely, the non-ALD coated catalyst, **1|SiO$_2$**, was only able to achieve roughly 25 turnovers before deactivation.

To ensure this catalyst is generally amenable to Suzuki cross-coupling reactivity and not just applicable to a single reaction, a modest substrate scope for this catalyst was examined. Figure 2.6 shows the range of cross-coupling partners explored and products obtained from this hybrid ALD catalyst. In general, **1|SiO2|TiO2** was able to couple a variety of aryl halide and aryl boronic acid substrates with yields that range between 49 to 90%. **1|SiO2|TiO2** exhibits greater reactivity towards aryl iodides compared to aryl bromides or chlorides. This reactivity trend has been previously observed for [(2,2':6',2''-terpyridine)Ni(II)]Cl_2 cross-coupling catalysis.[62] As can be seen in Figure 2.6, a range of electron donating and electron withdrawing substrates are amenable to cross-coupling using **1|SiO2|TiO2** as the catalyst. This result illustrates that the reported hybrid catalyst motif may be a general approach towards designing cross-coupling catalysts.

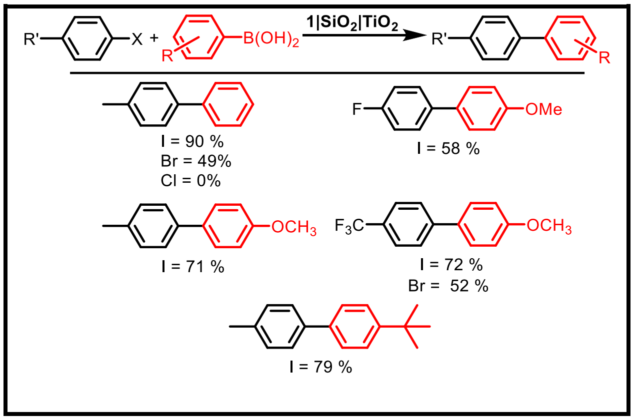

Figure 2.6. Catalytic Suzuki cross-coupling achieved by hybrid ALD catalyst. % Yields are isolated yield and based on limiting reagent. 0.82 mmol phenylboronic acid, 0.68 mmol iodotoluene, 1.7 mmol K_3PO_4 in 20 ml 1:1 ethanol/water. 105 ^oC 24 hr. 100 mg **1|SiO2|TiO2**.

2.4 Conclusions

This study demonstrates a new paradigm in the design of hybrid catalysts in which ALD is used to improve the attachment and stability of molecular catalysts on solid metal oxide supports. Generating hybrid catalysts with increased catalyst lifetimes makes the catalysts amenable for the use of green solvents and easily separable from reaction solutions. At an optimal ALD layer thickness, the molecular catalyst remains highly active while still being resistant to surface detachment and subsequent deactivation. Through a series of control experiments and spectroscopic characterizations, we provide strong evidence for the active species to be the unperturbed molecular catalyst attached to the metal oxide surface and encased with an optimal ALD deposited TiO_2 layer. Interestingly, the exemplary molecular catalyst studied here is not catalytically active by itself in homogeneous solution for the target carbon-carbon cross-coupling reaction due to extremely short catalyst lifetimes. Thus, a combination of ligand-first surface attachment with molecular design and ALD application could lead to new approaches in catalyst discovery. Noteworthy here for green chemistry principles is that this hybrid catalyst was able to perform cross-coupling catalysis using a non-noble metal (nickel) and earth abundant oxides and is active in a near-neutral pH, primarily aqueous solution. Moreover, since the optimal ALD coating requires only about 10 reaction cycles, this process is technologically and economically viable for large-scale manufacturing.

2.5 Experimental

Materials: Compound **1** was synthesized according to previously reported procedures.[6] **1|SiO$_2$** was prepared following the one-step method previously reported.[6] Atomic layer deposition was carried out in a custom-built, hot-wall, flow-tube reactor with automated control software[63] using a $TiCl_4$ + H_2O chemistry at 120 °C in a ~2 Torr flowing N_2 (>99.99% purity) atmosphere. ALD runs on catalyst powder were limited to a few grams sealed in a polyester fabric bag that permitted permeation of the precursor gases. To assist precursor gas permeation, a “hold” step was included in each ALD cycle. One full ALD cycle included: (1) close the gate valves, (2) pump down for 420 seconds, (3) reaction chamber isolation for 60 seconds, (4) $TiCl_4$ dose for 1 second directly into the isolated reaction chamber, (5) hold for 120 seconds, (6) pump down the reaction chamber for 30 seconds, (7) open the gate valves, (8) purge for 30 seconds, (9) H_2O dose for 1 second, (10) purge for 30 seconds. The water dose, steps (9) and (10), were repeated three times for each cycle. Monitor silicon wafers were included in each run to estimate approximate TiO_2 film thickness using spectroscopic ellipsometry (Woollam Alpha-SE).[64] The procedure for the synthesis of Nickel nanoparticle catalysts prepared by charge enhanced dry impregnation (CEDI) has been reported.[58] The SiO_2 support is Aerosil 300 (Evonik) and is a fumed, amorphous silica with 300 m^2/g surface area and an average particle size of ~ 20 nm. Cross-coupling reaction solutions were prepared with ultra-pure (18 MΩ) water and 200 proof ethanol. All other materials and supplies were used as received from the supplier unless otherwise noted.

Instrumentation: A Bruker Advance III HD 300 was used for NMR spectroscopy. ^{1}H data were collected at 300 MHz and ^{13}C at 75 MHz. Bruker TopSpin software was used to process the NMR data. Inductively coupled plasma-mass spectrometry (ICP-MS) was collected on a Finnigan ELEMENT XR with a double focusing magnetic field with a quartz torch and injector (Thermo Fisher Scientific) and a 0.2 mL/min micromist U-series nebulizer (GE). Gas chromatography-mass spectrometry analyses were performed with a Shimadzu QP-20105 containing a RXI-5MS (Restek) column (30 m, 0.25 mm id). Mass spectrometer electron ionization was at 70 eV and the spectrometer was scanned from 1000 to 50 *m/z* at low resolution. Powder X-ray diffraction (XRD) was carried out with a Rigaku Miniflex-II with a D/teX Ultra silicon strip detector. Cu α radiation (l – 1.5406 Å) was operated at 15 kV and 30 mA. Samples were loaded on a zero-background holder and scanned from 20-80° 2θ range at a scan rate of 3° 2θ/min. Fourier transform infrared-attenuated total reflection (FTIR-ATR) was performed on a Nicolet iS Fourier transform infrared spectrometer with an iD7 attenuated total reflectance attachment (diamond crystal). Before each sample set, a background scan of ambient atmosphere was collected and then subtracted from the experimental signal to calculate the final spectra reported. EPR spectra were collected on a Bruker EMXplus instrument equipped with a Bruker X-band microwave bridgehead. Spectra were recorded in a quartz EPR tube at room temperature at a power of 1.589 mW with a modulation amplitude of 2.0 G using the Xenon v1.1b.66 software. Nitrogen physisorption measurements were performed on samples pretreated for by placing the samples under 10 mmHg vacuum at room temperature, then ramping the temperature to 90 °C at 10 °C/minute and holding for 6 hours. Nitrogen physisorption measurements were collected at 77 K and surface area characterized by BET.

General Cross-Coupling Reaction Set Up: In a 50 mL round-bottom flask, 0.68 mmol aryl halide and 0.82 mmol of boronic acid were added to a 20 mL solution comprise of 1:1 ethanol: water. 1.7 mmol of K_3PO_4 and 0.1 g of **1|SiO_2|TiO_2** were added to the flask (unless otherwise stated in the manuscript). The solution was heated to 105 °C for 24 hours. The reaction was then allowed to cool to room temperature and the products were extracted with 3 rinses with pentane and purified by preparative scale TLC (90:10 pentane: ethyl acetate mobile phase). For catalyst recycling, the solid catalyst was gravity filtered from the reaction solution and rinsed three times with pentane and three times with ethanol and dried under a stream of N_2 (99.999%, Airgas) before being used in a new reaction.

2.6 Spectroscopic Results

Multiplicity was indicated as follows: s (singlet), d (doublet), t (triplet), q (quartet), m (multiplet).

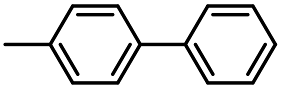

^{1}H NMR (DMSO, 300 MHz) δ 2.62 (s, 3H), 7.46 (d, *J* = 9.0 Hz, 2H), 7.55-7.57 (m, 1H), 7.63 (t, *J* = 7.3 Hz, 2H), 7.71-7.74 (d, *J* = 9.0 Hz, 2H), 7.80-7.82 (m, 2H). ^{13}C NMR ($CDCl_3$, 300 MHz) δ (ppm): 21.13, 127.00, 128.74, 129.51, 131.23, 137.05, 138.39, 141.19.

Figure 2.7 ^{1}H and ^{13}C NMR of 4-Methyl-1,1'-biphenyl

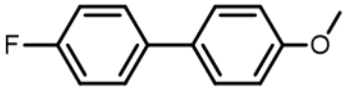

^{1}H NMR (CD_2Cl_2, 300 MHz) δ 3.84 (s, 3H), 6.96-6.99 (m, 2H), 7.09-7.15 (m, 2H), 7.48-7.55 (m, 4H). ^{13}C NMR (CD_2Cl_2, 300 MHz) δ (ppm): 55.28, 114.18, 115.27, 115.55, 127.91, 128.20, 132.55, 136.95, 159.25, 163.69.

Figure 2.8 ^{1}H and ^{13}C NMR of 4-Fluoro-4'-methoxy-1,1'-biphenyl

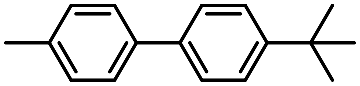

^{1}H NMR ($CDCl_3$, 300 MHz) δ 1.37 (s, 9H), 2.40 (s, 3H), 7.24-7.26 (d, *J* = 7.9 Hz, 2H), 7.45-7.55 (m, 6H). ^{13}C NMR ($CDCl_3$, 300 MHz) δ (ppm): 21.11, 31.39, 34.51, 125.67, 126.60, 126.87, 129.43, 131.21, 136.71, 137.24, 138.26.

Figure 2.9 ^{1}H and ^{13}C NMR of 4-(*tert*-butyl)-4'-methyl-1,1'-biphenyl

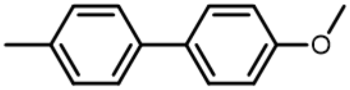

^{1}H NMR (CD_2Cl_2, 300 MHz) δ 2.36 (s, 3H), 3.82 (s, 3H), 6.94-6.96 (d, *J* = 8.8 Hz, 2H), 7.20-7.23 (d, *J* = 8.0 Hz, 2H), 7.43-7.46 (d, *J* = 8.13, 2H), 7.49-7.52 (d, *J* = 8.8 Hz, 2H). ^{13}C NMR (CD_2Cl_2, 300 MHz) δ (ppm): 20.72, 55.26, 114.10, 126.35, 127.75, 129.39, 133.47, 136.46, 137.74, 159.05.

Figure 2.10 ^{1}H and ^{13}C NMR of 4-methoxy-4'-methyl-1,1'-biphenyl

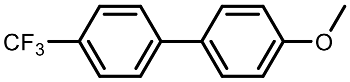

^{1}H NMR (DMSO, 300 MHz) δ 3.85 (s, 3H), 6.99-7.02 (d, *J* = 8.6 Hz, 2H), 7.56-7.59 (d, *J* = 8.6 Hz, 2H), 7.65-7.71 (m, 4H). ^{13}C NMR ($CDCl_3$, 300 MHz) δ (ppm): 55.33, 114.09, 114.36, 125.62, 126.82, 127.53, 128.28, 160.30.

Figure 2.11 ^{1}H and ^{13}C NMR of 4-methoxy-4'-(trifluoromethyl)-1,1'-biphenyl

2.7 References

1. Cornils, B.; Herrmann, W. A., Concepts in homogeneous catalysis: the industrial view. *Journal of Catalysis* **2003**, *216* (1), 23-31.

2. Duan, L.; Bozoglian, F.; Mandal, S.; Stewart, B.; Privalov, T.; Llobet, A.; Sun, L., A molecular ruthenium catalyst with water-oxidation activity comparable to that of photosystem II. *Nature Chem.* **2012**, *4* (5), 418-423.

3. Payard, P.-A.; Perego, L. A.; Ciofini, I.; Grimaud, L., Taming Nickel-Catalyzed Suzuki-Miyaura Coupling: A Mechanistic Focus on Boron-to-Nickel Transmetalation. *ACS Catalysis* **2018**, *8* (6), 4812-4823.

4. Inatomi, T.; Fukahori, Y.; Yamada, Y.; Ishikawa, R.; Kanegawa, S.; Koga, Y.; Matsubara, K., Ni(i)–Ni(iii) cycle in Buchwald–Hartwig amination of aryl bromide mediated by NHC-ligated Ni(i) complexes. *Catalysis Science & Technology* **2019**, *9* (8), 1784-1793.

5. Rull, S. G.; Funes-Ardoiz, I.; Maya, C.; Maseras, F.; Fructos, M. R.; Belderrain, T. R.; Nicasio, M. C., Elucidating the Mechanism of Aryl Aminations Mediated by NHC-Supported Nickel Complexes: Evidence for a Nonradical Ni(0)/Ni(II) Pathway. *ACS Catal.* **2018**, *8* (5), 3733-3742.

6. Key, R. J.; Tengco, J. M. M.; Smith, M. D.; Vannucci, A. K., A Molecular/Heterogeneous Nickel Catalyst for Suzuki–Miyaura Coupling. *Organometallics* **2019**, *38* (9), 2007-2014.

7. Fillol, J. L.; Codolà, Z.; Garcia-Bosch, I.; Gómez, L.; Pla, J. J.; Costas, M., Efficient water oxidation catalysts based on readily available iron coordination complexes. *Nature Chem.* **2011**, *3* (10), 807-813.

8. Kilgore, U. J.; Roberts, J. A. S.; Pool, D. H.; Appel, A. M.; Stewart, M. P.; DuBois, M. R.; Dougherty, W. G.; Kassel, W. S.; Bullock, R. M.; DuBois, D. L., [Ni(PPh2NC6H4X2)2]2+ Complexes as Electrocatalysts for H2 Production: Effect of Substituents, Acids, and Water on Catalytic Rates. *J. Am. Chem. Soc.* **2011**, *133* (15), 5861-5872.

9. Das, S.; Rodrigues, R. R.; Lamb, R. W.; Qu, F.; Reinheimer, E.; Boudreaux, C. M.; Webster, C. E.; Delcamp, J. H.; Papish, E. T., Highly Active Ruthenium CNC Pincer Photocatalysts for Visible-Light-Driven Carbon Dioxide Reduction. *Inorg. Chem.* **2019**, *58* (12), 8012-8020.

10. Shirley, H.; Su, X.; Sanjanwala, H.; Talukdar, K.; Jurss, J. W.; Delcamp, J. H., Durable Solar-Powered Systems with Ni-Catalysts for Conversion of CO2 or CO to CH4. *J. Am. Chem. Soc.* **2019**, *141* (16), 6617-6622.

11. Cui, X.; Li, W.; Ryabchuk, P.; Junge, K.; Beller, M., Bridging homogeneous and heterogeneous catalysis by heterogeneous single-metal-site catalysts. *Nature Catalysis* **2018**, *1* (6), 385-397.

12. Vannucci, A. K.; Alibabaei, L.; Losego, M. D.; Concepcion, J. J.; Kalanyan, B.; Parsons, G. N.; Meyer, T. J., Crossing the divide between homogeneous and heterogeneous catalysis in water oxidation. *Proc. Natl. Acad. Sci.* **2013**, *110*, 20918-20922.

13. Phan, N. T. S.; Van Der Sluys, M.; Jones, C. W., On the Nature of the Active Species in Palladium Catalyzed Mizoroki–Heck and Suzuki–Miyaura Couplings – Homogeneous or Heterogeneous Catalysis, A Critical Review. *Adv. Synth. Catal.* **2006**, *348* (6), 609-679.

14. Copéret, C.; Comas-Vives, A.; Conley, M. P.; Estes, D. P.; Fedorov, A.; Mougel, V.; Nagae, H.; Núñez-Zarur, F.; Zhizhko, P. A., Surface Organometallic and Coordination Chemistry toward Single-Site Heterogeneous Catalysts: Strategies, Methods, Structures, and Activities. *Chem Rev* **2016**, *116* (2), 323-421.

15. Lu, J.; Elam, J. W.; Stair, P. C., Synthesis and Stabilization of Supported Metal Catalysts by Atomic Layer Deposition. *Accounts of Chemical Research* **2013**, *46* (8), 1806-1815.

16. Mouat, A. R.; Mane, A. U.; Elam, J. W.; Delferro, M.; Marks, T. J.; Stair, P. C., Volatile Hexavalent Oxo-amidinate Complexes: Molybdenum and Tungsten Precursors for Atomic Layer Deposition. *Chemistry of Materials* **2016**, *28* (6), 1907-1919.

17. Samantaray, M. K.; Pump, E.; Bendjeriou-Sedjerari, A.; D'Elia, V.; Pelletier, J. D. A.; Guidotti, M.; Psaro, R.; Basset, J.-M., Surface organometallic chemistry in heterogeneous catalysis. *Chemical Society Reviews* **2018**, *47* (22), 8403-8437.

18. Camacho-Bunquin, J.; Ferrandon, M.; Sohn, H.; Yang, D.; Liu, C.; Ignacio-de Leon, P. A.; Perras, F. A.; Pruski, M.; Stair, P. C.; Delferro, M., Chemoselective Hydrogenation with Supported Organoplatinum(IV) Catalyst on Zn(II)-Modified Silica. *J. Am. Chem. Soc.* **2018**, *140* (11), 3940-3951.

19. Syed, Z. H.; Kaphan, D. M.; Perras, F. A.; Pruski, M.; Ferrandon, M. S.; Wegener, E. C.; Celik, G.; Wen, J.; Liu, C.; Dogan, F.; Goldberg, K. I.; Delferro, M., Electrophilic Organoiridium(III) Pincer Complexes on Sulfated Zirconia for Hydrocarbon Activation and Functionalization. *J. Am. Chem. Soc.* **2019**, *141* (15), 6325-6337.

20. Tafazolian, H.; Culver, D. B.; Conley, M. P., A Well-Defined Ni(II) α-Diimine Catalyst Supported on Sulfated Zirconia for Polymerization Catalysis. *Organometallics* **2017**, *36* (13), 2385-2388.

21. Culver, D. B.; Tafazolian, H.; Conley, M. P., A Bulky Pd(II) α-Diimine Catalyst Supported on Sulfated Zirconia for the Polymerization of Ethylene and Copolymerization of Ethylene and Methyl Acrylate. *Organometallics* **2018**, *37* (6), 1001-1006.

22. Pelletier, J. D. A.; Basset, J.-M., Catalysis by Design: Well-Defined Single-Site Heterogeneous Catalysts. *Acc. Chem. Res.* **2016**, *49* (4), 664-677.

23. Witzke, R. J.; Chapovetsky, A.; Conley, M. P.; Kaphan, D. M.; Delferro, M., Nontraditional Catalyst Supports in Surface Organometallic Chemistry. *ACS Catalysis* **2020**, *10* (20), 11822-11840.

24. Malakar, C. C.; Helmchen, G., Immobilized Catalysts for Iridium-Catalyzed Allylic Amination: Rate Enhancement by Immobilization. *Chem. Eur. J.* **2015**, *21* (19), 7127-7134.

25. Zhou, Y.-B.; Liu, Z.-K.; Fan, X.-Y.; Li, R.-H.; Zhang, G.-L.; Chen, L.; Pan, Y.-M.; Tang, H.-T.; Zeng, J.-H.; Zhan, Z.-P., Porous Organic Polymer as a Heterogeneous Ligand for Highly Regio- and Stereoselective Nickel-Catalyzed Hydrosilylation of Alkyne. *Org. Lett.* **2018**, *20* (24), 7748-7752.

26. Kramer, S.; Bennedsen, N. R.; Kegnæs, S., Porous Organic Polymers Containing Active Metal Centers as Catalysts for Synthetic Organic Chemistry. *ACS Catal.* **2018**, *8* (8), 6961-6982.

27. Wisser, F. M.; Mohr, Y.; Quadrelli, E. A.; Canivet, J., Porous Macroligands: Materials for Heterogeneous Molecular Catalysis. *ChemCatChem* **2020**, *12* (5), 1270-1275.

28. Dhakshinamoorthy, A.; Asiri, A. M.; Garcia, H., Formation of C–C and C–Heteroatom Bonds by C–H Activation by Metal Organic Frameworks as Catalysts or Supports. *ACS Catal.* **2019**, *9* (2), 1081-1102.

29. Chen, X. B.; Li, C.; Gratzel, M.; Kostecki, R.; Mao, S. S., Nanomaterials for renewable energy production and storage. *Chem. Soc. Rev.* **2012**, *41* (23), 7909-7937.

30. Dalle, K. E.; Warnan, J.; Leung, J. J.; Reuillard, B.; Karmel, I. S.; Reisner, E., Electro- and Solar-Driven Fuel Synthesis with First Row Transition Metal Complexes. *Chem. Rev.* **2019**, *119* (4), 2752-2875.

31. Ashford, D. L.; Gish, M. K.; Vannucci, A. K.; Brennaman, M. K.; Templeton, J. L.; Papanikolas, J. M.; Meyer, T. J., Molecular Chromophore–Catalyst Assemblies for Solar Fuel Applications. *Chemical Reviews* **2015**, *115* (23), 13006-13049.

32. Hanson, K.; Brennaman, M. K.; Ito, A.; Luo, H. L.; Song, W. J.; Parker, K. A.; Ghosh, R.; Norris, M. R.; Glasson, C. R. K.; Concepcion, J. J.; Lopez, R.; Meyer, T. J., Structure-Property Relationships in Phosphonate-Derivatized, Ru-II Polypyridyl Dyes on Metal Oxide Surfaces in an Aqueous Environment. *J. Phys. Chem. C* **2012**, *116* (28), 14837-14847.

33. Vannucci, A. K.; Chen, Z.; Concepcion, J. J.; Meyer, T. J., Nonaqueous Electrocatalytic Oxidation of the Alkylaromatic Ethylbenzene by a Surface Bound RuV(O) Catalyst. *ACS Catal.* **2012**, *2* (5), 716-719.

34. Chen, Z. F.; Concepcion, J. J.; Hull, J. F.; Hoertz, P. G.; Meyer, T. J., Catalytic water oxidation on derivatized nanoITO. *Dalton Trans.* **2010**, *39* (30), 6950-6952.

35. Materna, K. L.; Crabtree, R. H.; Brudvig, G. W., Anchoring groups for photocatalytic water oxidation on metal oxide surfaces. *Chemical Society Reviews* **2017**, *46* (20), 6099-6110.

36. Opanasenko, M.; Štěpnička, P.; Čejka, J., Heterogeneous Pd catalysts supported on silica matrices. *RSC Advances* **2014**, *4* (110), 65137-65162.

37. Hübner, S.; de Vries, J. G.; Farina, V., Why Does Industry Not Use Immobilized Transition Metal Complexes as Catalysts? *Adv. Synth. Catal.* **2016**, *358* (1), 3-25.

38. Hyde, J. T.; Hanson, K.; Vannucci, A. K.; Lapides, A. M.; Alibabaei, L.; Norris, M. R.; Meyer, T. J.; Harrison, D. P., Electrochemical Instability of Phosphonate-Derivatized, Ruthenium(III) Polypyridyl Complexes on Metal Oxide Surfaces. *ACS Appl. Mater. Inter.* **2015**, *7* (18), 9554-9562.

39. Vicente, B. C.; Huang, Z.; Brookhart, M.; Goldman, A. S.; Scott, S. L., Reactions of phosphinites with oxide surfaces: a new method for anchoring organic and organometallic complexes. *Dalton Trans.* **2011**, *40* (16), 4268-4274.

40. Brown, D. G.; Schauer, P. A.; Borau-Garcia, J.; Fancy, B. R.; Berlinguette, C. P., Stabilization of Ruthenium Sensitizers to TiO_2 Surfaces through Cooperative Anchoring Groups. *J. Am. Chem. Soc.* **2013**, *135* (5), 1692-1695.

41. Losego, M. D.; Hanson, K., Stabilizing molecular sensitizers in aqueous environs. *Nano Energy* **2013**, *2* (5), 1067-1069.

42. Liu, S.; Tan, J. M.; Gulec, A.; Crosby, L. A.; Drake, T. L.; Schweitzer, N. M.; Delferro, M.; Marks, L. D.; Marks, T. J.; Stair, P. C., Stabilizing Single-Atom and Small-Domain Platinum via Combining Organometallic Chemisorption and Atomic Layer Deposition. *Organometallics* **2017**, *36* (4), 818-828.

43. Lu, Z.; Tracy, R. W.; Abrams, M. L.; Nicholls, N. L.; Barger, P. T.; Li, T.; Stair, P. C.; Dameron, A. A.; Nicholas, C. P.; Marshall, C. L., Atomic Layer Deposition Overcoating Improves Catalyst Selectivity and Longevity in Propane Dehydrogenation. *ACS Catal.* **2020**, *10* (23), 13957-13967.

44. Handa, S.; Slack, E. D.; Lipshutz, B. H., Nanonickel-Catalyzed Suzuki–Miyaura Cross-Couplings in Water. *Angew. Chem. Int. Ed.* **2015**, *54* (41), 11994-11998.

45. Lipshutz, B. H., When Does Organic Chemistry Follow Nature’s Lead and “Make the Switch”? *J. Org. Chem.* **2017**, *82* (6), 2806-2816.

46. Jana, R.; Pathak, T. P.; Sigman, M. S., Advances in Transition Metal (Pd,Ni,Fe)-Catalyzed Cross-Coupling Reactions Using Alkyl-organometallics as Reaction Partners. *Chem. Rev.* **2011**, *111* (3), 1417-1492.

47. Gildner, P. G.; Colacot, T. J., Reactions of the 21st Century: Two Decades of Innovative Catalyst Design for Palladium-Catalyzed Cross-Couplings. *Organometallics* **2015**, *34* (23), 5497-5508.

48. Bryan, M. C.; Dunn, P. J.; Entwistle, D.; Gallou, F.; Koenig, S. G.; Hayler, J. D.; Hickey, M. R.; Hughes, S.; Kopach, M. E.; Moine, G.; Richardson, P.; Roschangar, F.; Steven, A.; Weiberth, F. J., Key Green Chemistry research areas from a pharmaceutical manufacturers' perspective revisited. *Green Chem.* **2018**, *20* (22), 5082-5103.

49. Jo, J.; Tu, Q.; Xiang, R.; Li, G.; Zou, L.; Maloney, K. M.; Ren, H.; Newman, J. A.; Gong, X.; Bu, X., Metal Speciation in Pharmaceutical Process Development: Case Studies and Process/Analytical Challenges for a Palladium-Catalyzed Cross-Coupling Reaction. *Organometallics* **2019**, *38* (1), 185-193.

50. Hanson, K.; Losego, M. D.; Kalanyan, B.; Parsons, G. N.; Meyer, T. J., Stabilizing Small Molecules on Metal Oxide Surfaces Using Atomic Layer Deposition. *Nano Lett.* **2013**, *13* (10), 4802-4809.

51. Hanson, K.; Losego, M. D.; Kalanyan, B.; Ashford, D. L.; Parsons, G. N.; Meyer, T. J., Stabilization of $[Ru(bpy)_{(2)}(4,4'-(PO_3H_2)bpy)]^{(2+)}$ on Mesoporous TiO_2 with Atomic Layer Deposition of Al_2O_3. *Chem. Mater.* **2013**, *25* (1), 3-5.

52. Kim, D. H.; Losego, M. D.; Hanson, K.; Alibabaei, L.; Lee, K.; Meyer, T. J.; Parsons, G. N., Stabilizing chromophore binding on TiO_2 for long-term stability of dye-sensitized solar cells using multicomponent atomic layer deposition. *PCCP* **2014**, *16* (18), 8615-8622.

53. Winter, A.; Schubert, U. S., Metal-Terpyridine Complexes in Catalytic Application – A Spotlight on the Last Decade. *ChemCatChem* **2020**, *12* (11), 2890-2941.

54. Brennan, B. J.; Llansola Portolés, M. J.; Liddell, P. A.; Moore, T. A.; Moore, A. L.; Gust, D., Comparison of silatrane, phosphonic acid, and carboxylic acid functional groups for attachment of porphyrin sensitizers to TiO2 in photoelectrochemical cells. *Physical Chemistry Chemical Physics* **2013**, *15* (39), 16605-16614.

55. Nazeeruddin, M. K.; Humphry-Baker, R.; Liska, P.; Gratzel, M., Investigation of sensitizer adsorption and the influence of protons on current and voltage of a dye-sensitized nanocrystalline TiO_2 solar cell. *J. Phys. Chem. B* **2003**, *107* (34), 8981-8987.

56. Norio, M.; Suzuki, A., Palladium-Catalyzed Cross-Coupling Reactions of Organoboron Compounds. *Chem. Rev.* **1995**, *95*, 2457-2483.

57. DeLucia, N. A.; Jystad, A.; Vander Laan, K.; Tengco, J. M. M.; Caricato, M.; Vannucci, A. K., A Silica Supported Molecular Palladium Catalyst for Selective Hydrogeoxygenation of Aromatic Compounds Under Mild Conditions. *ACS Catal.* **2019**, *9*, 9060-9071.

58. Zhu, X.; Cho, H.-r.; Pasupong, M.; Regalbuto, J. R., Charge-Enhanced Dry Impregnation: A Simple Way to Improve the Preparation of Supported Metal Catalysts. *ACS Catal.* **2013**, *3* (4), 625-630.

59. Campbell, K. C.; Hislop, J. S., Mercury adsorption, catalyst poisoning, and reactivation phenomena on metal catalysts. *J. Catal.* **1969**, *13* (1), 12-19.

60. Anastas, P. T.; Warner, J. C., *Green Chemistry: Theory and Practice*. Oxford University Press: New York, 1998.

61. Li, C.-J.; Trost, B. M., Green Chemistry for Chemical Synthesis. *Proc. Natl. Acad. Sci.* **2008**, *105* (36), 13197-13202.

62. Paul, A.; Smith, M. D.; Vannucci, A. K., Photoredox-Assisted Reductive Cross-Coupling: Mechanistic Insight into Catalytic Aryl–Alkyl Cross-Couplings. *J. Org. Chem.* **2017**, *82* (4), 1996-2003.

63. Piercy, B. D.; Losego, M. D., Tree-based control software for multilevel sequencing in thin film deposition applications. *J. Vac. Sci. Technol., B* **2015**, *33* (4).

64. Piercy, B. D.; Leng, C. Z.; Losego, M. D., Variation in the density, optical polarizabilities, and crystallinity of TiO_2 thin films deposited via atomic layer deposition from 38 to 150 °C using the titanium tetrachloride-water reaction. *J. Vac. Sci. Tech. A* **2017**, *35* (3), 03E107.

CHAPTER 3

STABILIZING MOLECULAR/HYBRID NICKELBIPYRIDINE CATALYSTS ONTO AN OXIDE SUPPORT VIA CARBOXYLIC ACID AND SILATRANE SURFACE ANCHORING GROUPS: SYNTHESIS AND REACTIVITY[2]

---

[2] Ayare, P. J.; Morrow, M.; Vannucci, A. K. Manuscript in Preparation

3.1 Abstract

Stable surface binding groups for attachment of molecular complexes to oxide supports are needed for building robust functional materials used in dye-sensitized solar cells and molecular/heterogeneous hybrid catalysis. Although molecular catalysts can be aptly tuned as per the desired reactivity by changing the coordinating ligand design, and thus, are highly selective for various chemical transformations, they lack industrial utility. Thus, the approach of immobilizing molecular catalysts onto oxide supports for chemical transformations needs to be keenly undertaken to increase the practical utility of these catalysts in further scale-up and recovery. An important parameter to consider while designing molecular/hybrid catalysts for longer catalytic lifetimes is the binding strength and stability of the surface anchoring groups. Although carboxylic acid anchors have been extensively used, they tend to dissociate from the surface in polar, protic solvents due to weaker bonding to the support. Herein, we demonstrate a comparative study on synthesis, characterization and stability of nickel bipyridine complexes anchored via carboxylic acid and silatrane linkages to oxide support for employing in cross-coupling reactions. Two nickel complexes, of [(2,2'-bipyridine-4,4'-dicarboxylic acid)Ni(II)]Cl_2 and [(2,2'-bipyridine-4,4'-diamidopropylsilatrane)Ni(II)]Cl_2 were synthesized and immobilized on silica oxide support. Characterization of the complexes pre and post immobilization indicates successful complex loading onto the support. Preliminary data indicates the nickel bipyridine silatrane complex to have higher loading onto solid support which can

be possibly attributed to stronger covalent bonding of the silatrane group leading to better catalyst stabilization.

3.2 Introduction

Synthesizing recoverable catalysts based on earth-abundant metals with broad applicability are a key to sustainable synthesis of fine chemicals, pharmaceuticals and agrochemicals. It is well known that traditional molecular catalysts exhibit high selectivity but suffer from lack of separation ease and recoverability from reaction solutions. Catalysis in homogeneous systems is well understood with respect to determining both the active catalytic center and the elementary steps involved in the reaction mechanism and this knowledge is advantageous in developing new catalytic systems. Thus, the transfer of molecular organometallic catalysis concepts to surface catalysis provides numerous applications and advantages over traditional approaches of both fields.[1-2] One advantage provided by immobilizing a molecular catalyst onto a surface support is the isolation of active sites which prevents the bimolecular deactivation frequently observed in these homogeneous catalytic systems.[3] Furthermore, a molecular approach to heterogeneous catalysis can help address the problem of low number of active sites and help gain insights into the mechanism of heterogeneous catalysis.

Binding motif and coordination environment also affects catalyst stability and overall reactivity since stronger binding to oxide supports, will lead to longer lifetimes of catalyst. Moreover, altering the coordination environment can help alter catalyst reactivity and enable new applications. 2,2'-Bipyridine(bpy) has been established as a prime ligand scaffold for Ni catalysis involving a single-electron redox process, which enable novel molecular transformations.[4-5] 2,2'-Bipyridine ligands have been extensively used in transition metal-based organometallic complex formation due to high redox stability and ease of functionalization. Furthermore, Nickel bipyridine complexes have played a major role in synthetic chemistry. Much of the fundamental information regarding reducing elimination reactions and redox events,[6-8] insertion reactions,[9-10] polymer synthesis,[11-12] and electrocatalytic couplings[13-14] using nickel comes from studies initiated with complexes bearing the bipyridine ligand.[15]

While designing the molecular/hybrid complexes, the anchoring groups for either dyes or catalysts should be chosen to maximize the robustness and efficiency of the supported organometallic complex. Carboxylic acids have been the most widely used anchoring group for attaching complexes to metal oxide supports for DSSCs.[16] However, carboxylic acids are prone to desorption from the metal oxide surface in aqueous conditions and are only moderately stable at low pH.[17-18] In comparison, hydroxamic acids and silatranes form more robust surface bonds and being stable under acidic, neutral, and basic conditions (pH 2–11). [17, 19-20] Among water-stable anchoring groups, silatranes are known to be stable in extreme hydrolytic conditions, are non-protic, non-ionic, and form strong siloxane surface bonds to metal oxides. Additionally, the caged trialkoxysilane precursor contains an electron-rich pentacoordinate silicon atom. Thus, this silicon is more stable to nucleophiles. This facilitates silatranes resistance to hydrolysis as compared to the more commonly used non-caged silane analogues and other anchoring groups.[21-24] Despite reports on high stability of the silatrane anchoring groups, of the various anchoring groups reviewed in literature, silatranes are less studied and their utility in cross-coupling catalysis has not been examined. A study on stability of silatrane anchoring group indicated that the silatrane anchor had the lowest level of desorption, in turn, suggesting that it has highest binding affinity to the solid support.[16]

Motivated by the results from previous reports on hybrid catalysis approach demonstrating excellent catalytic performance of ALD stabilized molecular/hybrid Nickel terpyridine catalyst,[25-26] this chapter explores the stability of the molecular complexes on the oxide supports. It discusses if stabilizing can be achieved by altering the surface anchoring group to silatrane instead of previously used carboxylic acid moieties. In addition, studying the interfacial chemistry of carboxylic acid and silatrane surface binding groups, with the understanding that the stronger covalently bonding silatranes will help further the goal of stabilizing molecular complexes onto the oxide support and thus increase robustness of these hybrid catalysts. Thus, we describe here the synthesis of Nickelbipyridine complexes with carboxylic acid and silatrane anchoring groups. Figure 3.1 presents the molecular and hybrid complexes studied in this paper. We also report the immobilization procedures for loading these molecular catalysts onto an oxide support. The reactivity trends of the molecular and immobilized versions of the synthesized catalyst needs to be investigated in detail. Here, we analyze the structure and stability of these complexes immobilized onto an oxide support. Preliminary characterization data supports molecular complex formation and its immobilization onto a surface to form hybrid catalyst 1b and 2b.

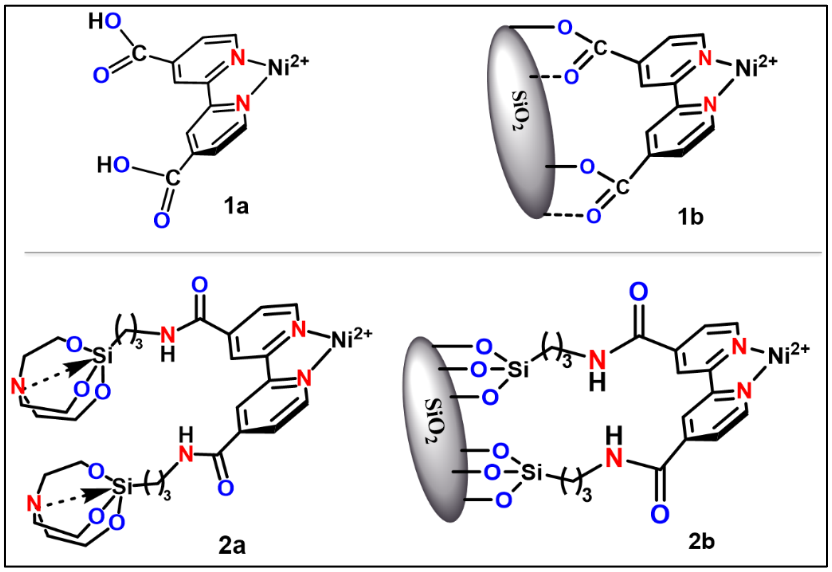

Figure 3.1: Molecular and supported versions of Nickel bipyridine based catalysts synthesized and studied.

3.3 Results and Discussion

3.3a *FT-IR characterization study*

ATR FT-IR spectroscopy has been previously used to study various anchoring groups anchored onto TiO_2 or SiO_2 surfaces. Structural characterization of 1a and hybrid 1aISiO_2 was carried out by ATR FTIR analysis. Figure 3.2 shows the ATR-FTIR overlay of molecular catalyst 1a and its immobilized analogue 1a**I**SiO_2.

The spectrum for molecular NibpyCOOH (orange) exhibits bands at 1616, 1558 and 1405 cm^{-1}, which are characteristic of the bipyridyl ligands.[27] The peak at 1700-1731 cm^{-1} is representative for carbonyl groups of 1a.

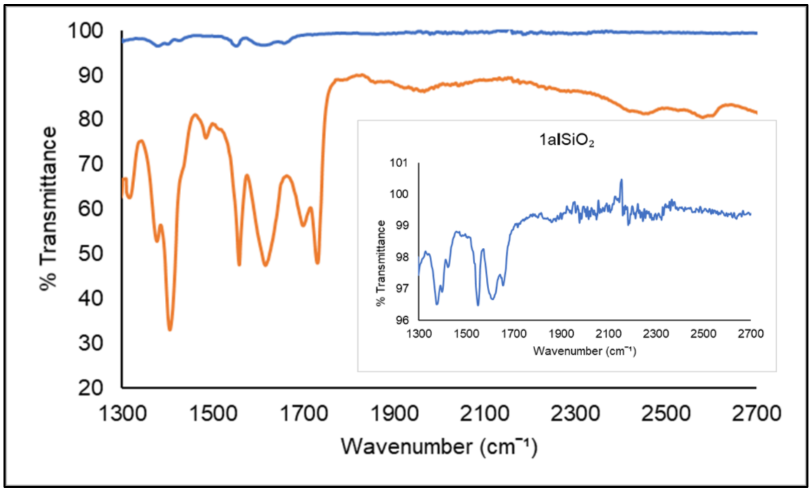

Figure 3.2: FT-IR overlay of 1a (molecular NibpyCOOH) and 1b (1a**I**SiO$_2$). (Inset 1a**I**SiO$_2$)

In the ATR-FTIR spectrum of 1a**I**SiO$_2$, after binding to the support the carbonyl peak at 1731 cm^{-1} disappears. Disappearance of the CO band indicates that the surface complexes are attached through a bidentate coordination, not a monodentate coordination, as observed in the literature. The band at 1700cm^{-1} for asymmetric CO stretch shifts to 1657 cm^{-1} with decreased intensity in the immobilized version, as consistent with the bridging bidentate binding mode.[17] This is indicative of COOH group binding to the metal oxide support.[16] ATR-FTIR of the bipyridine ligand on SiO$_2$ was little changed in the 1300-1700 cm^{-1} region. Thus, this ATR-FTIR analysis of 1a and 1b suggested successful immobilization of the catalyst onto silica support without altering the molecular catalyst.

Figure 3.3 shows ATR-FTIR overlay of the ligand bpy-sil, molecular complex 2a and 2**I**SiO$_2$. As seen, the CO frequency for the amide group continues as observed in all three spectra without any modification in the ligand structure.

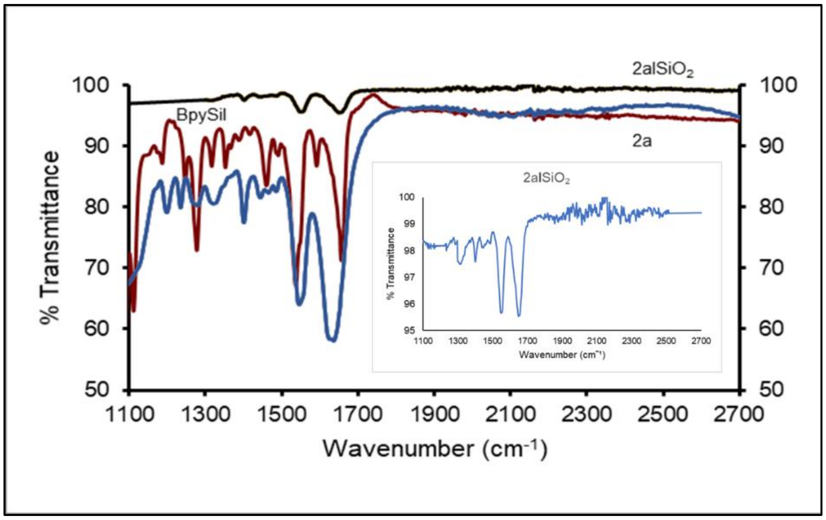

Figure 3.3: ATR FTI-IR spectra of bipyridine silatrane ligand, complex 2a, complex on 2a**I**SiO$_2$. (Inset: 2a**I**SiO$_2$)

Furthermore, the silatrane cage ATR-FTIR bands of bpy-sil at 1452 cm^{-1} for δ(CH$_2$) disappears upon formation of 2a**I**SiO$_2$ by surface binding, as previously observed for other systems, including porphyrin-silatranes bound to metal oxide surfaces. The functional groups C=O (1657 cm^{-1} stretch), N−H (1538 cm^{-1} bend) and the bands at 1406, 1431, 1462, and 1547 cm-^{1} for bipyridyl ligand vibration modes were identified in the ATR-FTIR of ligand bpysil. In the ATR-FTIR of complex 2a and 2b(2a**I**SiO$_2$), all the major the bands for CO and NH functional groups and the bands for bipyridyl ligand appear close to the theoretically determined values (within 25 cm^{-1}), thus supporting our assignments.[17] ATR-FTIR spectroscopy is consistent with incorporation of complexes 1a and 2a onto the silica support without alterations in the structure of complex.

3.3b ESI-MS analysis

Due to the paramagnetic nature of the nickel complex characterization via NMR could not be recorded. Thus, complex formation was monitored and confirmed through ESI MS analysis. ESI MS for 1a shows a prominent peak at m/z 192 ($C_{16}H_{14}NiO_4$, bpyNi(MeCN)$_2$) confirming the complex formation.

ESI MS analysis for 2a confirmed the formation of 2a with prominent peak at m/z 406.1. Remaining peaks can be arising due to sensitivity of the silatrane organic group to the chemicals and technique used in ESI MS analysis.

3.3c ICP-MS analysis

To examine the amount of nickel metal loading onto silica support, ICP-MS analysis was carried out on both hybrid complexes 1b and 2b. ICP-MS analysis indicated that 1b (COOH**I**SiO$_2$) contained 0.10 wt % nickel. This equates to 7.77×10^{-9} mol of catalyst per m^2 of silica support. Furthermore, ESI-MS of the resulting filtrate obtained post filtration of the immobilized catalyst, presented m/z at 192 (z=2) as the prominent peak, thus, implying that the molecular catalyst was intact during the immobilizing procedure and weight % nickel reported is indeed from the surface immobilization of the molecular catalyst. However, this is very low loading in comparison to previously studied [(2,2′:6′,2″-terpyridine-4′-benzoic acid)Ni(II)]Cl$_2$ immobilized on SiO$_2$ (3.9×10^{-8}).[25] This could be possibly due to formation of monocoordinated COOH or overcrowding on the support oxide sites due to two COOH moieties hindering the site of attachment and thus leading to lesser immobilization on the surface. ICP-MS of 2b (2a**I**SiO$_2$) indicated 2.03 wt% nickel and 1.6×10^{-7} mol of catalyst per m^2 of A300 support. It is to be noted that, the catalyst loading onto the support is significantly higher than its carboxylic acid counterpart. This can be primarily attributed to the formation of strong covalent Si-

O bonds on binding to the oxide support. Thus, utilizing silatrane anchoring group can be advantageous in achieving higher catalyst loading onto the support. Furthermore, stronger covalent interactions between the molecular catalyst and oxide support, results in formation of a highly stabilized molecular/hybrid catalyst onto the surface, which can prevent catalyst leaching from the surface during reactions.

3.4d EPR Analysis

EPR spectroscopy of solid samples offers a deliberate view of the electronic configuration of definite structural forms for several complexes, especially in determining the paramagnetic metal centers which are NMR silent. Thus, EPR spectroscopy was conducted to study the paramagnetic nickel metal center. However, due to lower weight % loading of 1a|SiO$_2$, it was difficult to detect any evident signal. Although ICP-MS detected higher weight % loading for 2b, unfortunately EPR spectroscopy of both complex 2|SiO$_2$ did not produce any evident signal. Further efforts to increase catalyst loading of 1a|SiO$_2$ for better signal output are underway.

3.4 Experimental

3.3a Synthesis procedures

Synthesis of 1a:

Ni(II)bpyCOOH

Bpy ligand precursor was synthesized using previously reported procedure and ligand formation was confirmed via ^{1}H NMR. To a round bottom, metal precursor, $NiCl_2.6H_2O$ was added with bpy ligand in 1.1:1 ratio and the resulting solution was refluxed overnight in ethanol. This solution was then placed on the rotary evaporator and evaporated to dryness. The resulting green solid was washed with diethyl ether and filtered. It was then isolated to dry and utilized for further characterization. Figure 3.2 shows synthesis route for 1a.

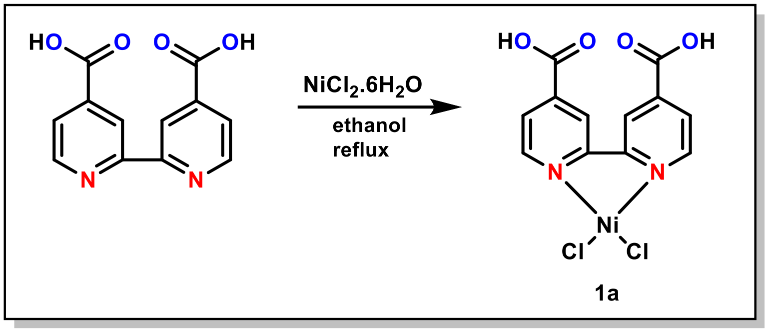

Figure 3.4: Synthesis of molecular complex 1a

Loading procedure to form 1b:

Ni(II)bpyCOOH**I**SiO_2

To a 500mL media bottle, 0.100g of complex 1a was added and sonicated to dissolve in 100mL ethanol. To this, 1.00g of Aerosil A300 silica was added, and the resulting solution was allowed to sit overnight in dark. The solid was then vacuum filtered, rinsed with hexanes/diethyl ether and dried prior to submitting for further analysis. Figure 3.2 depicts the immobilizing technique for formation of 1b.

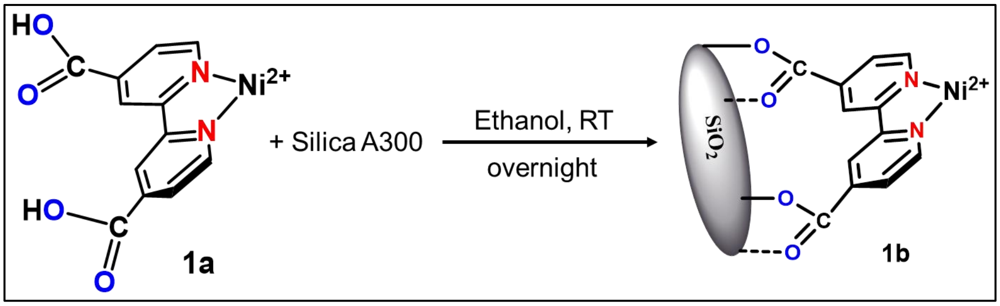

Figure 3.5: Synthesis of molecular/hybrid catalyst 1b

Structural analysis of complexes 1a and 1b will be discussed further in detail. The synthesized complex was NMR silent, thus, formation of complex 1a was confirmed using ESI MS analysis. Furthermore, ATR-FTIR of both 1a and 1b and ICP-MS of 1b confirms successful immobilization of the complex on silica support.

Synthesis of complex 2a:

Ni(II)bpySil

Synthesis of complex 2a comprised of a three-part procedure. Ligand framework was synthesized as a combination of two different fragments. Thus, the procedure consisted of synthesizing a 2-aminopropyl silatrane ligand and combining it with bipyridyl ligand to form 2,2’-bipyridine-4,4’-diamidopropylsilatrane ligand (bpySil). This was then used for synthesis of complex 2a.

Synthesis of 1-(3-aminopropyl) silatrane ligand:

Aminopropylsilatranes are of high interest due to their potential for the preparation of new silatranes by the derivatization of the amino group. Literature studies on synthesis of silatrane ligands are very well established. Silatranes are relatively stable to moisture being more difficult to hydrolyze as compared to alkoxysilanes, carboxylates etc. Thus, they are generally used as precursors for a number of silatrane derivatives.[28]

1-(3-aminopropyl) silatrane was synthesized by following the procedure reported earlier.[28] To a round bottom, (3-aminopropyl)triethoxysilane (0.24 mol, 4.3 g, 4.4 mL), triethanolamine(6.7 mol, 1.49 g, 1.57 mL), MeOH 14.2 mL, BuOH 1 mL and toluene 50 mL were added inside the glovebox. The mixture was stirred for 3 h at 60°C and then concentrated by rotavap. White crystals of the ligand were obtained after 24 h. ^{1}H-NMR studies confirmed the ligand formation.

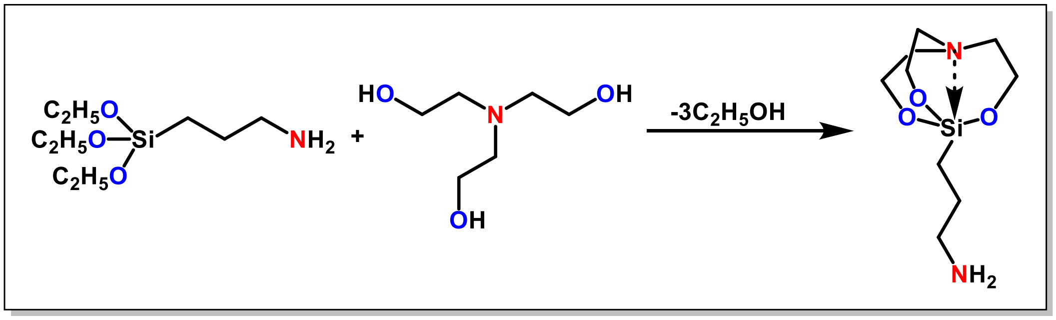

Figure 3.6: Synthesis of 1-(3-aminopropyl) silatrane

^{1}H NMR δ_H (400 MHz, $CDCl_3$), ppm: 0.33–0.35 (2H, t, CH_2), 1.16–1.18 (2H, s, NH_2); 1.45-1.47 (2H, p, CH_2); 2.58–2.60 (2H, t, CH_2); 2.73–2.75 (6H, t, CH_2); 3.65–3.68 (6H, t, CH_2); intensity ratio: 1:1:1:3:3.

Synthesis of 2,2'-Bipyridine-4,4'-diamidopropylsilatrane ligand:

This synthesis was performed following a known procedure.[21] To a dry round bottom flask was added 0.200 g (0.82 mmol) of 2,2'-bipyridine-4,4'-dicarboxylic acid and 4 mL (54 mmol) thionyl chloride. The suspension was refluxed overnight under nitrogen atmosphere. The solvent was removed under reduced pressure, yielding a yellow solid. The solid was dissolved in 10 mL of warm, dry dichloromethane along with 0.417 g (1.79 mmol) 3- aminopropyl silatrane and 0.560 mL (4.01 mmol) triethylamine. The solution stirred under a nitrogen atmosphere at room temperature for three hours, over which time a pale pink precipitate formed. The reaction was cooled to 0°C overnight and then filtered to afford a light pink solid (0.548 g, 92 %).

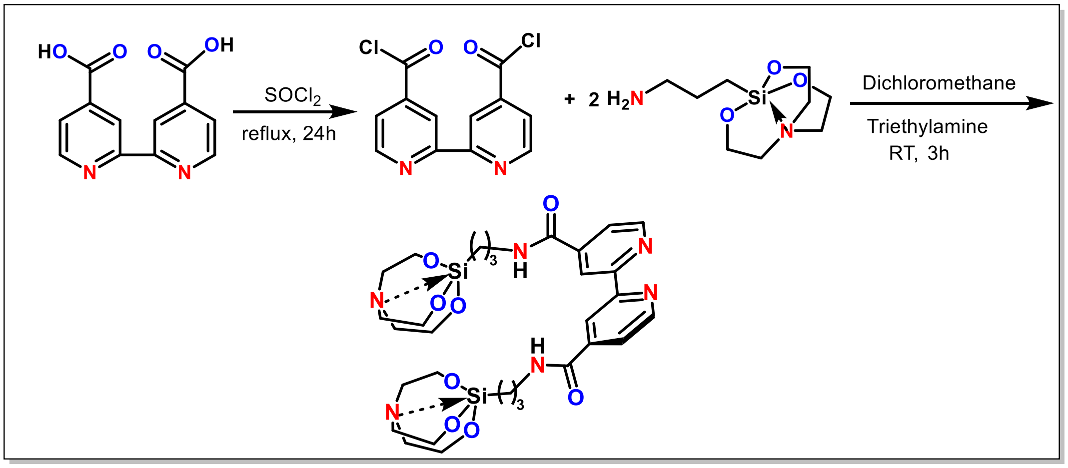

Figure 3.7: Synthesis of 2,2'-bipyridine-4,4'-diamidopropylsilatrane (bpysil)

^{1}H NMR: δ_H (400 MHz; $CDCl_3$) 8.77 – 8.73 (4H, m, CH), 7.9 (2H, s, CH), s, 7.68 (2H, m, NH), 3.78 (12H, t, CH_2), 3.49 (4H, q, CH_2), 2.80 (12H, t, CH_2), 1.80 (4H, p, CH_2), 0.56 (4H, t, CH_2).

Synthesis of complex 2a:

Ni(II)bpySil

The above synthesized bipyridine silatrane ligand was added to a round bottom and purged under N_2. On transferring to the glovebox, the ligand was allowed to dissolve in 25mL warm (~40°C) acetonitrile and excess $NiBr_2$.DME was added. The resulting green solution was allowed to stir overnight and filtered outside the glovebox to yield complex 2a.

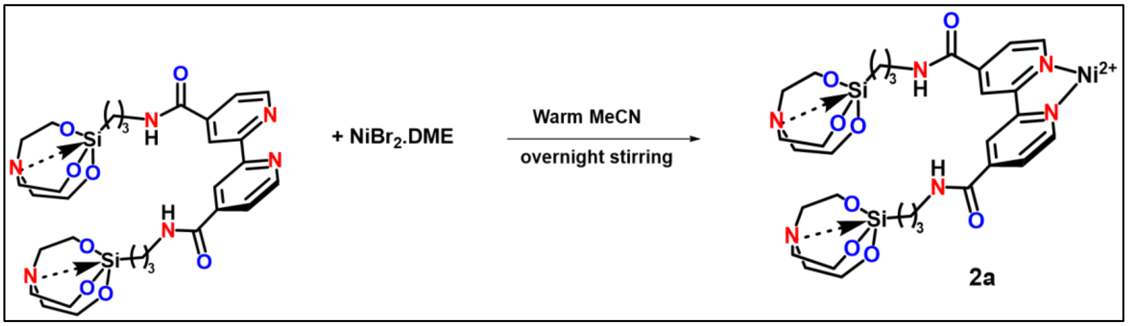

Figure 3.8: Synthesis of molecular complex 2a

Synthesis route to form immobilized 2b:

Ni(II)bpySilISiO$_2$

As surface-anchoring functional groups are designed to chelate metals, stability during formation of an inorganic complex is crucial. Reports based on hydroxamic acids functional groups with strong metal oxide binding, have found them to be incompatible during metal complex formation due to their strong tendency to chelate.[17, 29] In contrast, the silatrane functional group linker is protected from these side-reactions due to its caged structure, thus limiting any unwanted side reactions. Thus, for anchoring 2a onto the silica oxide support, a procedure previously reported by Brudvig and coworkers was followed.[21] 1mmol of synthesized complex 2a and 100mg silica A300 added to 25mL anhydrous MeCN. The resulting mixture was then refluxed in MeCN overnight under nitrogen. The solution was then filtered, and the solid (2a|SiO_2) was rinsed with diethyl ether and air dried prior to further analysis.

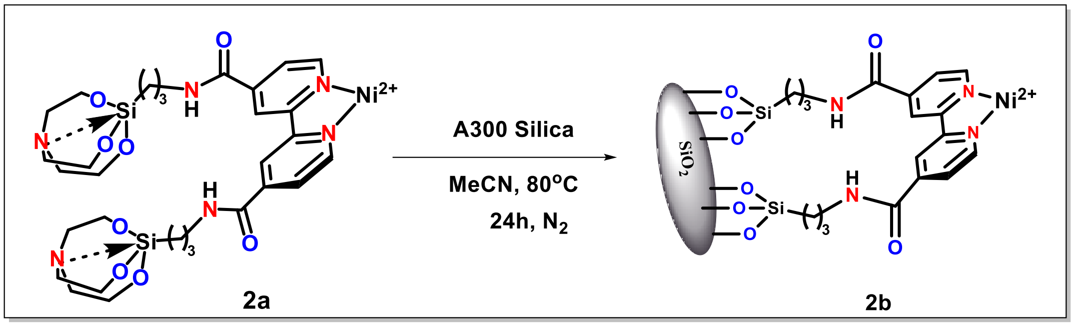

Figure 3.9: Procedure for immobilizing complex 2a onto silica support.

As discussed previously, the silatrane cage deprotects on the metal oxide surface to form covalent siloxyl bonds. Although deprotection of the silatrane cage on TiO_2 and SnO_2 surfaces has been well studied, its stability on SiO_2 supports hasn't been explored yet. Thus, its comparison to the carboxylic acid analogue provides a good basis for understanding interfacial chemistry of both the anchoring groups and in turn, help understand the reactivity trends during catalysis.

3.3b Instrumentation

Inductively coupled plasma-mass spectrometry (ICP-MS, Finnigan ELEMENT XR double focusing magnetic field) analysis was used for the analysis of nickel present on silica with rhenium as internal standard. A quartz torch and injector (Thermo Fisher Scientific) and a 0.2 mL/min Micromist U-series nebulizer (GE, Australia) were used for sample introduction. GC−MS (Shimadzu QP-2010S) analysis was performed with a 30 m long Rxi-5 ms (Restek) separation column with a 0.25 mm id, and the oven temperature program was 40 °C for 0.5 min, followed by a 10 °C/min ramp to 280 °C and held for 2 min. Mass spectrometer electron ionization was at 70 eV, and the spectrometer was scanned from 1000 to 50 m/z at low resolution. NMR spectroscopy was performed using a Bruker Advance III HD 400. Data were processed using Bruker TopSpin software. ^{1}H NMR spectroscopy was performed using a 400 MHz instrument using deuterated chloroform or deuterated dimethyl sulfoxide as the solvent with a calibrated peak at 7.26 or 2.50 ppm, respectively.

3.3c Materials

All reagents were used as received from the manufacturer and were used without any further purification. The silica oxide support used throughout was Aerosil 300 (A300, Evonik). A300 is amorphous SiO_2 with a 300 m_2 /g surface area and an average particle size of 20 nm.

3.5 Conclusions

The results of the present study demonstrate successful synthesis of molecular/hybrid complexes and the differences between binding of carboxylic acid and silatrane anchoring groups. In summary, we find that the expected anchoring modes via the silatrane groups present the most stable surface binding for the molecular catalyst to A300 via the covalent Si-O-Si linkages. Since the findings discussed in this report are preliminary, future work on structural characterization via crystal structure, XES, XRD and elemental analysis of both NiBpyCOOH and NiBpySil molecular and hybrid complexes will provide further evidence for stability of these complexes on silica support. Preliminary assessment of these immobilized catalysts in cross coupling catalysis is currently ongoing. Additionally, we hypothesize that higher loading of NiBpySil on silica surface will lead to greater cross-coupled product yields compared to previously reported hybrid catalysts. Since, bimolecular degradation is a major inhibitor of homogeneous nickel catalysis, results from reactivity studies of these supported nickelbipyridine based molecular catalysts can help understand if stabilization due to silatrane linker can increase catalyst lifetimes, robustness, reactivity and prevent catalyst leaching. Thus, our study makes a further contribution to designing new generation of sustainable metal based molecular/hybrid catalysts.

3.6 References

1. Samantaray, M. K.; Pump, E.; Bendjeriou-Sedjerari, A.; D'Elia, V.; Pelletier, J. D. A.; Guidotti, M.; Psaro, R.; Basset, J.-M., Surface organometallic chemistry in heterogeneous catalysis. *Chemical Society Reviews* **2018**, *47* (22), 8403-8437.

2. Samantaray, M. K.; D'Elia, V.; Pump, E.; Falivene, L.; Harb, M.; Ould Chikh, S.; Cavallo, L.; Basset, J.-M., The Comparison between Single Atom Catalysis and Surface Organometallic Catalysis. *Chem Rev* **2020**, *120* (2), 734-813.

3. Pelletier, J. D. A.; Basset, J.-M., Catalysis by Design: Well-Defined Single-Site Heterogeneous Catalysts. *Accounts of Chemical Research* **2016**, *49* (4), 664-677.

4. Kim, Y.; Iwai, T.; Fujii, S.; Ueno, K.; Sawamura, M., Dumbbell-Shaped 2,2'-Bipyridines: Controlled Metal Monochelation and Application to Ni-Catalyzed Cross-Couplings. *Chemistry – A European Journal* **2021**, *27* (7), 2289-2293.

5. Kaes, C.; Katz, A.; Hosseini, M. W., Bipyridine: The Most Widely Used Ligand. A Review of Molecules Comprising at Least Two 2,2‘-Bipyridine Units. *Chemical Reviews* **2000**, *100* (10), 3553-3590.

6. Klein, A.; Kaiser, A.; Sarkar, B.; Wanner, M.; Fiedler, J., The Electrochemical Behaviour of Organonickel Complexes: Mono-, Di- and Trivalent Nickel. *European Journal of Inorganic Chemistry* **2007**, *2007* (7), 965-976.

7. Lin, B. L.; Clough, C. R.; Hillhouse, G. L., Interactions of Aziridines with Nickel Complexes: Oxidative-Addition and Reductive-Elimination Reactions that Break and Make C−N Bonds. *Journal of the American Chemical Society* **2002**, *124* (12), 2890-2891.

8. Yamamoto, T.; Wakabayashi, S.; Osakada, K., Mechanism of C□C coupling reactions of aromatic halides, promoted by Ni(COD)2 in the presence of 2,2′-bipyridine and PPh3, to give biaryls. *Journal of Organometallic Chemistry* **1992**, *428* (1), 223-237.

9. Davis, J. L.; Arndtsen, B. A., Comparison of Imine to Olefin Insertion Reactions: Generation of Five- and Six-Membered Lactams via a Nickel-Mediated CO, Olefin, CO, Imine Insertion Cascade. *Organometallics* **2011**, *30* (7), 1896-1901.

10. Matsunaga, P. T.; Mavropoulos, J. C.; Hillhouse, G. L., Oxygen-atom transfer from nitrous oxide (N□N□O) to nickel alkyls. Syntheses and reactions of nickel(II) alkoxides. *Polyhedron* **1995**, *14* (1), 175-185.

11. Bialek, M.; Cramail, H.; Deffieux, A.; Guillaume, S. M., Styrene polymerization using nickel(II) complexes as catalysts. *European Polymer Journal* **2005**, *41* (11), 2678-2684.

12. Khanduyeva, N.; Senkovskyy, V.; Beryozkina, T.; Bocharova, V.; Simon, F.; Nitschke, M.; Stamm, M.; Grötzschel, R.; Kiriy, A., Grafting of Poly(3-hexylthiophene) from Poly(4-bromostyrene) Films by Kumada Catalyst-Transfer Polycondensation: Revealing of the Composite Films Structure. *Macromolecules* **2008**, *41* (20), 7383-7389.

13. Déjardin, C.; Renou, A.; Maddaluno, J.; Durandetti, M., Nickel-Catalyzed Electrochemical Cyclization of Alkynyl Aryl Iodide and the Domino Reaction with Aldehydes. *The Journal of Organic Chemistry* **2021**, *86* (13), 8882-8890.

14. Mikhaylov, D. Y.; Gryaznova, T. V.; Budnikova, Y. G.; Sinyashin, O. G., Electrocatalytic fluoroalkylation of olefins. *Russian Chemical Bulletin* **2010**, *59* (10), 1918-1920.

15. Yamaguchi, Y.; Ichioka, H.; Klein, A.; Brennessel, W. W.; Vicic, D. A., Linear Bis(perfluoroalkyl) Complexes of Nickel Bipyridine. *Organometallics* **2012**, *31* (4), 1477-1483.

16. Brennan, B. J.; Llansola Portolés, M. J.; Liddell, P. A.; Moore, T. A.; Moore, A. L.; Gust, D., Comparison of silatrane, phosphonic acid, and carboxylic acid functional groups for attachment of porphyrin sensitizers to TiO2 in photoelectrochemical cells. *Physical Chemistry Chemical Physics* **2013**, *15* (39), 16605-16614.

17. Materna, K. L.; Crabtree, R. H.; Brudvig, G. W., Anchoring groups for photocatalytic water oxidation on metal oxide surfaces. *Chemical Society Reviews* **2017**, *46* (20), 6099-6110.

18. Bae, E.; Choi, W.; Park, J.; Shin, H. S.; Kim, S. B.; Lee, J. S., Effects of Surface Anchoring Groups (Carboxylate vs Phosphonate) in Ruthenium-Complex-Sensitized TiO2 on Visible Light Reactivity in Aqueous Suspensions. *The Journal of Physical Chemistry B* **2004**, *108* (37), 14093-14101.

19. McNamara, W. R.; Snoeberger Iii, R. C.; Li, G.; Richter, C.; Allen, L. J.; Milot, R. L.; Schmuttenmaer, C. A.; Crabtree, R. H.; Brudvig, G. W.; Batista, V. S., Hydroxamate anchors for water-stable attachment to TiO2 nanoparticles. *Energy & Environmental Science* **2009**, *2* (11), 1173-1175.

20. McNamara, W. R.; Milot, R. L.; Song, H.-e.; Snoeberger Iii, R. C.; Batista, V. S.; Schmuttenmaer, C. A.; Brudvig, G. W.; Crabtree, R. H., Water-stable, hydroxamate anchors for functionalization of TiO2 surfaces with ultrafast interfacial electron transfer. *Energy & Environmental Science* **2010**, *3* (7), 917-923.

21. Materna, K. L.; Brennan, B. J.; Brudvig, G. W., Silatranes for binding inorganic complexes to metal oxide surfaces. *Dalton Transactions* **2015**, *44* (47), 20312-20315.

22. Brennan, B. J.; Keirstead, A. E.; Liddell, P. A.; Vail, S. A.; Moore, T. A.; Moore, A. L.; Gust, D., 1-(3′-amino)propylsilatrane derivatives as covalent surface linkers to nanoparticulate metal oxide films for use in photoelectrochemical cells. *Nanotechnology* **2009**, *20* (50), 505203.

23. Brennan, B. J.; Gust, D.; Brudvig, G. W., Organosilatrane building blocks. *Tetrahedron Letters* **2014**, *55* (5), 1062-1064.

24. Frye, C. L.; Vincent, G. A.; Finzel, W. A., Pentacoordinate silicon compounds. V. Novel silatrane chemistry. *Journal of the American Chemical Society* **1971**, *93* (25), 6805-6811.

25. Key, R. J.; Tengco, J. M. M.; Smith, M. D.; Vannucci, A. K., A Molecular/Heterogeneous Nickel Catalyst for Suzuki–Miyaura Coupling. *Organometallics* **2019**, *38* (9), 2007-2014.

26. Ayare, P. J.; Gregory, S. A.; Key, R. J.; Short, A. E.; Tillou, J. G.; Sitter, J. D.; Yom, T.; Goodlett, D. W.; Lee, D.-C.; Alamgir, F. M.; Losego, M. D.; Vannucci, A. K., Immobilization of molecular catalysts on solid supports via atomic layer

deposition for chemical synthesis in sustainable solvents. *Green Chemistry* **2021**, *23* (23), 9523-9533.

27. Gerasimova, T. P.; Katsyuba, S. A., Bipyridine and phenanthroline IR-spectral bands as indicators of metal spin state in hexacoordinated complexes of Fe(ii), Ni(ii) and Co(ii). *Dalton Transactions* **2013**, *42* (5), 1787-1797.

28. Dumitriu, A. M.-C.; Cazacu, M.; Shova, S.; Turta, C.; Simionescu, B. C., Synthesis and structural characterization of 1-(3-aminopropyl)silatrane and some new derivatives. *Polyhedron* **2012**, *33* (1), 119-126.

29. Brewster, T. P.; Konezny, S. J.; Sheehan, S. W.; Martini, L. A.; Schmuttenmaer, C. A.; Batista, V. S.; Crabtree, R. H., Hydroxamate Anchors for Improved Photoconversion in Dye-Sensitized Solar Cells. *Inorganic Chemistry* **2013**, *52* (11), 6752-6764.

CHAPTER 4

MOLECULAR HYDROGEN PRODUCTION VIA DUAL PHOTOCATALYTIC CYCLES[3]

---

[3] Pooja J. Ayare, Noelle Watson, Maizie R. Helton, Matthew J. Warner, Tristan Dilbeck, Kenneth Hanson, Aaron K. Vannucci. Manuscript in Preparation

4.1 Abstract

Hydrogen is a sustainable and renewable energy source that is a potential clean alternative to fossil fuel energy sources. Although extensive research has been done on hydrogen production by artificial photosynthesis, molecular Z-scheme based hydrogen formation by using efficient aryl-alcohol photocatalysts has not yet been reported. Here, we have developed a novel Z-scheme based molecular photocatalytic system by utilizing the light absorbing properties of aryl-alcohol photocatalysts for hydrogen production. We have shown that on simultaneous excitation of an Iridium-based photocatalyst and an aryl alcohol based photoacid in presence of a sacrificial electron donor, catalytic hydrogen production at significantly low reaction overpotentials (≤40meV) was achieved. Spectroscopic and electrochemical studies, control reactions, and GC analysis of headspace gas supports a Z-scheme based mechanism consisting of consisting of: 1) photoexcitation of PC, 2) reduction of excited state PC, 3) electron transfer from PC^- to photoexcited ROH, and 4) generation of H_2 from reduced ROH. This molecular Z-scheme thus circumvents the thermodynamic and overpotential constraints associated with reduction of weak acids in their ground-state and offers a new paradigm for the conversion of light energy into H_2 bond energy.

4.2 Introduction

The conversion of solar energy into chemical bond energy via photosynthetic organisms is the foundation of life on earth. Given its ubiquity and utility, considerable efforts are underway to realize efficient “artificial” photosynthesis[1-3] that harnesses solar energy for the production of chemical fuels such as hydrogen (H_2) to meet the energy consumption needs of humans.[4] The inherent thermodynamic driving forces combined with reaction overpotentials[5] make it difficult to form chemical bonds with the energy of a single photon that is typically absorbed by photosynthetic chromophores.[6] Nature circumvents this limitation by using a Z-Scheme (Figure 4.1, left) which combines the energies of two independent light absorption events to meet the energetic requirements necessary to drive chemical bond breaking/making.[7-8]

For both natural and artificial photosynthetic systems, there are stringent thermodynamic requirements that must be met for chemical fuels generation. For example, the minimum energy required to generate H_2 from a weak acid is dependent on the pK_a of the acid (p$K_{a,HA}$) as described in equation 4.1:

$$E_{HA}^{o} = E_{H+}^{o} - \frac{2.303RT}{F}\mathrm{p}K_{a,HA} \quad (4.1)$$

where $E°_{HA}$ is the reduction potential of the weak acid in its ground-state, $E°_{H^+}$ is the thermodynamic potential required to reduce a proton in a given solvent, R and F are the gas and Faraday's constants respectively, and T is the temperature.[9] Consequently, the reduction of weak acids in acetonitrile solution thermodynamically require between -0.3 to -1.5 eV vs. the saturated calomel electrode (SCE) at room temperature. Additionally, experimental results consistently show that an overpotential energy, beyond the minimal thermodynamic requirement, is needed to reduce weak acids at reasonable rates.[5, 10] Overpotentials between 0.1 and 1.0 eV are common,[5, 10] even for platinum metal catalysts.[9, 11] Thus, Z-schemes require photon energies much greater than the thermodynamic reduction potentials in order to achieve H_2 production at reasonable rates.[4] Designing a catalytic H_2 generation scheme that efficiently exploits excited-state electron transfers for the reduction event could minimize reaction overpotentials and would represent a breakthrough in solar energy conversion.[12]

There has been progress in developing Z-schemes for artificial photosynthetic systems using a variety of approaches including multijunction solar cells, quantum dots, and tandem dye-sensitized photoelectrosynthesis cells.[13-20] These artificial Z-schemes are composed of inorganic (i.e. semiconductor based) light absorbing/charge transport materials and often require additional, optically inactive, transition metal catalysts to perform the bond breaking/making reactions. While the transition metal catalysts are used to help minimize reduction overpotentials, overpotentials of > 0.1 eV are still commonly observed.[13] Judicious construction of the systems is also necessary to ensure proper charge transfer and redox reactivity. To date, however, a fully molecular based artificial Z-scheme for converting solar energy to chemical bonds has yet to be realized.

Here we show that upon excitation of both a photocatalyst (PC) and an aryl alcohol (ROH) in the presence of a sacrificial electron donor and a proton source results in the photocatalytic generation of H_2. The proposed dual catalytic cycle consists of reduction of excited state PC ($PC^* + e^- \rightarrow PC^-$), electron transfer from PC^- to the excited ROH ($PC^- + ROH^* \rightarrow PC^- + ROH^-$), followed by the production of H_2. Regeneration of ROH can also be achieved with phenol (PhOH) as the sacrificial proton source ($RO^- + PhOH \rightarrow ROH + PhO^-$).

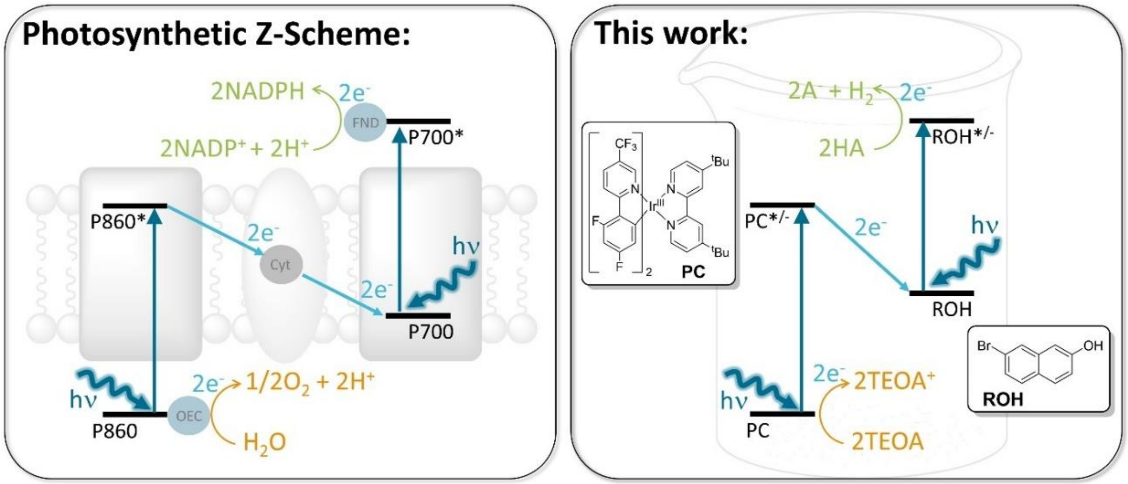

Figure 4.1. A simplified depiction of the natural photosynthetic Z-scheme (left), and the molecular Z-scheme reported here (right). TEOA = triethanolamine, HA = weak acid.

This “molecular Z-scheme” (Figure 4.1, right) circumvents the thermodynamic and overpotential constraints associated with reduction of weak acids in their ground-state and offers a new paradigm for the conversion of light energy into H_2 bond energy.

4.3 Results and Discussion

To realize a molecular Z-scheme, 7-bromo-2-naphthol (ROH) was chosen as an aryl alcohol proton source due to its long-lived triplet excited state ($\tau^{3}_{ROH^{*}}$ = 15 ms; as shown in Figure 4.2) to enable diffusion limited, bimolecular reactions.[21] Also, in the ground state, ROH has a relatively high reduction potential (E^{o}_{red} = -1.39 V vs SCE in MeCN) and is only weakly acidic (pK_a = 27.9 in MeCN) such that it is unfavorable for direct reduction of ROH to ROH^- and/or H^+ to H_2 by common reduction photocatalysts. Ir(dF-CF_3-ppy)$_2$(dtbpy)$^+$, where dF-CF_3-ppy is 2-(2,4-difluorophenyl)-5-(trifluoromethyl)pyridine and dtpby is 4,4′-tertbutyl-2,2′-

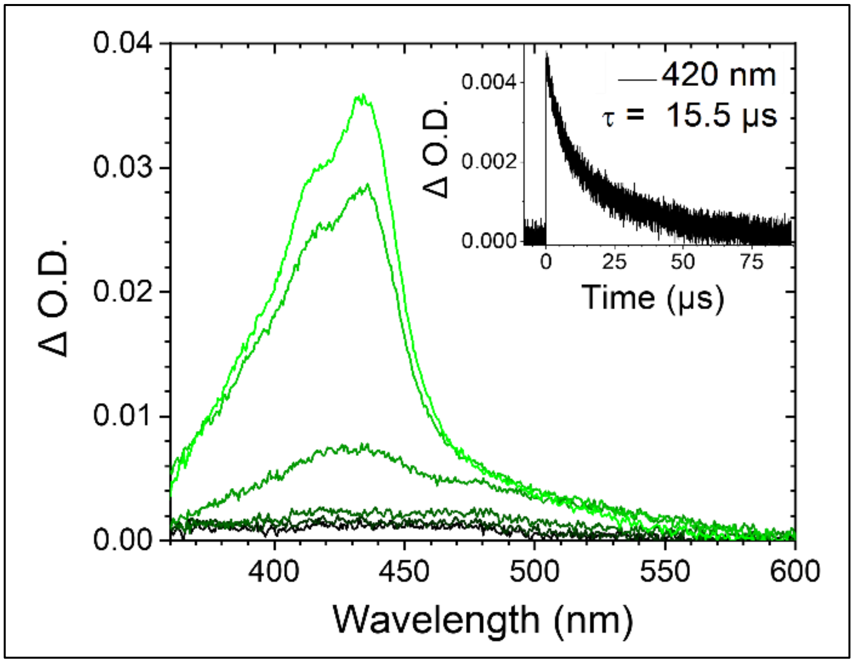

Figure 4.2: Transient absorption spectra for ROH in MeCN (lex = 335 nm). Inset: DO.D. at 420 nm versus time with the lifetime determined from a single exponential fit to this decay

bipyridine, was chosen as the photocatalyst (PC) due to its long triplet excited-state lifetime (PC) due to its long triplet excited-state lifetime ($t_{^3PC^*}$ = 2.2 ms; Figure 4.3) and its excited-state oxidation potential is thermodynamically below the reduction potential of the ground state of ROH.22 Lastly, triethanolamine (TEOA) was used as the sacrificial electron donor because its potential is favorable for the reduction of 3PC* but not 3ROH*.

With system design in hand, broadband irradiation of an MeCN solution containing 100 mM ROH, 150 mM TEOA, and 2.5 mol% PC (0.07 mmols) for six hours resulted in 0.16 mmol of H_2 corresponding to a turnover number (TON) of 4.5 and 0.1 for the PC and ROH, respectively. While these initial TONs are modest, the results confirm the ability of the system to photocatalytically produce H_2, with respect to the PC, without the need for a secondary transition metal catalyst to

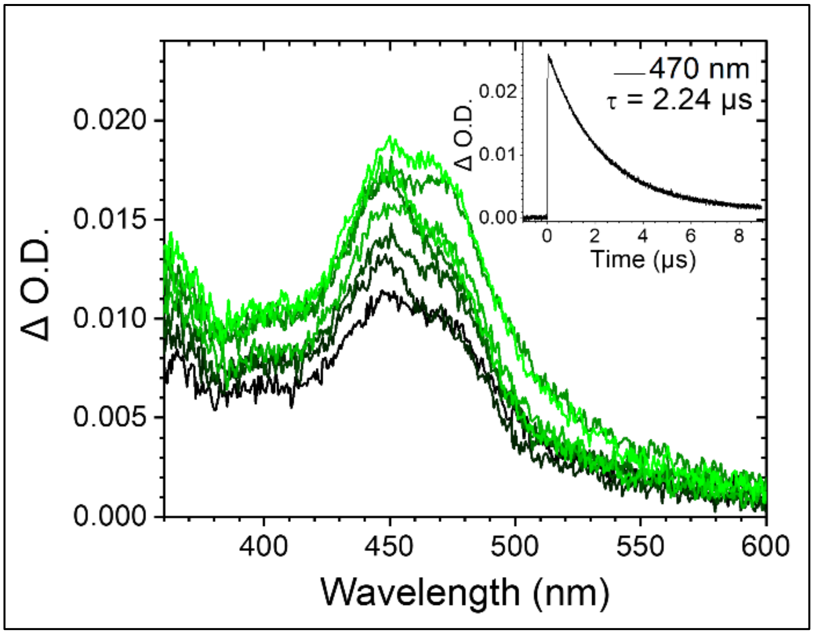

Figure 4.3: Transient absorption spectra for PC in MeCN (l$_{ex}$ = 375 nm). Inset: DO.D. at 470 nm versus time with the lifetime determined from a single exponential fit to this decay.

promote the hydrogen bond making reaction.[22] To investigate the mechanism of this reaction, a series of control experiments were performed, and the results are summarized in Table 4.1. Three different light conditions were used 1) broadband light (200-700 nm) capable of exciting both PC and ROH, 2) blue light (400-500nm) that can excite PC but not ROH in darkness where no photoexcitation is occurring. Only with broadband light capable of exciting both the PC and ROH was a measurable quantity of H_2 observed (entry 1, Table 4.1). The lack of H_2 generation under blue light (entry 2) and in the dark (entry 3) implies that both the PC and ROH must be excited for the reaction to occur. Selective removal of TEOA (entry 4) or PC (entry 5) resulted in no measurable quantities of H_2 suggesting that PC* and its reduction product by TEOA (i.e. PC$^-$) are necessary events in the catalytic solution.

Table 4.1: Summary of various reaction conditions and the resulting quantity of H_2

Entry	**Reaction Condition**					**Product Outcome**		
	[PC] (mM)	**[ROH] (mM)**	**[TEOA] (mM)**	**Light[b]**	**Other**	**mmol H_2[c]**	**TON $_{PC}$[d]**	**TON $_{ROH}$[e]**
1	2.5	100	150	Broadband	-	0.16	4.5	0.1
2	2.5	100	150	Blue	-	0	0	0
3	2.5	100	150	-	-	0	0	0
4	2.5	100	-	Broadband	-	0	0	0
5	-	100	150	Broadband	-	0	0	0
6	-	100	-	-	100 mM PC^-	0	0	0
7	-	100	-	Broadband	100 mM PC^-	0.42	0.3	0.3
8	2.5	-	150	Broadband	-	0.03	0.9	N/A
9	-	100	-	-	3.08 mM K	0.95	N/A	0.7
10	2.5	-	150	Broadband	100 mM MCA	0.06	1.6	N/A
11	***2.5***	***10***	***150***	***Broadband***	***100 mM PhOH***	***1.50***	***42.9***	***10.7***
12	2.5	-	150	Broadband	100 mM PhOH	0.08	2.3	N/A

[a]Reaction vessel contained 28 mL of acetonitrile and 3.5 mL of N_2 purged headspace. [b]450W Hanovia Hg lamp (Broadband) or 34 W Kessil H150 (Blue). [c]All reactions performed in at least duplicate and mmol of H_2 are reported with ±5% accuracy. [d]TON with respect to PC. [e]TON with respect to ROH.

The lack of H_2 generation under blue light (entry 2) and in the dark (entry 3) implies that both the PC and ROH must be excited for the reaction to occur. Selective removal of TEOA (entry 4) or PC (entry 5) resulted in no measurable quantities of H_2 suggesting that PC* and its reduction product by TEOA (i.e. PC^-) are necessary events in the catalytic solution. To gain further insights into the role of PC^- and ROH, PC^- was prepared by chemical reduction with potassium and then stirred with ROH in the dark for 6 hours (entry 6). GC analysis showed no H_2 production suggesting that PC^- does not reduce ground-state ROH. However, a mixture of PC^- and ROH under broadband irradiation for 6 hours (entry 7) resulted in similar H_2 production () to the complete reaction mixture (TON = 0.3 relative to ROH versus TON = 0.1, entry 1). In addition, electrochemical measurements using an indium tin oxide electrode modified with PC[23] under reducing bias (-0.4 V vs. SCE) gave minimal photocurrent response (<10 mA) (Figure 4.4).

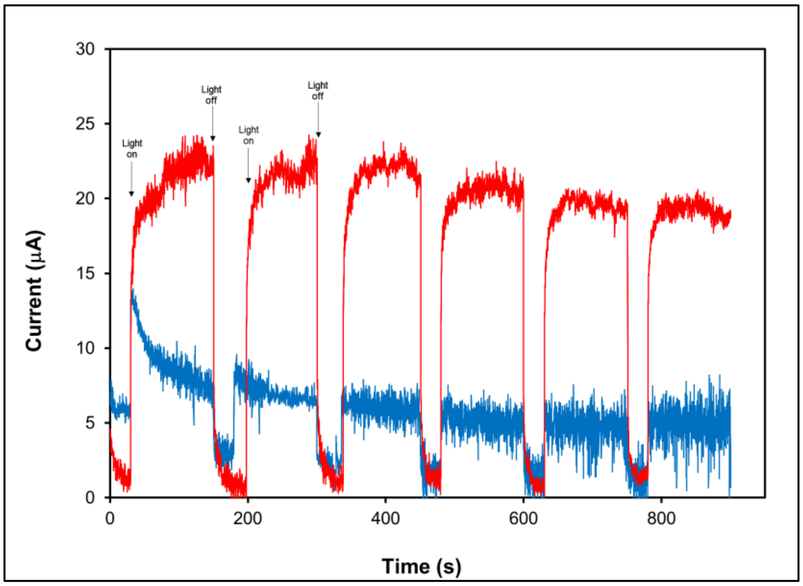

Figure 4.4: Controlled potential electrolysis of a PC functionalized ITO working electrode held at -0.4 V vs. SCE in an N_2 deaerated MeCN solution containing 0.1 M NBu_4PF_6, without (blue) and with (red) 4mM ROH. Irradiation of the sample with light from the broadband light source was turned on and off as denoted in the figure.

Upon the addition of ROH, however, switchable photocurrents of >15 mA were observed indicating that ROH* can serve as an electron transfer relay in the electrolyte solution (i.e. PC^- + ROH* → PC^- + ROH^-). Collectively these results suggest that the formation of PC^- and photoexcitation of ROH are necessary for H_2 production in this catalytic system. As an aside, it is worth noting that a small but measurable amount of H_2 was produced from a solution containing just PC and TEOA (i.e. without ROH, entry 8), This H_2 production most likely occurred from chemical decomposition of the oxidized TEOA.[24] This is an important observation because TEOA is a commonly used sacrificial electron donor in photocatalytic H_2 producing systems,[25] however we were unable to find a report that considered TEOA as a source for H_2. Regardless, in the current study, the amount of H_2 from TEOA was negligible compared to the system containing PC^- and ROH* indicating that TEOA is not necessary for the production of H_2.

We envisioned two possible pathways for the photocatalytic generation of H_2 from PC^- and ROH*: the reduction of ROH* by PC^- to generate ROH^-, followed by H_2 production (eq 4.2) or the generation of acidic protons by ROH* (eq 4.3) that are then reduced by PC^- (eq 4.4).

$$2ROH^* + 2e^- \rightarrow 2ROH^- \rightarrow H_2 + 2RO^- \qquad (4.2)$$

$$2ROH^* \rightarrow 2RO^- + 2H^+ \qquad (4.3)$$

$$2H^+ + 2e^- \rightarrow H_2 \qquad (4.4)$$

To investigate a possible bimolecular reaction between two ROH^- molecules to generate H_2, ROH was chemically reduced with potassium metal (Table 1, entry 9) and significant H_2 production (0.95 mmol) was observed with the primary organic product being RO^-. This corresponds to a nearly 70% conversion of the protons from ROH to H_2. Furthermore, kinetic studies under chemical reduction conditions showed that H_2 production scaled linearly with the concentration of ROH to the second power, consistent with a second order reaction with respect to ROH. Electrochemical reduction of ROH was also monitored with UV-visible absorption spectra, and a clear isosbestic point for the conversion of ROH to RO^- was observed as shown in Figure 4.5. This result indicates that the bimolecular reaction that generates H_2 is rapid in comparison to the experimental time frame as ROH^- was not observed. These experiments are consistent with the mechanism proposed in equation 1, but do not necessarily rule out the photoacid mechanism shown in eq 3 and 4.

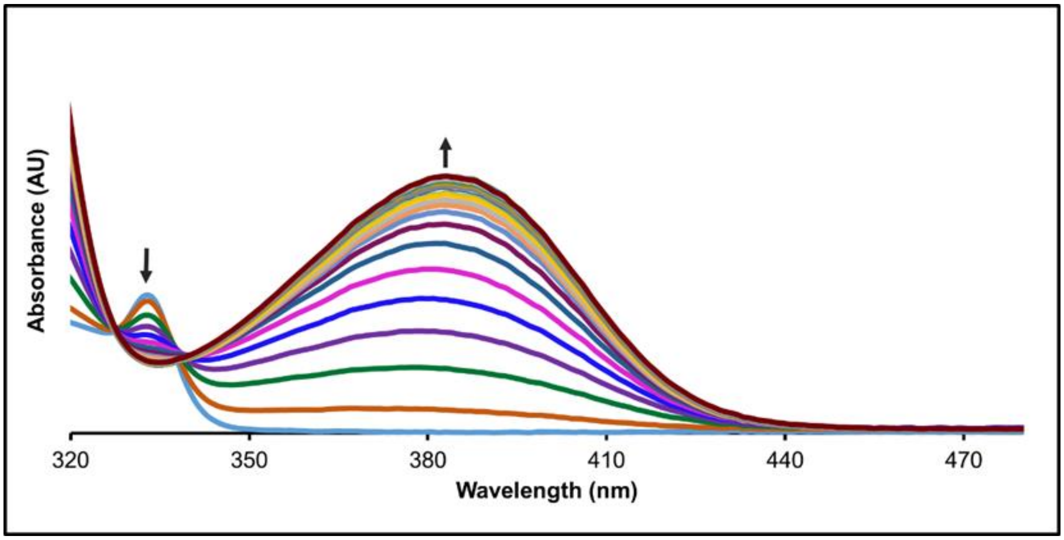

Figure 4.5: UV-Visible absorption spectra of an MeCN solution containing 4.0 mM ROH and 0.1 M NBu_4PF_6 under an applied bias of -1.5 V vs. SCE. Absorption spectra were acquired every 2 seconds.

Naphthol and its derivatives are known transient photoacids with notably increased acidities in the excited state.[26] Following excitation and $^3ROH^*$ formation, the pK_a of ROH decreases from 27.9 (in MeCN) to 16.4 as determined from a Förster cycle analysis (see SI for details).[27-29] This transient acidity increases the H^+ concentration in solution (eq 4.2) which could be followed by the reduction of H^+(eq 4.3). To test the role of solution acidity in H_2 production, chloroacetic acid (MCA, pK_a = 15.3) was used as a surrogate for $^3ROH^*$. Under standard reaction conditions 0.06 mmol H_2 was produced from 100 mM MCA (entry 10), which is nearly three-fold lower than the solution containing ROH (entry 1). It is important to note that the effective concentration of $^3ROH^*$ is <0.1 mM because it is limited by photon flux and the excited state lifetime, and thus the H^+ concentration for a solution containing 100 mM ROH is many orders of magnitude lower than for 100 mM MCA. Consequently, the low H_2 production from MCA indicates that solution acidity plays a minimal role in H_2 production from the catalytic solution. Instead, ROH* is acting as an electron acceptor/shuttle which then facilitates H_2 formation via a bimolecular reaction between ROH^- (eq 4.1). This observation opens interesting opportunities for aryl alcohol molecules to serves as the chemical, electrochemical, and/or photochemical catalysts for the production of H_2. It is worth note that the catalytic production of H_2 from excitation of a brominated naphthol containing solution has been observed before.[28] In that report, the authors proposed that the excited state photoacidity of 6-bromo-2-naphthol was sufficient to protonate a well-known cobalt-diglyoxime secondary catalyst, followed by H_2 generation.[30-31] However, their "anomalously large" rate constant for the proposed protonation[28] and the results above suggest that reduction of excited 6-bromo-2-naphthol by Co^I-diglyoxime followed by H_2 generation may have been an operable reaction mechanism in their study.

Collectively the above results are consistent with the energy level diagram depicted in Figure 4.6. Photon absorption by PC is followed by reductive quenching of $^3PC^*$ by TEOA to generate PC^- (1). A photon is also absorbed by ROH, and the resulting $^3ROH^*$ is reduced by PC^- [2]. ROH^- molecules then undergo a rapid bimolecular reaction to generate H_2 and RO^- [3]. Electron transfer events 4-6 in Figure 2 are thermodynamically unfavorable and not observed. The net reaction is the reduction of ROH by TEOA to generate H_2, which cannot occur in the ground-state or by ROH excitation alone. The reaction is made energetically accessible via the excitation of both PC and ROH, analogous to the Z-scheme of photosynthesis. This cooperative strategy puts less energetic restrictions on the catalyst and light harvesting components enabling new design strategies for solar fuels formation.

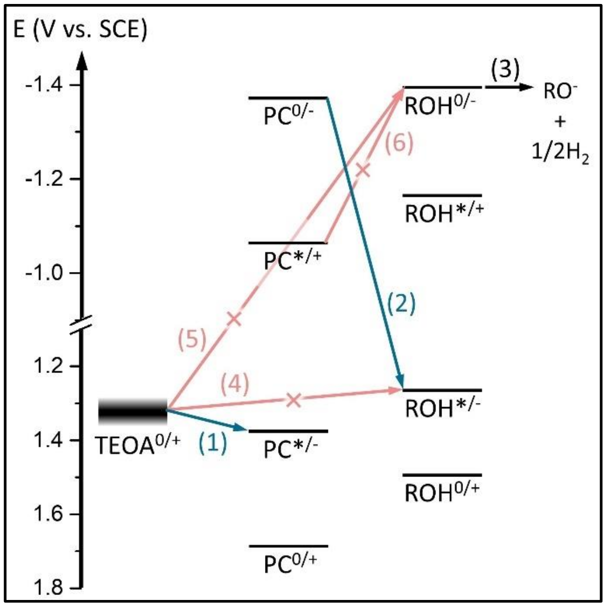

Figure 4.6: Energy level diagram for TEOA, PC, and ROH with energetically favorable and unfavorable processes depicted by blue and red arrows, respectively. Excited state potentials are for triplet excited states (i.e. $^3PC^*$ and $^3ROH^*$).

As described above, irradiation of a solution containing PC, ROH, and TEOA results in the photocatalytic production of H_2 and RO^-. That reaction, however, is only catalytic with respect to PC, and not ROH, and will stop when ROH is consumed. To regenerate ROH during the catalytic reaction, phenol (PhOH) was added as a sacrificial proton source. Broadband irradiation of an acetonitrile solution containing 2.5 mM PC, 10 mM ROH, 100 mM PhOH, and 150 mM TEOA resulted in the formation of 1.5 mmols of H_2 which corresponds to a TON of 42.9 with respect to the PC and 10.7 with respect to ROH (Table 4.1, entry 11). Removal of ROH from the reaction (entry 12) resulted in a nearly 20-fold decrease in H_2 indicating that PhOH is not solely responsible for the H_2 increase, and $^3ROH^*$ is needed for high H_2 production.

The pK_a of PhOH[9] and ROH in MeCN are 27.2 and 27.9, respectively. Consequently, the acid-base equilibrium constant (equation 4.5) indicates that PhOH to RO^- proton transfer is favorable.

$$RO^- + PhOH \rightleftharpoons ROH + PhO^- \qquad K_{eq} = 5.0 \qquad (4.5)$$

Furthermore, ^1H NMR spectra of a solution containing RO^- and PhOH shows the formation of ROH and confirms that PhOH can protonate RO^-. This regeneration step closes the catalytic cycle with respect to ROH and results in a dramatic increase in TON_{ROH}. The regeneration of ROH from RO^- may also prevent homoconjugation between ROH and its conjugate base ($RO^{-\cdots}H\text{-}OR$), an interaction that is known to impede catalytic H_2 generation.[32-33]

The proposed photocatalytic mechanism for the production of H_2 from a solution of PC, ROH, TEOA, and PhOH is shown in Figure 4.7. This reaction generates H_2 from the relatively unreactive TEOA and PhOH, a thermodynamically unfavorable process by 2.65 eV, but is enabled by the additive effects of two independent excitation events in a dual catalytic Z-scheme. Furthermore, the highest energy electron generated (ROH^-) has a thermodynamic energy of only

0.04 eV above the thermodynamic potential required to reduce PhOH. Thus, this molecular Z-scheme minimizes the overpotentials associated with catalytic H_2 production.

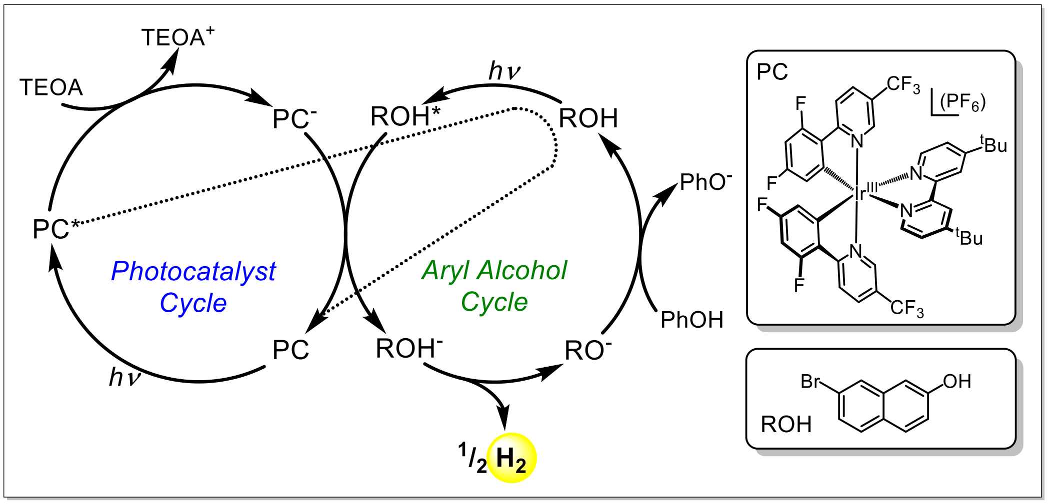

Figure 4.7: Proposed mechanism for the catalytic generation of H_2 from PhOH and TEOA in molecular Z-scheme consisting of photocatalyst (PC) and aryl alcohol (ROH) cycles.

Further support for the mechanism in Figure 4.7 is provided by transient absorption spectroscopy (TA); the key results are shown in Figure 4.8.

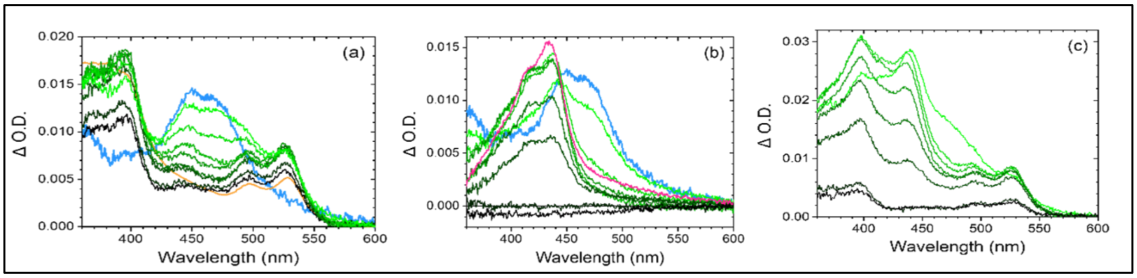

Figure 4.8: Transient absorption spectra of a) PC and TEOA (1:10; l_{ex} = 375 nm) with ^{3}PC* (at 5 ns) in blue and the chemically generated PC$^-$ spectrum in orange, b) PC and ROH (1:10; l_{ex} = 375 nm) with ^{3}PC* and ^{3}ROH* (at 5 ns) in blue and red, respectively, and c) PC, TEOA, and ROH (1:20:10; l_{ex} = 335 nm) in MeCN. Time slices progress from green to black at 0.005, 0.5, 1.0, 2.0, 5.0, 10.0, 100, and 1000 ms.

Two different excitation wavelengths were used: 375 nm for the excitation of PC and 335 nm for excitation of both PC and ROH. Upon 375 nm excitation of a MeCN solution containing only PC and TEOA (Figure 4.8a), there is a rapid (<1 ms) decrease in the ^{3}PC* feature (425-500 nm, followed by the formation of a structured absorption spectra resembling that of the chemically generated PC$^-$ via reduction with potassium. This is consistent with the previously reported reductive quenching reaction, ^{3}PC* + TEOA → PC$^-$ + TEOA$^+$, that occurs with a near diffusion limited Stern-Volmer quenching constant of 7 × 10^8 M/s as shown in Figure 4.9.[34]

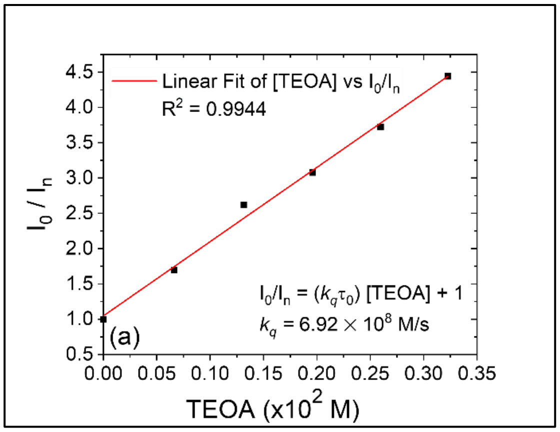

Figure 4.9: Stern-Volmer analysis of the integrated intensity for quenching of 20 mM PC by TEOA in MeCN (l_{ex} = 375 nm, l_{em} = 473 nm

The resulting PC$^-$ lifetime is significantly longer than our acquisition time window (>1 ms). In contrast, the excited state decay of ^{3}ROH* (t ≈ 15 ms) was unperturbed by the addition of TEOA.

For a solution containing only PC and ROH, excitation of only the PC at 375 nm (Figure 4.8b) resulted in a TA spectral shift consistent with the ^{3}PC* to ROH triplet energy transfer with a Stern-Volmer quenching constant of ~8 × 10^9 M/s as can be seen in Figure 4.10.

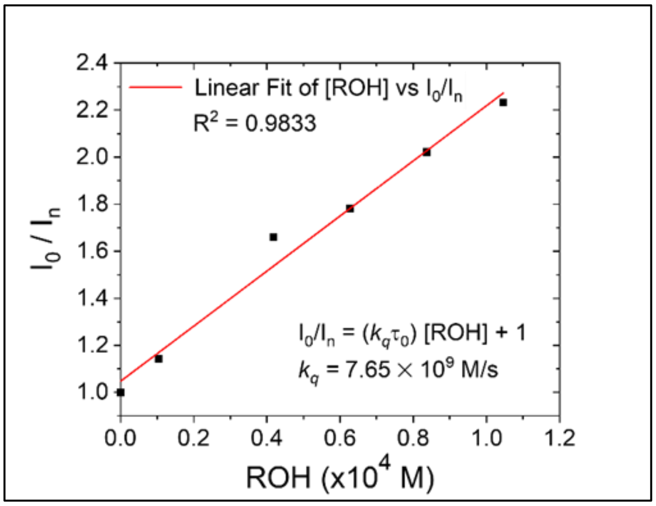

Figure 4.10: Stern-Volmer analysis for the integrated emission quenching of 20 mM PC* by ROH in MeCN (l_{ex} = 375 nm).

Importantly, in Figure 4.8b there are no indications of the formation of PC^+/PC^- or an increased rate of ^{3}ROH* decay (375-475 nm) demonstrating that no redox events are occurring and that ^{3}PC* to ROH energy transfer is the only excited state interaction upon sole excitation of the PC. Also, as indicated in Figure 4.11, excitation of both PC and ROH at 335 nm resulted in a similar ^{3}PC* to ^{3}ROH* spectral evolution, but with a larger initial contribution from ^{3}ROH* ($l_{max} \approx 440$ nm) from direct excitation of ROH. Interestingly, although this triplet sensitization mechanism (dashed line in Figure 4.7) is competitive with the formation of PC^-, it is still a productive pathway as it also generates the reactive ^{3}ROH* species.

In a solution containing PC, ROH, and TEOA, 335 nm excitation was again followed by the rapid disappearance of ^{3}PC* feature, but now with the sustained presence of PC^- and ^{3}ROH* spectral signatures (Figure 4.8c) consistent with the

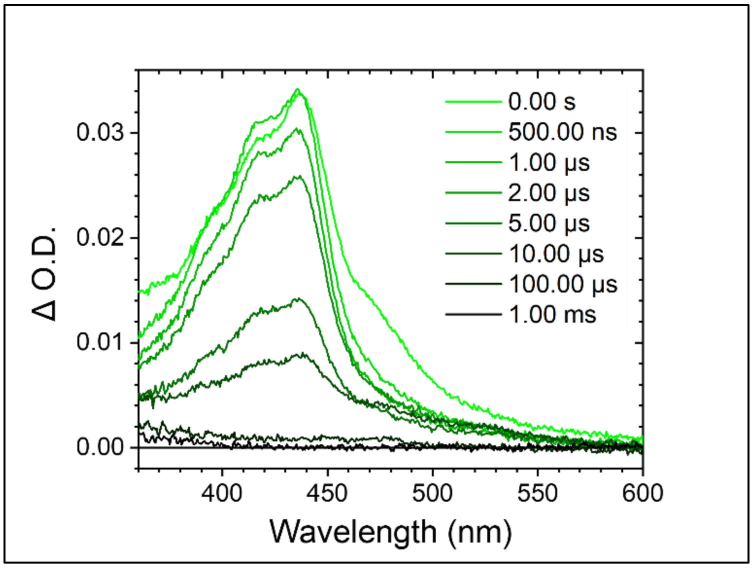

Figure 4.11: Transient absorption spectra for PC and ROH (1:10) in MeCN (l_{ex} = 335 nm).

mechanistic steps at the top of the catalytic cycles in Figure 4.7. Similar results were observed with 375 nm excitation presumably through the triplet sensitization mechanism (dashed line in Figure 4.7). Concomitant decay for PC^- ($l_{max} \approx 370$ nm) and $^3ROH^*$ ($l_{max} \approx 440$ nm) occurs with a lifetime of ~10 ms which is faster than the intrinsic decay of PC^- (t >1 ms) and $^3ROH^*$ (t ≈ 15 ms) suggesting a cooperative decay mechanism. Based on the results above, we attribute this cooperative decay to reduction of $^3ROH^*$ by PC^-. We observed no spectral features that would be indicative of ROH^- formation, which is also consistent with the electrochemical reduction of ROH where H_2 generation was the rapid step.

Collectively, these spectroscopic results are consistent with the mechanism in Figure 4.7 which was proposed based on the experiments in Table 4.1 and the electrochemical data. The spectroscopic studies also indicate that $^3ROH^*$ generation via $^3PC^*$ sensitization can occur, effectively making this a tri-catalytic reaction solution but with the sensitization process being redundant and less efficient than direct excitation of ROH. Nonetheless, with sufficient blue photon flux we anticipate that H_2 generation could occur via the $^3PC^*$ to ROH triplet sensitization step, but minimal H_2 was observed under our excitation conditions (35 W blue LED).

4.4 Conclusions

A fully molecular Z-scheme for the production of H_2 has been realized. Concurrent photoexcitation of a molecular photocatalyst and an aryl alcohol in the presence of an amine electron-donor and a phenol proton source resulted in the catalytic generation of H_2. A series of chemical and electrochemical control reactions support a dual catalytic mechanism that exploits excited-state electron transfers involving the photocatalyst and a substituted naphthol molecule as the aryl alcohol. These electron transfers catalyze the reduction of phenol by triethanol amine to generate H_2. TA data further supports this proposed mechanism and gives evidence for a possible third catalytic cycle involving energy transfer between the excited-state photocatalyst and the ground-state naphthol molecule. Importantly, this molecular Z-scheme also operates under low reaction overpotentials (≤ 0.04 eV), thus illustrating the advantages of utilizing aryl alcohols for light absorption *and* proton reduction. This new paradigm for the conversion of light energy into H_2 bond energy offers new research possibilities for solar energy conversion.

4.5 Experimental Section

Materials

All reagents were used as received from the manufacturer without further purification unless otherwise noted.

Instrumentation.

Photolysis Light Sources. The broadband light source used for photolysis experiments was a Hanovia 450 W medium arc Hg lamp (PC451.050) cooled in a quartz immersion well. The blue light source used in entry 2 of Table 4.1 was a 34 W Kessil H150W-BLUE LED.

H_2 measurements: Hydrogen gas was measured using a thermocouple detector installed in HP 5890 Series II gas chromatograph instrument. A Carboxen 1010 plot capillary GC column was used, and the carrier gas was high purity nitrogen (99.999%).

Absorption Spectra: Both standard and spectroelectrochemical absorption spectra were acquired on an Agilent Technologies Cary 8454 UV-Vis Spectrometer.

Steady-state Emission: An Edinburgh FLS980 fluorescence spectrometer was used to record emission spectra at room temperature and 77K. Excitation was provided by a a housed 450 W Xe lamp passed through a single grating 1800 l mm^{-1} Czerny-Turner monochromator (250 nm blaze). Emission was then passed through the appropriate long pass filter, a single grating Czerny−Turner monochromator (1800 l mm^{-1}, 500 nm blaze), and finally detected by a Peltier-cooled Hamamatsu R928 photomultiplier tube. Room temperature spectra were acquired on samples in a 1×1 cm quartz cuvette after either deaerating with N_2 or were prepared in a glovebox (N_2 atmosphere). A cold finger dewar filled with liquid nitrogen was used for measurements at 77K.

Time-resolved Emission: An Edinburgh FLS980 spectrometer was used to acquire time-resolved emission traces using multichannel scaling (MCS) acquisition mode. Samples were excited using a 60 W microsecond flashlamp (pulse width <2.5 μs) at a 100 Hz repetition rate. The Edinburgh software package was used to fit time-resolved data with a single exponential function, $y = A_1 e^{-kx} + y_0$.

Transient Absorption: For TA measurements, all samples were prepared in a glovebox (N_2 atmosphere) in a 1×1 cm quartz cuvette. Samples were kept optically dilute (O.D. < 0.5) in the visible region to ensure sufficient light transmission for the measurement. Data was acquired using Edinburgh LP980 laser flash photolysis spectrometer system equipped with a Continuum Surelite EX Nd:YAG laser and a Continuum Horizon OPO (5 ns IRF, operated at 1 Hz, beam diameter ~0.5 cm, 2.5−5 mJ/pulse). White probe light was generated using a 150 W Xe lamp, passed through the sample and monochromator before being detected using an intensified Andor iStar CCD camera. For time-resolved traces, a TMS302-A monochromator (1800 grooves/mm grating) with a 300 mm focal length in Czerny Turner configuration and a Hamamatsu R928 side window PMT were used. Edinburgh's L900 (version 8.2.3, build 0) software package was used to process detector outputs.

FT-IR: Samples for IR measurements were placed in an Omni-Cell liquid transmission cell and recorded by Nicolet S10 spectrometer with a 1 cm^{-1} resolution.

NMR spectroscopy: ^{1}H NMR was performed using a Bruker Advance III 400 with deuterated chloroform or deuterated dimethyl sulfoxide as the solvent with a calibrated peak at 7.26 and at 2.50 ppm, respectively. Data were processed using Bruker TopSpin software.

Spectroelectrochemical Measurements: Experiments were performed using a platinum honeycomb spectroelectrochemical cell-kit (Pine Research Instrumentation) with a saturated calomel electrode (SCE) reference, and 0.1 M tetrabutylammonium hexafluorophosphate (NBu_4PF_6) acetonitrile as the electrolyte solution. The experiment was monitored/controlled using a CH Instruments 601 potentiostat and Agilent Technologies Cary 8454 UV-Vis Spectrometer. Acetonitrile (99.8%, water ≤ 50 ppm) was used without further drying but was purged with N_2 for five minutes before measurements were performed. The 0.1 M tetrabutylammonium hexafluorophosphate supporting electrolyte was further purified by recrystallization from ethanol and dried under vacuum at 80 ˚C for 24 hours prior to use.

Experimental Procedures.

General Photolysis Reaction: All samples were prepared inside a N_2-filled glove box. 2.5 mmol of 7-bromo-2-naphthol, 3.75 mmol triethanolamine, and 0.07 mmol $(Ir[dF(CF_3)ppy]_2(dtbpy))PF_6$ were added to 28 mL of anhydrous acetonitrile in a round-bottomed flask that was then sealed with a rubber septa leaving 3.5 ml of head space volume for collecting and analyzing the gas produced during the reaction. The solution was stirred and irradiated with the Hanovia 450 W medium pressure mercury lamp (emission from 200 to 700 nm) for 6 hours with a constant temperature range of 26 °C to 28 °C. On completion of the reaction, 0.8 mL of the head space volume was collected via Hamilton Luer-Lock precision gas tight syringe and the sample was analyzed using gas chromatography. Control experiments were performed with variation of this general procedure (i.e. not adding reagents, adding PhOH or MCA, blue light source, etc.).

Electrochemical Reduction of ROH: Using the spectroelectrochemical apparatus described above, an acetonitrile solution containing 4.0 mM ROH and 0.1 M NBu_4PF_6 was held under an applied bias of -1.5 V vs. SCE. Absorption spectra were acquired every 2 seconds until no further changes were observed in the absorption spectra and the results are shown in Figure 4.5 of the manuscript. Over time, the spectral signature of ROH (l_{max} = 334 nm) decreased while the spectral signature for RO^- (l_{max} = 387 nm) increased with an isosbestic point at ~340 nm.

Chemical Reduction of ROH: Inside a N_2-filled glove box, 2.5 mmol of ROH and 2.75 mmol of potassium were mixed in 28 mL of anhydrous tetrahydrofuran in a round bottom flask. THF was selected as the solvent due to the instability of acetonitrile towards potassium metal. The reaction flask was sealed with a rubber septum leaving 3.5 mL of gas headspace. The reaction mixture was stirred for 6 hours at room temperature, then 0.8 mL of the headspace gas was collected in a gas tight syringe and analyzed for hydrogen using gas chromatography (entry 9 of Table 4.1 in the manuscript). Following head space analysis, excess solid potassium was filtered from the solution under inert atmosphere. Anhydrous pentane was then added to the filtrate, and a light pink solid precipitated from solution. The solid was then filtered and dried and analyzed with ^{1}H NMR with the spectral features assigned to the 7-bromo-2-naphthalate (RO^-) molecule (i.e. $2ROH + 2K \rightarrow 2K^+ + 2ROH^- \rightarrow H_2 + 2RO^-$). An independently obtained ^{1}H NMR spectrum of RO^- obtained by stirring an acetonitrile solution of ROH and NaOH was consistent with the spectrum of 7-bromo-2-naphthalate analyzed in direct reduction using potassium.

Reduction of PC: Using the spectroelectrochemical apparatus described above, an acetonitrile solution containing 1.0 mM PC and 0.1 M NBu_4PF_6 was held under an applied bias of -1.4 V vs. SCE. The charge passed was monitored until 1.1 F of charge was passed to ensure complete reduction of the PC and the absorption spectrum was obtained and the results are shown as the orange spectrum in Figure 4.8a of the manuscript.

Surface Bound Electrochemical Measurements: PC was adsorbed to an indium tin oxide working electrode[35] from an 0.1 mM solution of PC in methanol. The working electrode was submerged in an N_2 deaerated MeCN solution containing 0.1 M tetrabutylammonium hexafluorophosphate (NBu_4PF_6) electrolyte in an H-cell. Platinum wire and SCE were used as the counter and working electrodes respectively. Current was measured with respect to time under an applied bias of -0.4 V vs. SCE, using the potentiostat described above, and the broadband light source (200 – 700 nm) turned on and off at intervals shown in Figure 4.4. The experiment was performed both without and with 4 mM ROH.

Ground State pK_a Determination: The pK_a value for ROH was determined by monitoring titrations of ROH with cyclopentadienyl iron(dicarobonyl) anion (Fp^-) with infrared (IR) spectroscopy as previously described.[36] IR spectra of standard concentrations of Fp^- in acetonitrile solution and mixtures of Fp^- and ROH are shown in Figure 4.12 and 4.13, respectively.

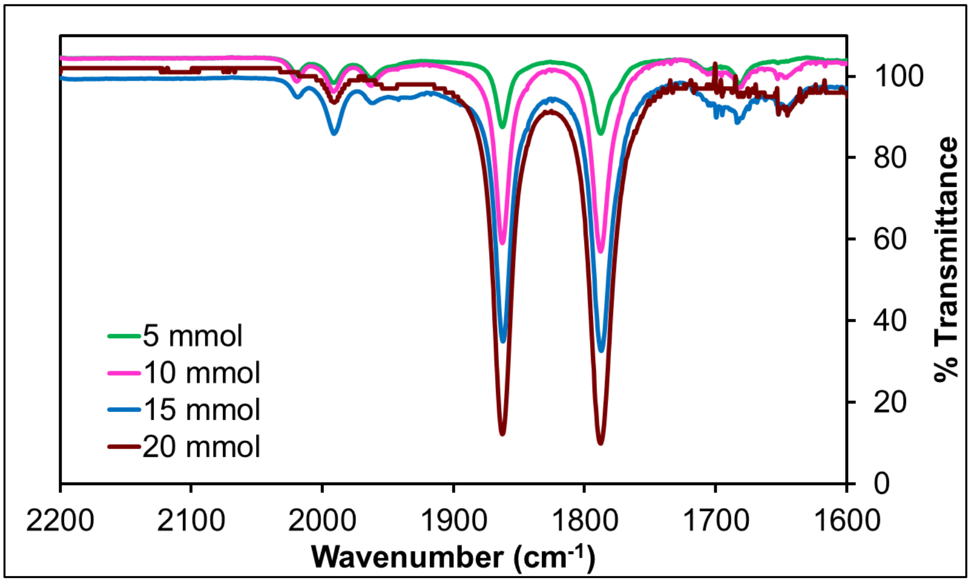

Figure 4.12: IR spectra of acetonitrile solutions containing various concentrations of cyclopentadienyl iron(dicarobonyl) anion (Fp^-).

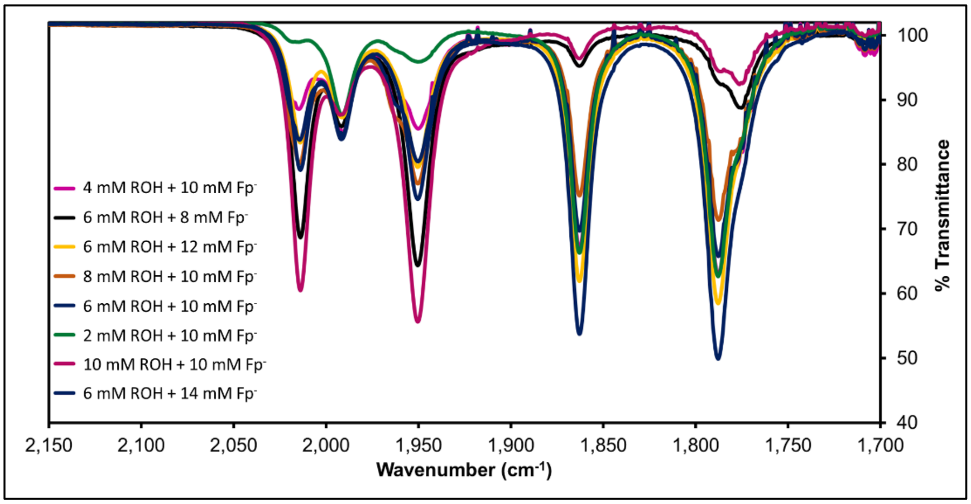

Figure 4.13: IR spectra of mixtures of various ratios of ROH and Fp^- in MeCN

The peaks at 2015 cm^{-1} and 1950 cm^{-1} have been previously assigned to the formation of cyclopentadienyl iron(dicarobonyl) hydride (FpH) which forms when Fp^- is protonated ($Fp^- + H^+ \rightarrow FpH$).[36] From the calibration curve shown in Figure

4.14, the known pK_a of FpH (27.1), and the data in Figure 4.13, a pK_a value of 27.9 was determined for ROH in the ground state.

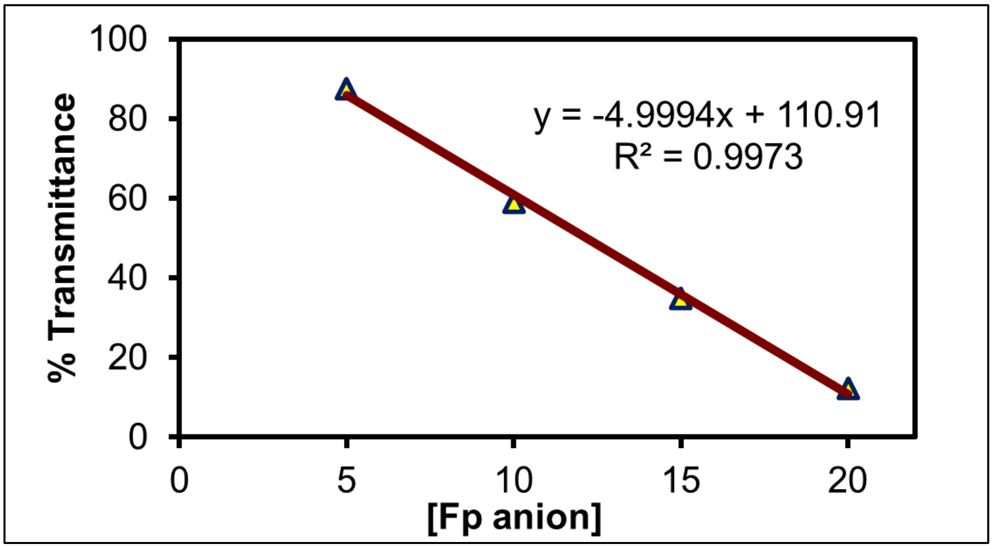

Figure 4.14: Calibration curve of % transmittance versus [Fp^-]. The slope of the line was used to determine the extent of Fp^- protonation by ROH ($Fp^- + ROH \rightarrow FpH + RO^-$).

Excited State pK$_a$ Determination: A pK_a for the triplet excited-state of 7-bromo-2-naphthol (p$K_{a,ROH*}$) of 16.4 was determined using a Forster cycle and equation 4.6:

$$pK_{a,ROH^*} = pK_{a,ROH} - \frac{N_A h(V_{OH} - V_{O-})}{2.303RT} \qquad (4.6)$$

where p$K_{a,ROH}$ = 27.9, N_A is Avogadro's number, *h* is Planck's constant, *R* is the gas constant, *T* is temperature (77 K), and V_{OH} and V_{O^-} are equal to the speed of light divided by $E_{0\text{-}0}$ of the triplet excited state of ROH (2.65 eV) and RO^- (2.48 eV), respectively. $E_{0\text{-}0}$ were estimated from the x-intercept of the tangent to the inflection point on the high energy side of the phosphorescent emission from ROH in Figure 4.16. We were unable to observe phosphorescent emission from RO^-, even at 77K. Consequently we used the phosphorescent emission onset value from the related 7-Br-NpOH for our calculations.[28]

Ground and excited state Redox Potential Determination: The ground state oxidation ($E°_{PC^{0/+}}$) and reduction ($E°_{PC^{0/-}}$) potentials for PC of 1.69 V and -1.37 V vs. SCE, were previously reported.[37] Following literature procedure,[38] triplet excited state oxidation ($E°_{PC^{*/+}}$) and reduction ($E°_{PC^{*/-}}$) potentials of -1.06 V and 1.38 V, respectively, and were estimated using equations 4.7 and 4.8 with an $E_{0\text{-}0}$ of 2.76 eV from phosphorescent emission spectra shown in Figure 4.15

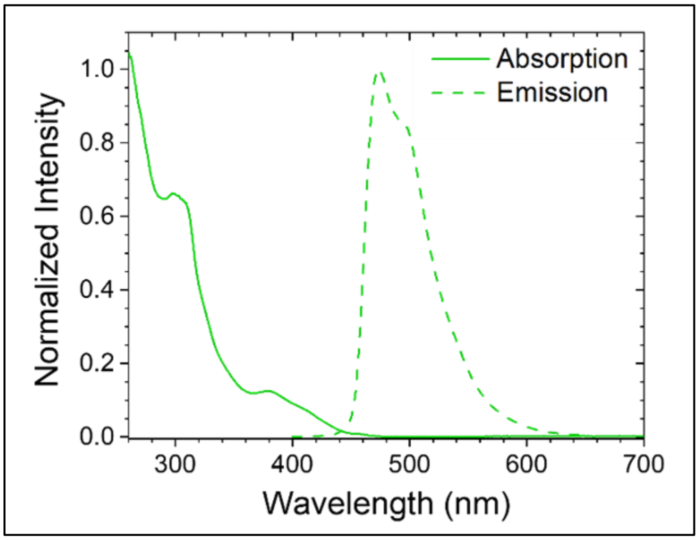

Figure 4.15: Absorption and emission spectra of PC in MeCN (λ_{ex} = 375 nm) at room temperature.

$$E°_{PC^{*/+}} = E°_{PC^{0/+}} - E_{0\text{-}0} \qquad (4.7)$$

$$E°_{PC^{*/-}} = E°_{PC^{0/-}} + E_{0\text{-}0} \qquad (4.8)$$

The oxidation potential for ROH ($E°_{ROH^{0/+}}$ = 1.50 V) was determined by cyclic voltammetry. The standard reduction potential for ROH ($E°_{ROH^{0/-}}$ = -1.39 V) was calculated from the pK_a value using equation 4:

$$E^o_{ROH0/-} = E^o_{H+} - \frac{2.303RT}{F}\mathrm{p}K_{a,ROH} \qquad (4.9)$$

where the temperature (T) is 298 K, R is the gas constant, F is Faraday's constant, and $E°_{H^+}$ = +0.26 V vs. SCE in MeCN.[9] Triplet excited state oxidation ($E°_{ROH^{*/+}}$) and reduction ($E°_{ROH^{*/-}}$) potentials for ROH of -1.16 V and 1.27 V, respectively, and were also estimated using equations 4.7 and 4.8 with an $E_{0\text{-}0}$ of 2.66 eV from phosphorescent emission spectra shown in Figure 4.16.

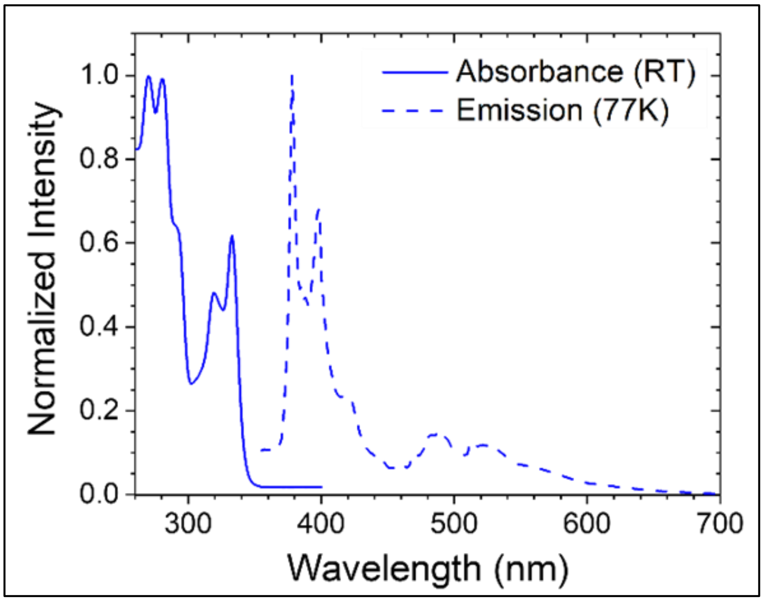

Figure 4.16: Absorption and emission spectra of ROH in MeCN (λ_{ex} = 335 nm). Absorption and emission measurements were acquired at room temperature and 77 K, respectively

Redox Reaction Potential Determination: The potential required to reduce phenol with TEOA was calculated using the half reactions shown in equations 4.10 and 4.11 and the full redox reaction 7.

$$TEOA^+ + e^- \rightarrow TEOA \qquad E^o = +1.30 \text{ V (vs. SCE)} \qquad (4.10)$$

$$PhOH + e^- \rightarrow PhOH- \qquad E^o = -1.35 \text{ V (vs SCE)} \qquad (4.11)$$

$$PhOH + TEOA \rightarrow PhOH^- + TEOA^+ \qquad DG = 2.65 \text{ eV} \qquad (4.12)$$

Stern-Volmer Analysis: Five or six 20 μM PC solutions were prepared in 1×1 cm cuvettes using anhydrous MeCN and deaerated with N_2 for 30 minutes prior to the addition 0 - 3800 μM of TEOA or 0 – 105 μM ROH. Steady-state and/or time-resolved emission from PC was then monitored under 375 nm excitation using the instrument described above.

4.6 References

1. Alstrum-Acevedo, J. H.; Brennaman, M. K.; Meyer, T. J., Chemical Approaches to Artificial Photosynthesis. 2. *Inorg. Chem.* **2005**, *44* (20), 6802-6827.

2. Dogutan, D. K.; Nocera, D. G., Artificial Photosynthesis at Efficiencies Greatly Exceeding That of Natural Photosynthesis. *Acc. Chem. Res.* **2019**, *52* (11), 3143-3148.

3. Zhang, B.; Sun, L., Artificial photosynthesis: opportunities and challenges of molecular catalysts. *Chem. Soc. Rev.* **2019**, *48* (7), 2216-2264.

4. Bard, A. J.; Fox, M. A., Artificial Photosynthesis - Solar Splitting of Water to Hydrogen and Oxygen. *Acc. Chem. Res.* **1995**, *28* (3), 141-145.

5. Felton, G. A. N.; Mebi, C. A.; Petro, B. J.; Vannucci, A. K.; Evans, D. H.; Glass, R. S.; Lichtenberger, D. L., Review of electrochemical studies of complexes containing the Fe2S2 core characteristic of [FeFe]-hydrogenases including catalysis by these complexes of the reduction of acids to form dihydrogen. *Journal of Organometallic Chemistry* **2009**, *694* (17), 2681-2699.

6. Kranz, C.; Wächtler, M., Characterizing photocatalysts for water splitting: from atoms to bulk and from slow to ultrafast processes. *Chem. Soc. Rev.* **2021**, *50* (2), 1407-1437.

7. Fukuzumi, S.; Lee, Y.-M.; Nam, W., Bioinspired artificial photosynthesis systems. *Tetrahedron* **2020**, *76* (14), 131024.

8. McConnell, I.; Li, G.; Brudvig, G. W., Energy Conversion in Natural and Artificial Photosynthesis. *Chemistry & Biology* **2010**, *17* (5), 434-447.

9. Felton, G. A. N.; Glass, R. S.; Lichtenberger, D. L.; Evans, D. H., Iron-Only Hydrogenase Mimics. Thermodynamic Aspects of the Use of Electrochemistry to Evaluate Catalytic Efficiency for Hydrogen Generation. *Inorg. Chem.* **2007**, *46* (19), 8098-8098.

10. Appel, A. M.; Helm, M. L., Determining the Overpotential for a Molecular Electrocatalyst. *ACS Catal.* **2014**, *4* (2), 630-633.

11. Quaino, P.; Juarez, F.; Santos, E.; Schmickler, W., Volcano plots in hydrogen electrocatalysis - uses and abuses. *Beilstein J Nanotechnol* **2014**, *5*, 846-854.

12. Stratakes, B. M.; Miller, A. J. M., H2 Evolution at an Electrochemical “Underpotential” with an Iridium-Based Molecular Photoelectrocatalyst. *ACS Catal.* **2020**, *10* (16), 9006-9018.

13. Maeda, K., Z-Scheme Water Splitting Using Two Different Semiconductor Photocatalysts. *ACS Catal.* **2013**, *3*, 1486-1503.

14. Wang, Y.; Suzuki, H.; Xie, J.; Tomita, O.; Martin, D. J.; Higashi, M.; Kong, D.; Abe, R.; Tang, J., Mimicking Natural Photosynthesis: Solar to Renewable H2 Fuel Synthesis by Z-Scheme Water Splitting Systems. *Chemical Reviews* **2018**, *118* (10), 5201-5241.

15. Guo, H.-L.; Du, H.; Jiang, Y.-F.; Jiang, N.; Shen, C.-C.; Zhou, X.; Liu, Y.-N.; Xu, A.-W., Artificial Photosynthetic Z-scheme Photocatalyst for Hydrogen Evolution with High Quantum Efficiency. *The Journal of Physical Chemistry C* **2017**, *121* (1), 107-114.

16. Sakata, Y.; Hayashi, T.; Yasunaga, R.; Yanaga, N.; Imamura, H., Remarkably high apparent quantum yield of the overall photocatalytic H2O splitting achieved by utilizing Zn ion added Ga2O3 prepared using dilute CaCl2 solution. *Chem. Commun.* **2015**, *51* (65), 12935-12938.

17. Yu, Z. B.; Xie, Y. P.; Liu, G.; Lu, G. Q.; Ma, X. L.; Cheng, H.-M., Self-assembled CdS/Au/ZnO heterostructure induced by surface polar charges for efficient photocatalytic hydrogen evolution. *Journal of Materials Chemistry A* **2013**, *1* (8), 2773-2776.

18. Li, X.; Garlisi, C.; Guan, Q.; Anwer, S.; Al-Ali, K.; Palmisano, G.; Zheng, L., A review of material aspects in developing direct Z-scheme photocatalysts. *Mater. Today* **2021**, doi.org/10.1016/j.mattod.2021.02.017.

19. Yu, Z.; Li, F.; Sun, L., Recent advances in dye-sensitized photoelectrochemical cells for solar hydrogen production based on molecular components. *Energy & Environmental Science* **2015**, *8* (3), 760-775.

20. Xiang, C.; Weber, A. Z.; Ardo, S.; Berger, A.; Chen, Y.; Coridan, R.; Fountaine, K. T.; Haussener, S.; Hu, S.; Liu, R.; Lewis, N. S.; Modestino, M. A.; Shaner, M. M.; Singh, M. R.; Stevens, J. C.; Sun, K.; Walczak, K., Modeling, Simulation, and Implementation of Solar-Driven Water-Splitting Devices. *Angew. Chem. Int. Ed.* **2016**, *55* (42), 12974-12988.

21. McClure, D. S.; Blake, N. W.; Hanst, P. L., Singlet-Triplet Absorption Bands in Some Halogen Substituted Aromatic Compounds. *The Journal of Chemical Physics* **1954**, *22* (2), 255-258.

22. Whittemore, T. J.; Xue, C.; Huang, J.; Gallucci, J. C.; Turro, C., Single-chromophore single-molecule photocatalyst for the production of dihydrogen using low-energy light. *Nature Chem.* **2020**, *12* (2), 180-185.

23. Bobo, M. V.; Paul, A.; Robb, A. J.; Arcidiacono, A. M.; Smith, M. D.; Hanson, K.; Vannucci, A. K., Bis-Cyclometalated Iridium Complexes Containing 4,4′-Bis(phosphonomethyl)-2,2′-bipyridine Ligands: Photophysics, Electrochemistry, and High-Voltage Dye-Sensitized Solar Cells. *Inorg. Chem.* **2020**, *59* (9), 6351-6358.

24. Paul, A.; Smith, M. D.; Vannucci, A. K., Photoredox-Assisted Reductive Cross-Coupling: Mechanistic Insight into Catalytic Aryl–Alkyl Cross-Couplings. *J. Org. Chem.* **2017**, *82* (4), 1996-2003.

25. Teets, T. S.; Nocera, D. G., Photocatalytic hydrogen production. *Chem. Commun.* **2011**, *47* (33), 9268-9274.

26. Tolbert, L. M.; Solntsev, K. M., Excited-State Proton Transfer: From Constrained Systems to “Super” Photoacids to Superfast Proton Transfer. *Acc. Chem. Res.* **2002**, *35* (1), 19-27.

27. Kütt, A.; Leito, I.; Kaljurand, I.; Sooväli, L.; Vlasov, V. M.; Yagupolskii, L. M.; Koppel, I. A., A Comprehensive Self-Consistent Spectrophotometric Acidity Scale of Neutral Brønsted Acids in Acetonitrile. *J. Org. Chem.* **2006**, *71* (7), 2829-2838.

28. Dempsey, J. L.; Winkler, J. R.; Gray, H. B., Mechanism of H2 Evolution from a Photogenerated Hydridocobaloxime. *J. Am. Chem. Soc.* **2010**, *132* (47), 16774-16776.

29. Forster, T. Z., Electrolytic Dissociation of Excited Molecules. *Elektrochem.* **1950**, *54*, 531-535.

30. Baffert, C.; Artero, V.; Fontecave, M., Cobaloximes as Functional Models for Hydrogenases. 2. Proton Electroreduction Catalyzed by Difluoroborylbis(dimethylglyoximato)cobalt(II) Complexes in Organic Media. *Inorg. Chem.* **2007**, *46* (5), 1817-1824.

31. Hu, X.; Brunschwig, B. S.; Peters, J. C., Electrocatalytic Hydrogen Evolution at Low Overpotentials by Cobalt Macrocyclic Glyoxime and Tetraimine Complexes. *J. Am. Chem. Soc.* **2007**, *129* (29), 8988-8998.

32. Izutsu, K., *Acid-Base Dissociation Constants in Dipolar Aprotic Solvents*. Blackwell Scientific: Oxford, U.K., 1990.

33. Margarit, C. G.; Asimow, N. G.; Thorarinsdottir, A. E.; Costentin, C.; Nocera, D. G., Impactful Role of Cocatalysts on Molecular Electrocatalytic Hydrogen Production. *ACS Catal.* **2021**, *11* (8), 4561-4567.

34. Lowry, M. S.; Goldsmith, J. I.; Slinker, J. D.; Rohl, R.; Pascal, R. A.; Malliaras, G. G.; Bernhard, S., Single-Layer Electroluminescent Devices and Photoinduced Hydrogen Production from an Ionic Iridium(III) Complex. *Chem. Mater.* **2005**, *17* (23), 5712-5719.

35. Hoertz, P. G.; Chen, Z. F.; Kent, C. A.; Meyer, T. J., Application of High Surface Area Tin-Doped Indium Oxide Nanoparticle Films as Transparent Conducting Electrodes. *Inorg. Chem.* **2010**, *49* (18), 8179-8181.

36. Estes, D. P.; Vannucci, A. K.; Hall, A. R.; Lichtenberger, D. L.; Norton, J. R., Thermodynamics of the Metal–Hydrogen Bonds in (η5-C5H5)M(CO)2H (M = Fe, Ru, Os). *Organometallics* **2011**, *30* (12), 3444-3447.

37. McDaniel, N. D.; Coughlin, F. J.; Tinker, L. L.; Bernhard, S., Cyclometalated iridium(III) aquo complexes: Efficient and tunable catalysts for the homogeneous oxidation of water. *J. Am. Chem. Soc.* **2008**, *130* (1), 210-217.

38. Bock, C. R.; Connor, J. A.; Gutierrez, A. R.; Meyer, T. J.; Whitten, D. G.; Sullivan, B. P.; Nagle, J. K., Estimation of excited-state redox potentials by electron-transfer quenching. Application of electron-transfer theory to excited-state redox processes. *J. Am. Chem. Soc.* **1979**, *101* (17), 4815-4824.

APPENDIX A

CHARACTERIZATION INFORMATION FOR CHAPTER 2

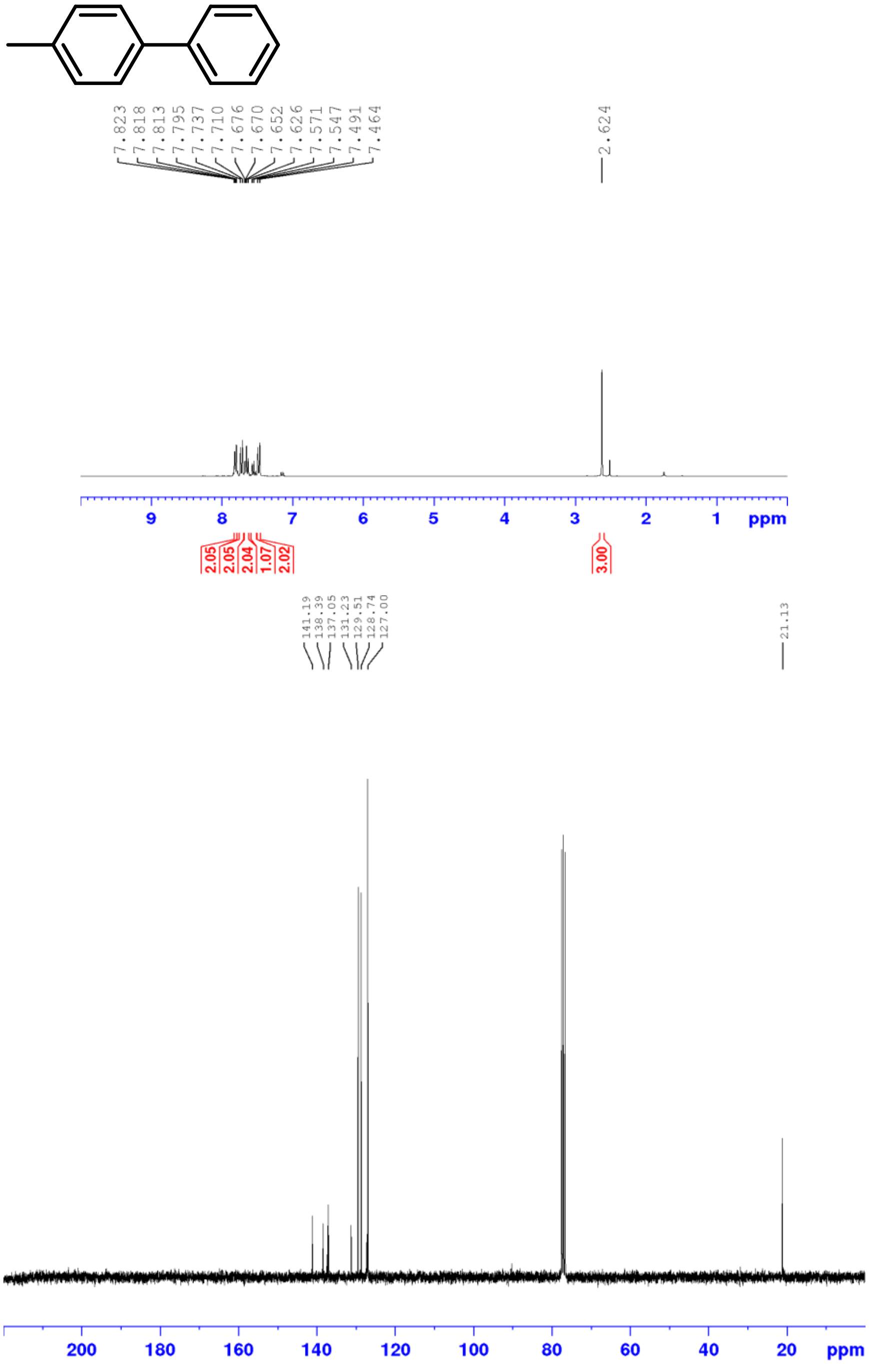

Figure A.1: ^{1}H and ^{13}C NMR of 4-Methyl-1,1'-biphenyl which matches the previously reported spectra.[1]

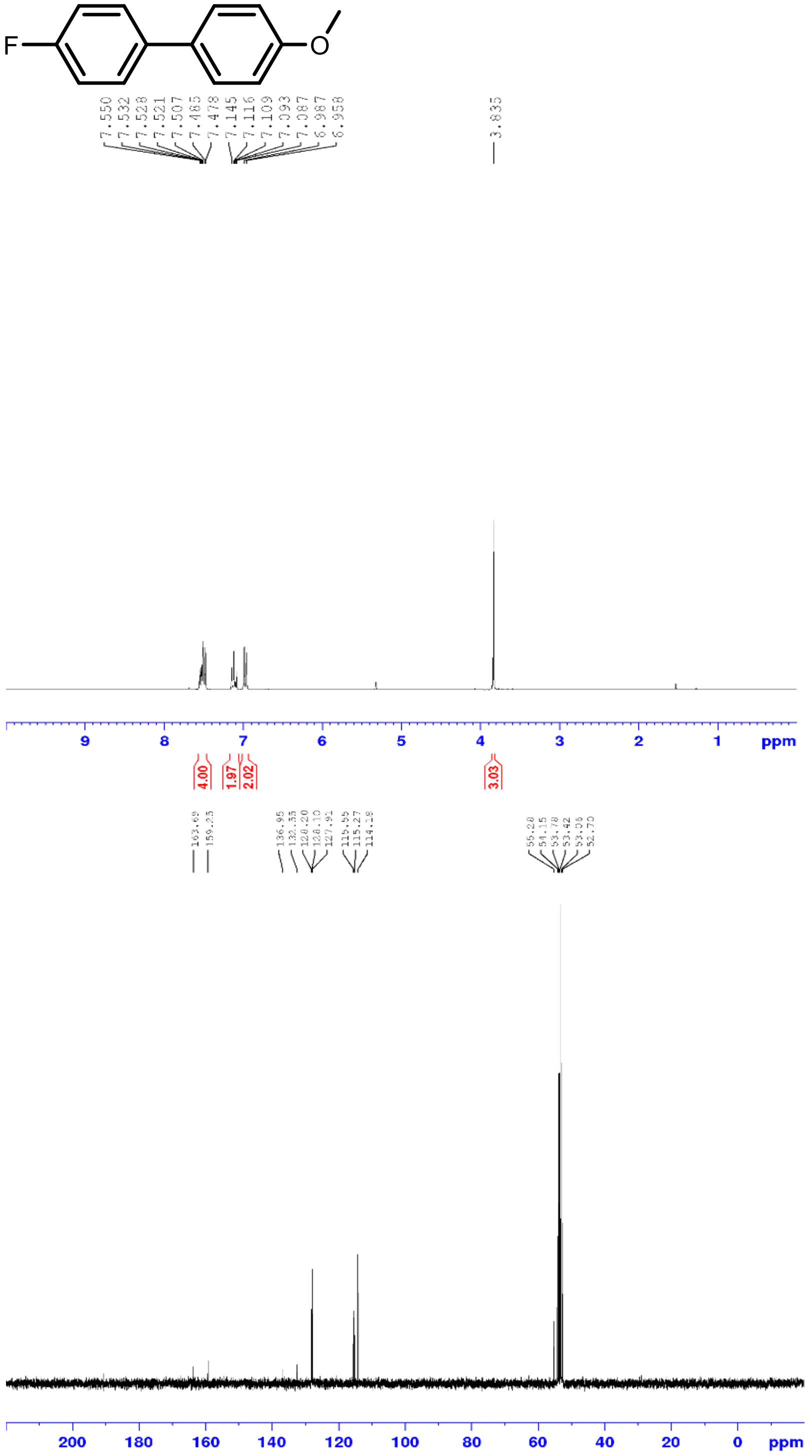

Figure A.2: ^{1}H and ^{13}C NMR of 4-Fluoro-4'-methoxy-1,1'-biphenyl which matches the previously reported spectra.[2]

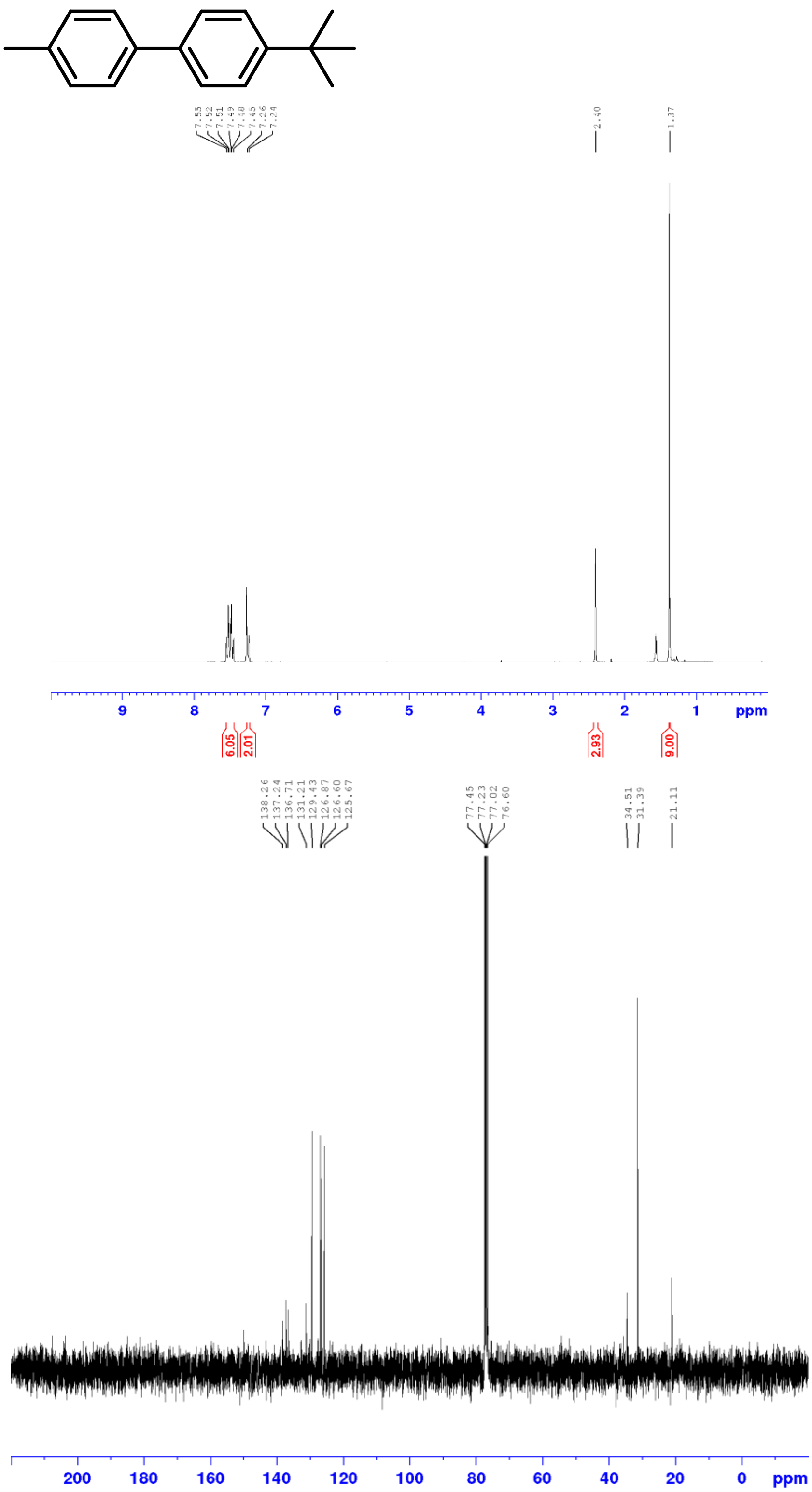

Figure A.3: ^{1}H and ^{13}C NMR of 4-(*tert*-butyl)-4’-methyl-1,1’-biphenyl which matches the previously reported spectra.[1]

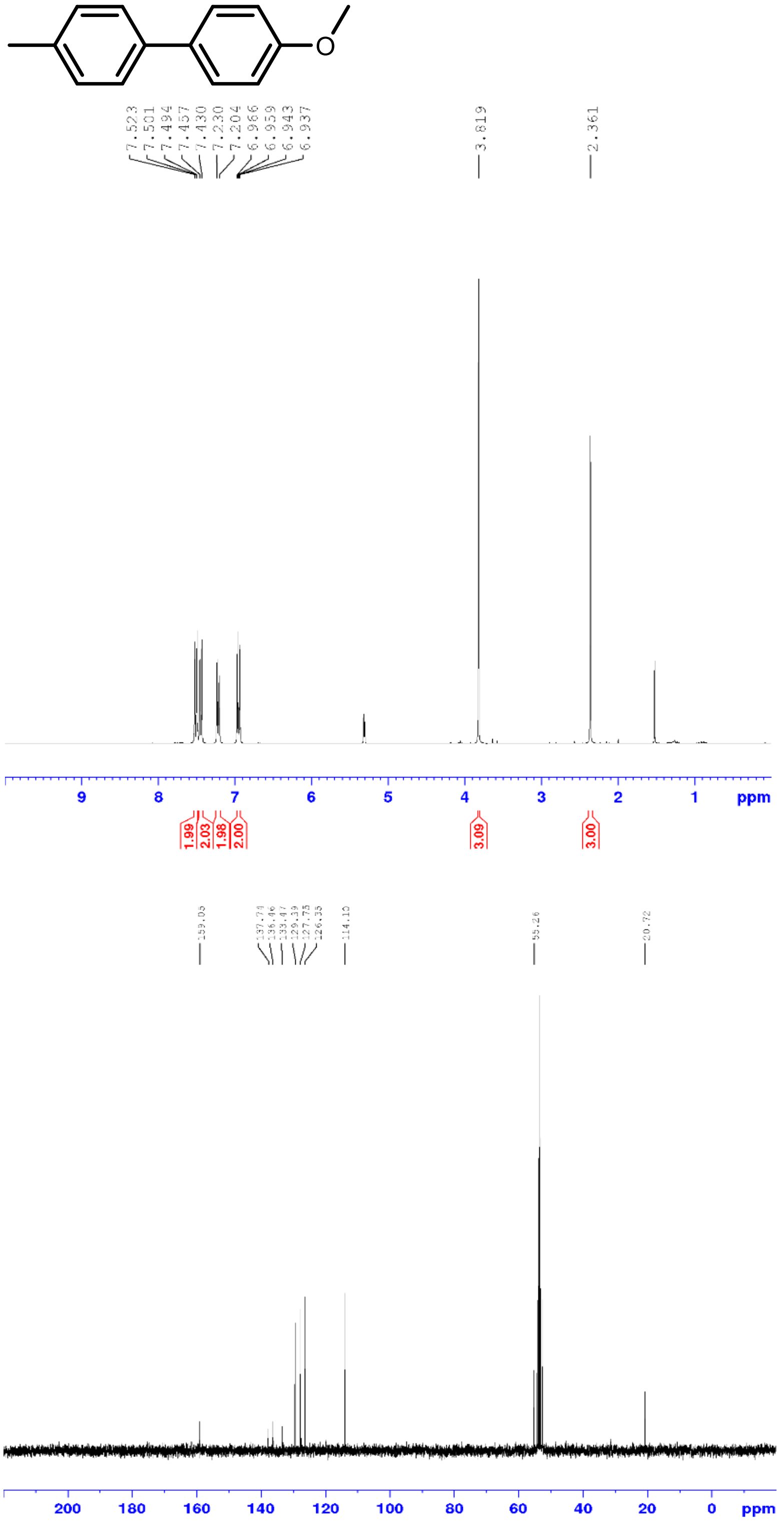

Figure A.4: ^{1}H and ^{13}C NMR of 4-methoxy-4'-methyl-1,1'-biphenyl which matches the previously reported spectra.[1]

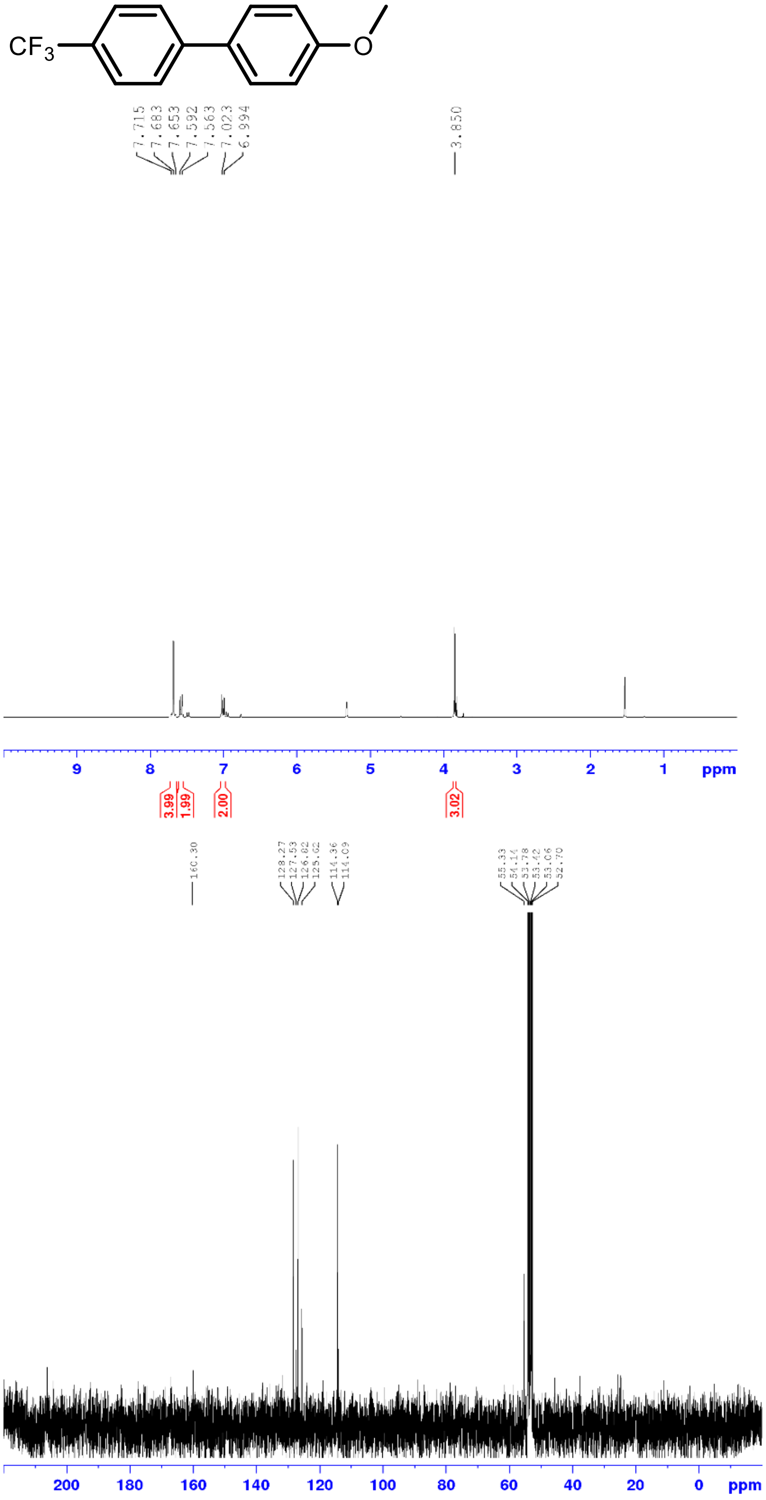

Figure A.5: ^{1}H and ^{13}C NMR of 4-methoxy-4’-(trifluoromethyl)-1,1’-biphenyl which matches the previously reported spectra.[3]

References:

1. P. Y. Choy, O. Y. Yuen, M. P. Leung, W. K. Chow, and F. Y. Kwong. *Eur. J. Org. Chem.* 2020, 2846-2853.
2. I. D. Inaloo, S. Majnooni, H. Eslahi, and M. Esmaeilpour. *ACS Omega,* 2020, **5**, 7406-7417.
3. C. P. Delaney, V. M. Kassel, and S. E. Denmark. *ACS Catal.*, 2020, **10***,* 73-80.

APPENDIX B

CHARACTERIZATION INFORMATION FOR CHAPTER 3

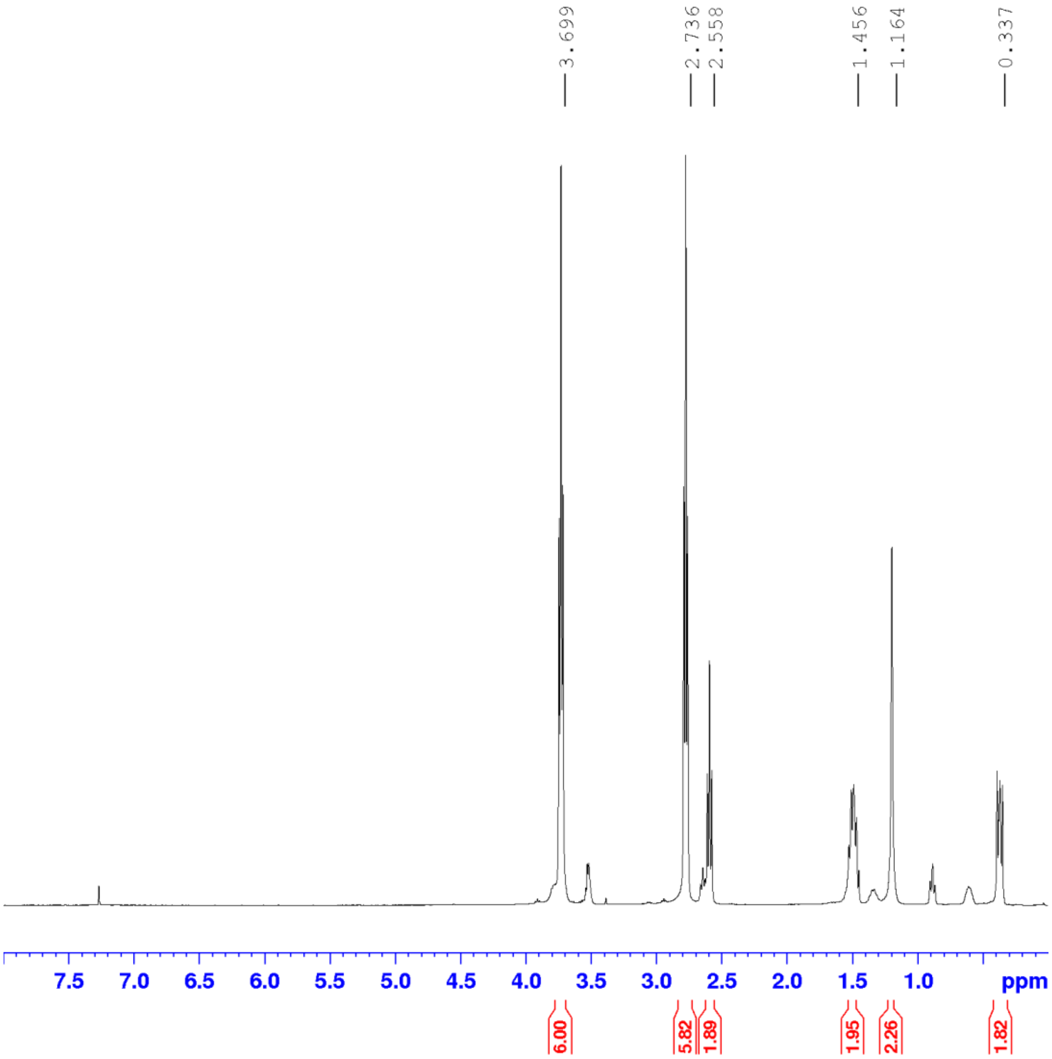

Figure B.1: ^{1}H NMR of 1-(3-aminopropyl) silatrane ligand.

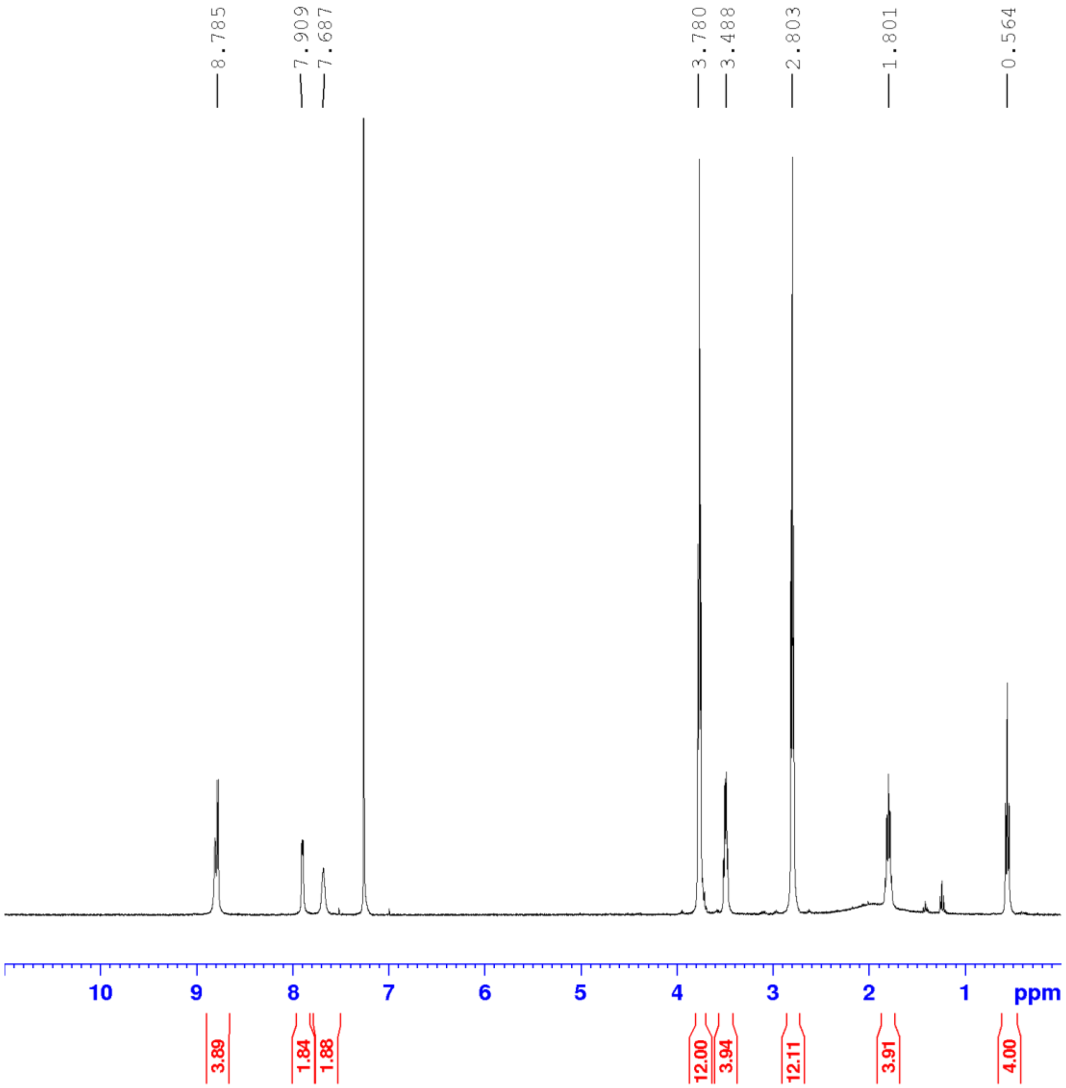

Figure B.2: ^{1}H NMR of 2,2’-bipyridine-4,4’-diamidopropylsilatrane (bpysil)

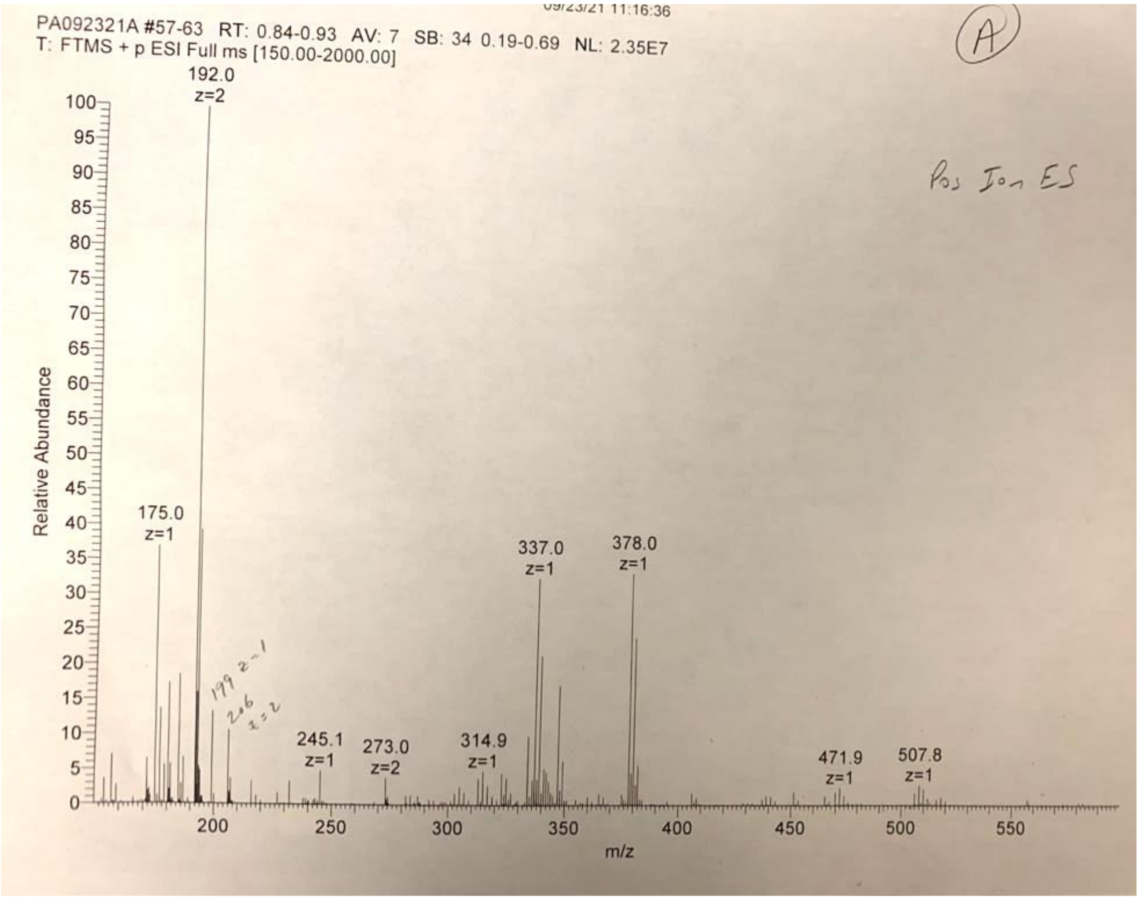

Figure B.3: ESI MS of molecular complex 1a (NibpyCOOH)

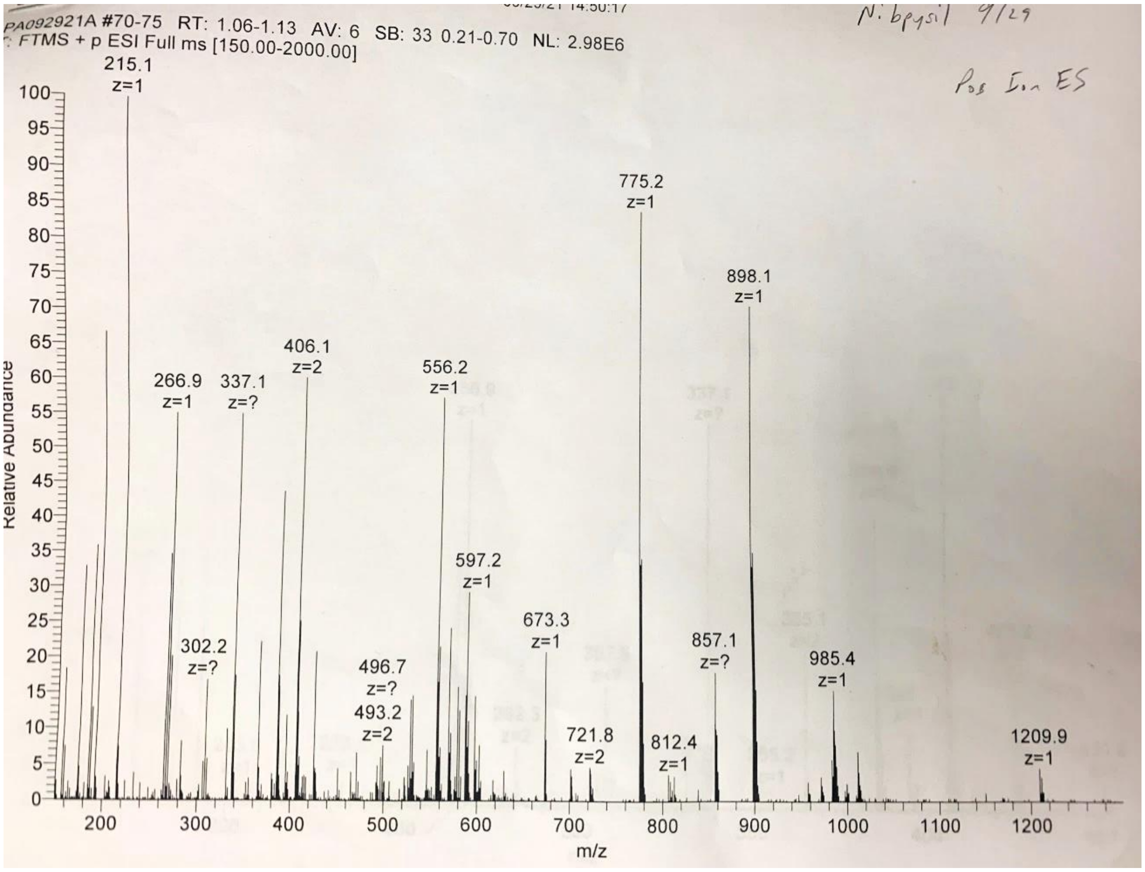

Figure B.4: ESI MS of molecular complex 2a (NibpySil).

APPENDIX C

CHARACTERIZATION INFORMATION FOR CHAPTER 4

Spectroscopic Results:

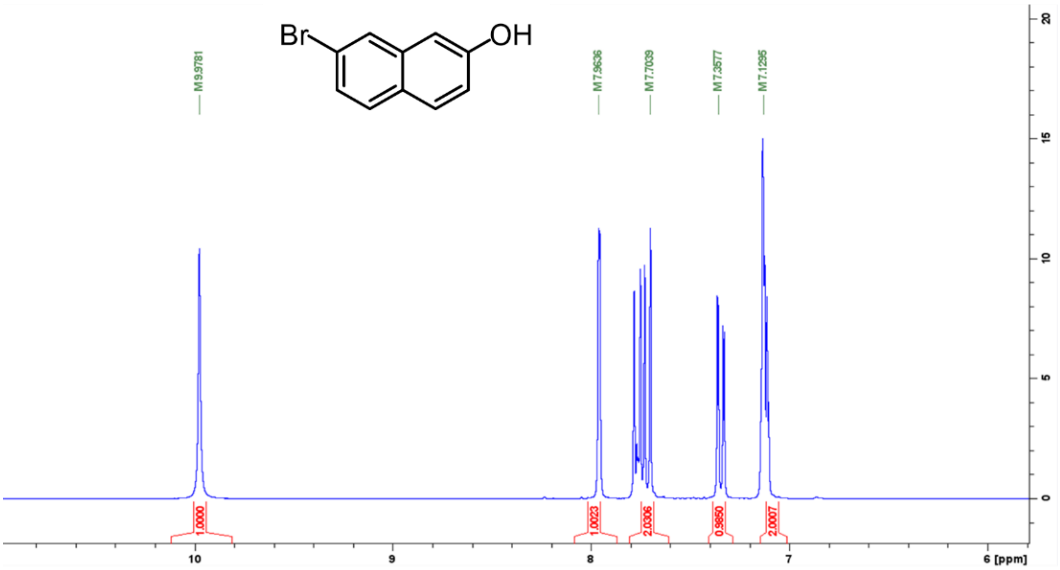

Figure C.1: ^{1}H NMR spectrum of ROH

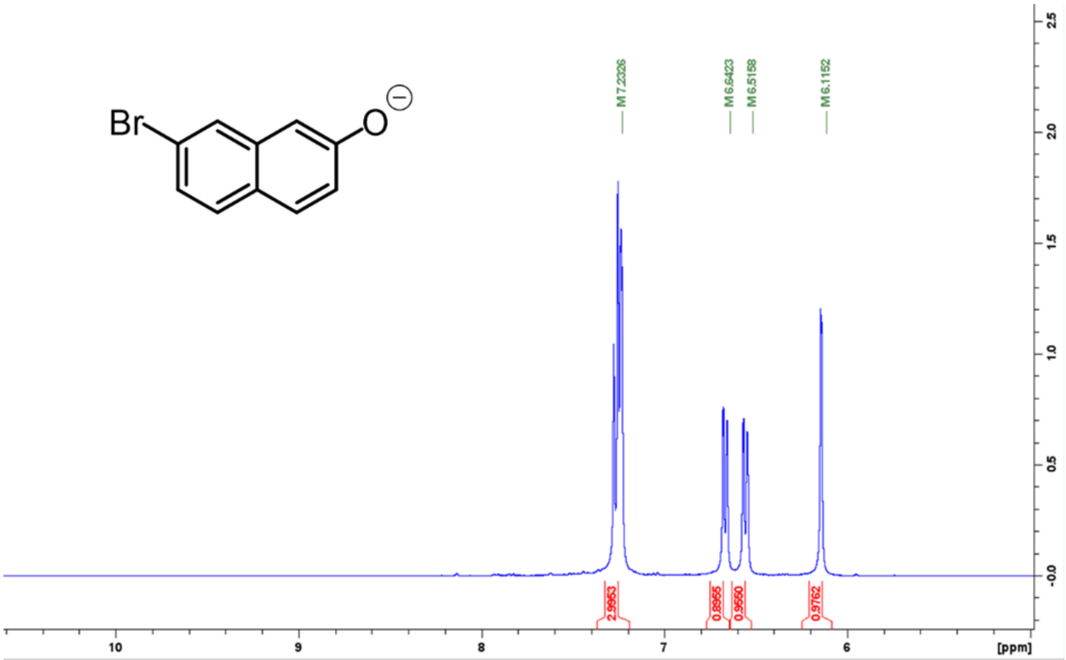

Figure C.2: . ^{1}H NMR spectrum of RO$^-$ in dimethyl sulfoxide-d$_6$ after chemical reduction of ROH with potassium metal.

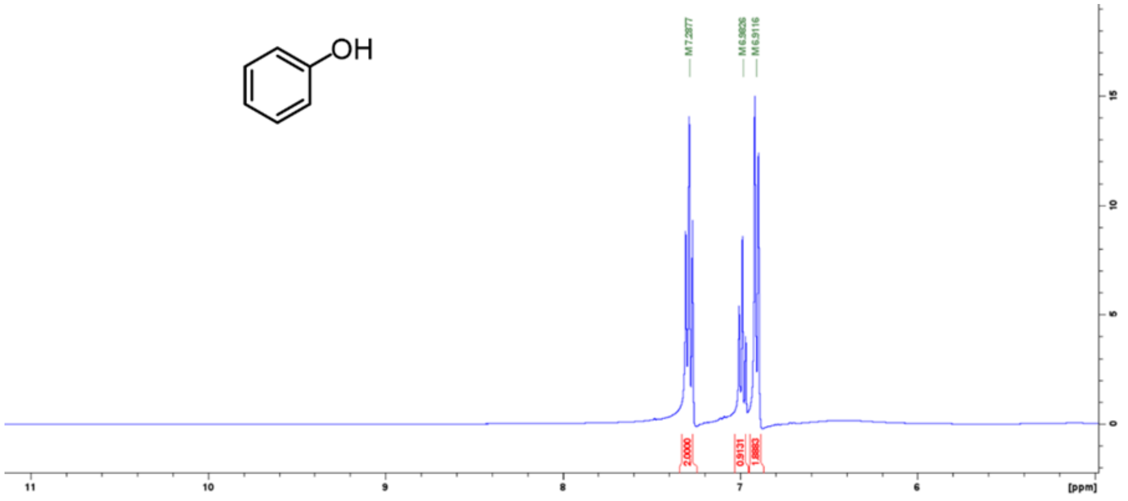

Figure C.3: ^{1}H NMR spectrum of Phenol

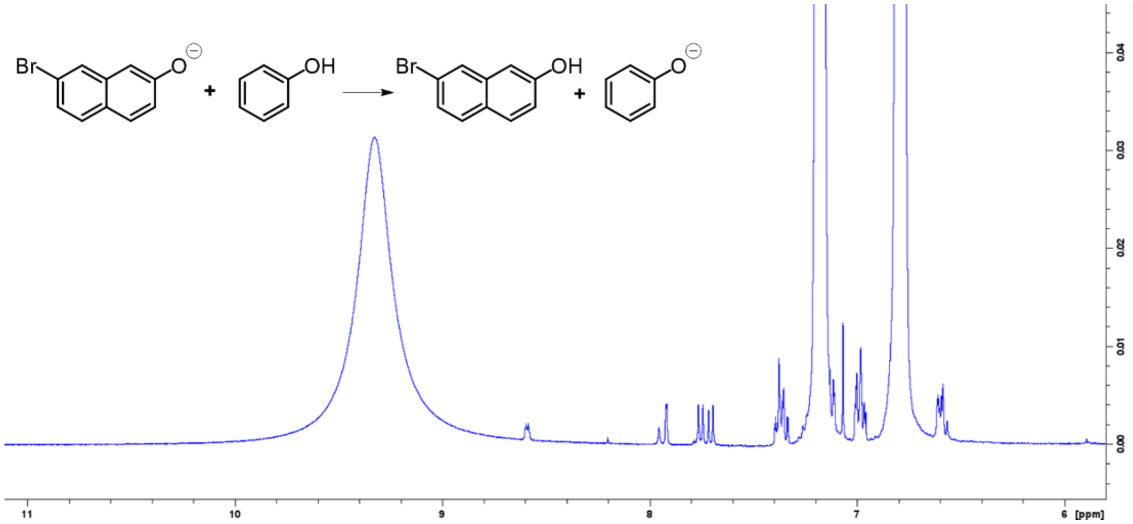

Figure C.4: ^{1}H NMR spectrum of a 1:10 mixture of RO$^-$ and PhOH in dimethyl sulfoxide-d$_6$.

APPENDIX D

PERMISSION TO REPRINT CHAPTER 2

Author reusing their own work published by the Royal Society of Chemistry

You do not need to request permission to reuse your own figure, diagrams, etc, that were originally published in a Royal Society of Chemistry publication. However, permission should be requested for use of the whole article or chapter except if reusing it in a thesis. If you are including an article or book chapter published by us in your thesis, please ensure that your co-authors are aware of this. Reuse of material that was published originally by the Royal Society of Chemistry must be accompanied by the appropriate acknowledgement of the publication. The form of the acknowledgement is dependent on the journal in which it was published originally, as detailed in ‘Acknowledgements’.

Acknowledgements

The Royal Society of Chemistry publishes some journals in partnership with, or on behalf of, other organizations; these journals require a specific wording of the acknowledgement when work is reproduced from them. The text for the acknowledgement for these journals, and the standard wording to be used by all other journals are given below.

Standard Acknowledgement

Reproduced from Ref. XX with permission from the Royal Society of Chemistry.